

RÉPUBLIQUE ALGÉRIENNE DÉMOCRATIQUE ET POPULAIRE

Ministère de l'Enseignement Supérieur et de la Recherche Scientifique



Université Hadj Lakhdar - BATNA 1
Faculté des Sciences de la Matière
Département de Physique



THÈSE

Présentée en vue de l'obtention du
Diplôme de Doctorat

par :

BOUAZIZ Hamza

Thème :

Sur la resommation des logarithmes non-globaux et logarithmes de
regroupement dans les observables de QCD à partir de l'évolution des
gluons de faible énergie

Domaine: Sciences de la Matière

Filière: Physique

Spécialité: Physique théorique

Soutenue le : 26/04/2023

Devant le jury :

Président :	Moumni Mustapha	Prof.	Université de Batna 1
Rapporteur :	Delenda Yazid	Prof.	Université de Batna 1
Examineurs :	Aouachria Mekki	Prof.	Université de Batna 1
	Redouane-Salah Essma	Prof.	Université de M'sila
	Aissaoui Habib	Prof.	Université de Constantine 1
Invité :	Khelifa-Kerfa Kamel	MCB	Université de Relizane

PEOPLE'S DEMOCRATIC REPUBLIC OF ALGERIA
Ministry of Higher Education and Scientific Research



Hadj Lakhdar University - BATNA 1
Faculty of Matter Sciences
Department of Physics



THESIS

Submitted in fulfillment of the requirement
for the degree of Doctorate

By:

HAMZA Bouaziz

Title:

On the resummation of non-global and clustering logarithms in QCD
observables from soft gluon evolution

Domain: Matter Sciences
Branch: Physics
Option: Theoretical Physics

Defended on: 26/04/2023

In front of the jury:

Chair:	Mustapha Mourni	Prof.	University of Batna 1
Supervisor:	Yazid Delenda	Prof.	University of Batna 1
Examiners:	Mekki Aouachria	Prof.	University of Batna 1
	Essma Redouane-Salah	Prof.	University of M'sila
	Habib Aissaoui	Prof.	University of Constantine 1
Invited:	Kamel Khelifa-Kerfa	MCB	University of Relizane

Contents

1	General Introduction	11
2	QCD preliminaries	15
2.1	QCD Lagrangian	16
2.2	Feynman rules	20
2.3	Radiative corrections	22
2.3.1	Regularization	23
2.3.2	Renormalization	24
2.3.3	Renormalization group	27
2.3.4	IR safety	30
2.4	Factorization	37
2.4.1	Collinear splittings	39
2.4.2	DGLAP evolution equations	43
2.4.3	Resummation	45
2.5	Jets & jet algorithms	48
2.5.1	Sequential recombination algorithms	48
2.5.2	Cone algorithms	49
3	Monte Carlo tools & methods.	50
3.1	Random number generation	51
3.2	Monte Carlo methods	52
3.2.1	Sampling	53
3.2.2	Variance reduction	55

3.3	Hard processes simulation	57
3.4	Tree level matrix element generators	59
3.5	Higher order corrections	62
3.6	Parton showers	63
3.6.1	Large N_c	66
3.7	Matching/merging	66
3.8	Monte Carlo tools	67
4	Azimuthal decorrelation in Z+jet process @ LHC.	69
4.1	Kinematics and observable definition	71
4.2	Global resummation	73
4.3	Results in Δ space	76
4.3.1	Evaluation of the b integral	76
4.3.2	Convolution with the Born cross-section	78
4.3.3	NNLL corrections at two loops	78
4.3.4	Comparison to MC results at fixed order	79
5	Non-global and clustering logarithms in Z+jet process	81
5.1	Non-global logarithms at 2-loops	81
5.2	Clustering logarithms at 2-loops	84
5.3	Non-global & clustering logarithms to all orders	87
5.4	Comparison to parton showers and experimental data	88
6	General conclusion.	93
A	Radiator.	95
A.1	In-in dipole	95
A.1.1	Integrating the whole phase space	95
A.1.2	Subtracting the jet region	97
A.2	In-jet dipole	98
A.2.1	First term	99

A.2.2	Second term	101
A.2.3	Assembled expression for the radiator	102
B	Fixed-order expansion.	104

List of Tables

2.1	QCD Feynman rules for external lines, quarks are represented by straight lines, gluons by curly lines, ghosts are unphysical thus do not appear as an external leg. $k(p)$ are the momenta of the gluon (quark or anti-quark) respectively, i, j, c are the color indices of the quark, anti-quark and the gluon respectively, while s, λ are their spin/polarization states in the same order.	21
2.2	QCD Feynman rules, quarks are represented by straight lines, gluons by curly lines and the massless Faddeev-Popov ghosts by dotted lines.	22
5.1	Fit parameters from numerically resummed NGLs for anti- k_t algorithm ($R = 0.5$).	88

List of Figures

1.1	Pictorial representation of a typical event at hadron colliders. Taken from [89]. . . .	12
1.2	A typical LHC event as seen by the CMS detector. The red lines are particle tracks while the blue cones represent hard jets.	13
2.1	Diagrams that contribute to the total (inclusive) cross section of the process $e^+e^- \rightarrow q\bar{q}$	31
2.2	The LO Altarelli-Parisi splitting kernels.	41
2.3	The leading order PDF sets from MSTW [119] & CTEQ [130] collaborations.	45
4.1	Leading order Feynman diagrams contributing to Z +jet process at Born level. . . .	71
4.2	Comparison of the differential distributions $d\sigma/d(\ln \delta\phi)$ obtained by expanding the resummed distribution up to $\mathcal{O}(\alpha_s)$ and output from fixed-order programs MadGraph5_aMC@NLO and MCFM.	80
5.1	The two loops NGL coefficients in k_t and anti- k_t algorithms for the two partonic Born channels $(\delta_{q,g})$	84
5.2	The two loops coefficients of CLs for the two partonic Born channels $(\delta_{q,g})$	86
5.3	The two loops combined NGL and CL coefficients for the two partonic Born channels $(\delta_{q,g})$	86
5.4	The differential distribution $1/\sigma d\sigma/d\delta\phi$ with anti- k_t clustering (top) and k_t clustering (bottom). We show here the global resummed distribution without NGLs/CLs, the full NLL resummed distribution (including NGLs/CLs), and the corrected NLL distribution including the constant C_1 . Also shown is the fixed-order MC result at NLO.	89

5.5	The differential distributions $1/\sigma d\sigma/d\delta\phi$ with anti- k_t clustering (top) and k_t clustering (bottom). Results are shown for the resummed distribution NLL+ C_1 and parton showers (PS) obtained with various MC event generators. Also shown is the fixed-order NLO MC result.	91
5.6	Comparison between the NLL-resummed distribution, the Pythia 8 parton shower result (including $Z + 2$ jet process), and the CMS data.	92

Acknowledgments

First of all, all praises due to ALLAH for all gratitudes and good things gifted including the health, patience and will to cut my way in life.

I would like to give a special thanks my supervisor, Pr. Delenda for his inspiration, encouragement and guidance throughout not only my PhD years, but also since I first sat in his class during my undergrad years.

A warm thank to my co-supervisor Dr. Khelifa-Kerfa to take the responsibility to take me under his banner, as it turned to be a fruitful collaboration and useful discussions and knowledge over the past 5 years.

I would like to express my gratitude towards the members of jury for taking the time to evaluate this work and traveling from far away to be a part in the jury.

A thank you also has to go to my teachers and professors who taught me from my elementary school until my graduation, this thesis is a culmination of the efforts they put day in and day out. I would also thank all administrative workers of HADJ LAKHDAR university and the staff of central library for making all they could at our disposal.

A big thank you to my friends and colleagues inside and outside the walls of the university that i had the luck to know. These include Mostefa, Sohaib, Abdellah, Oussama, Samir, Riadh, Fouad, Youssef and many many others. Also without forgetting the colleagues of PRIMA lab for letting the workplace alive with discussions and sharing many ideas and help among its members.

Finally, this wouldn't have been possible without the unconditional and constant support from my family members: my brothers and sisters: Abdelhak, Nouha, Fouzi, Linda, Nabil and my grandmother.

Dedication

To my mother and in the memory of my late father.

Chapter 1

General Introduction

One of the oldest ideas that remained from the days of the ancient Greeks is the idea that the universe was made out of indivisible microscopic entities called atoms. Their existence was only proven towards the second half of the nineteenth century. The attempts made thereafter to describe the internal structure of matter and the forces in play at that level using the knowledge acquired of physics over the past centuries all ended with unexpected outcomes, thus a new framework is needed. Today, in the era of modern physics, this new framework is known as the standard model of particle physics (SM). Based on the well established field theories, it replaced the centuries-old idea of sub-atomic particles being the basic building blocks by the concept of *fields* that permeate all space and the entire known spectrum of particles is a mere disturbances or excitations of their respective fields. In spite of being the most precise and most tested theory mankind has ever created, the SM is sometimes referred to as the 4% model due to the overwhelmingly vast wealth of questions that it never was able to answer concerning our universe (e.g dark matter, dark energy, gravitational force, ...) in equivalence to ones that it did.

The SM is based on two very successful field theories, the first being the electroweak theory (EW) that was tested precisely time and time again. The EW theory is based on the symmetry group $U(1) \otimes SU(2)$, it provides an extraordinarily accurate prediction (alongside many others) of the anomalous magnetic dipole moment of the electron and also successfully hypothesizing the existence of massive weak gauge bosons, i.e the W^\pm and Z^0 which alongside the newly discovered Higgs boson [6, 57] that provides a mechanism of generating masses for all known particles, play a

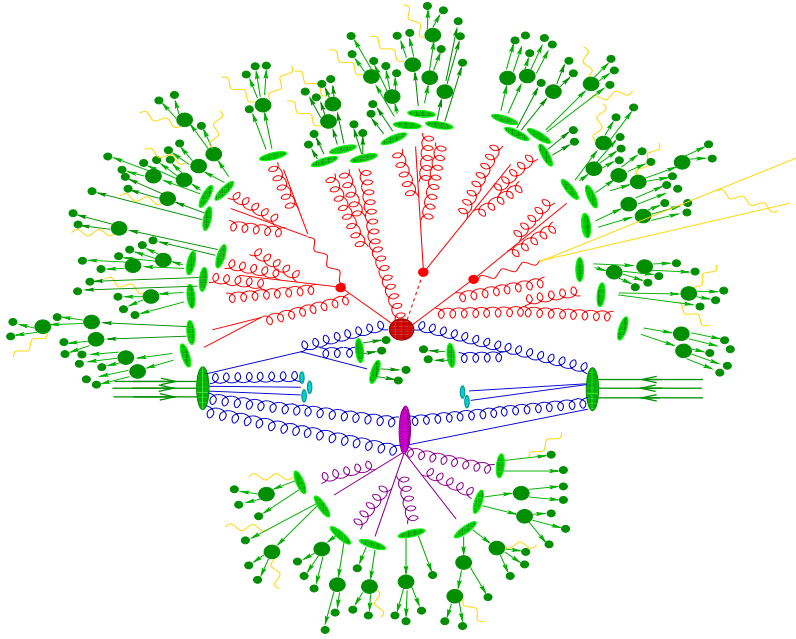


Figure 1.1: Pictorial representation of a typical event at hadron colliders. Taken from [89].

major role in uncovering new signals beyond our current models and predictions and can therefore be regarded as a window into new physics.

The second field theory with which we are concerned in this thesis is the theory of strong interactions or quantum chromo dynamics (QCD). It is based on the $SU(3)$ group, it describes the interaction between the fundamental quantas of quarks by exchanging color charged boson called the gluon. Successes at both of QCD & EW theories cemented the SM's position as a theory of quantas and their interactions.

Tests of QCD are performed at particle colliders, where beams composed of billions of protons are accelerated toward each other. The interesting events are kept to be analyzed later while the majority of events are discarded. The stored events are analyzed for making kinematical properties of events or try to capture new signals indicating a new prospect for particle physics. Often times, the signature of such events of interest is overwhelmed by those coming from far less interesting ones. This renders the discrimination hard and even more challenging at hadron-hadron colliders. To get a grasp of how complex the environment at hadron colliders can get, we show in figure 1.2 a view of a typical event at the LHC¹ while figure 1.1 is a pictorial representation of it.

Many extensions to SM or beyond the standard model (BSM) propose answers/solution to SM's

¹The picture is taken from PHOENIX event display framework [10] which can be found in: <https://hepsoftwarefoundation.org/phoenix>

unanswered questions by hypothesizing the existence of many exotic new particles, with masses at the TeV scale. Studies and searches conducted at different colliders proved fruitless in finding such signals. This suggests that such new states do not exist at all or are buried well within other backgrounds. Either way this calls for a change in our search strategies. Thus a better understanding of the current models and making more and more precise predictions from the experiment and theory side. Also more recently, the searches were supplemented by use of machine learning (ML) techniques to further dig maybe previously missed signals.

From figure (1.b), the pictorial representation can be described by factorizing all the effects shown into two regimes: a perturbative one where the primary hard interaction as well as gluon emission at fixed-order (FO) or to all orders and the subjugation of all outgoing particles to jet algorithms are all described withing the framework of perturbative QCD (pQCD). While on the side, effects such as hadronization, resonance decays, parton distributions inside initial colliding hadrons, underlying events (UE) of all kinds taking place along side the hard interaction are all an example of non-perturbative effects which in the current day, are only described by models with free parameters tuned from experiments.

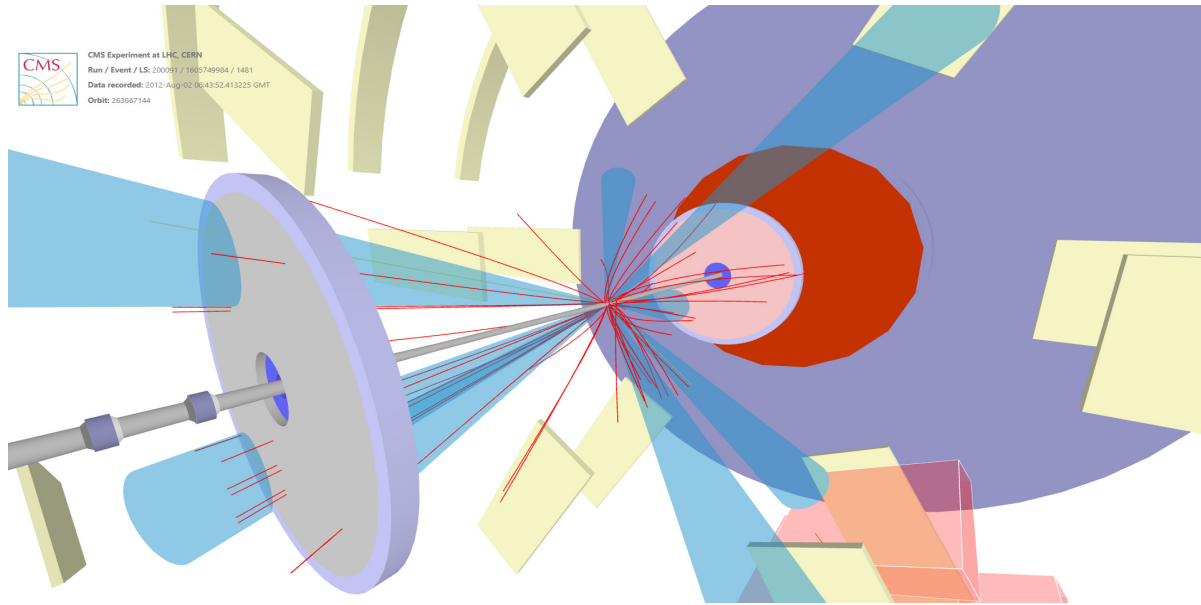


Figure 1.2: A typical LHC event as seen by the CMS detector. The red lines are particle tracks while the blue cones represent hard jets.

This Thesis deals only with effects occurring well within the range of validity of the former regime i.e the perturbative one.

The perturbative aspect can advance in two ways: either a FO approach to describe a finite set of energetic & well-separated partons inclusively or exclusively by considering enhanced gluon emissions in soft/collinear regions of phase space (PS). This is similar to what is considered in Monte Carlo codes where the user chooses at their desire to generate either parton-level weighted events, such that from these weights kinematical histograms of many observables can be filled on the fly and get an estimate of the cross section at the same time, or try and simulate full events with the help of parton shower algorithms (PS) that employ semi-empirical models.

In this thesis, we are interested in the phenomenology of QCD observables at hadron colliders, with the aim of establishing the accuracy of resummed predictions relative to both Monte Carlo event generators and experimental data. We choose a process which includes all sectors of the SM, namely the production of a Z boson together with a jet (or more), and study an interesting observable known as the azimuthal decorrelation between the produced Z boson and the leading hard jet in the event. Our choice is motivated by recent measurements of both the ATLAS and CMS collaborations at the LHC of this same quantity. Our main focus in this thesis will be the resummation of non-global (NGLs) and clustering logarithms (CLs) that arise in the distribution of this observable when a jet algorithm is applied in the final-state. We calculate these logarithms at fixed order and estimate them to all orders. We also address the issue of the resummation of the global logarithms by making a detailed calculation of the resummed form factor.

This thesis is organized as follows, chapter 2 is a brief review of QCD ideas that are in relation to the work presented here. Concepts from the basic QCD Lagrangian up to jet phenomenology at hadron-hadron colliders are presented. Being heavily used in this work as well as an indispensable tool to make predictions and comparisons with data, chapter 3 is a mere short review of MC tools and methods, where principles and generalities over them are discussed. Chapter 4 contains definitions for the observable under study and steps that lead to the principle resummed formula and comparison with fixed-order Monte Carlo codes to check its correctness. We present our results obtained in previous chapter and incorporate the effects of CLs & NGLs and make a comparison with both experimental data and various parton showers predictions. Chapter 6 contains concluding remarks and details of calculation can be found in appendices A and B.

Chapter 2

QCD preliminaries

One of the biggest human triumphs in explaining the microscopic aspect of nature is the development of a theory called the Standard model of particle physics (SM). Based on both of the well-established quantum mechanics as well as special theory of relativity, it is a quantum field theory (QFT) with a symmetry group $SU(3)_C \otimes SU(2)_L \otimes U(1)_Y$. The theory explains the creation, propagation and annihilation of the matter sector (i.e fermions) and their different interactions¹ by exchanging quanta of force carriers (i.e bosons).

In this chapter, we briefly review the $SU(3)$ component of the SM, namely the theory of strong interactions: Quantum Chromo Dynamics or simply QCD. We begin by giving the complete QCD Lagrangian and discuss its symmetries and Feynman rules extracted from it. Then, from well-established principles such as Factorization, we present the QCD master formula, important for doing calculations in the framework of perturbation theory thus bridging between theoretical expectations and experimental measurements. After that, we discuss some aspects of QCD: such as running of the strong coupling, PDFs, . . . and aspects that sets it apart from other quantum field theories notably asymptotic freedom, confinement. Finally, being almost a synonym (acronym) for QCD due to their ubiquity at hadron colliders, we conclude with definitions for the notion of jets and jet algorithms.

¹All known interactions except for gravity, which for now is explained classically by Einstein's general relativity.

2.1 QCD Lagrangian

Predictions in QFTs for the standard model or any BSM model start at the Lagrangian level, where the creation, propagation, annihilation and interactions of fermionic and/or bosonic fields are described (by virtue of dimensionless action) by a set of dimension four operators ². For the case of strong interactions, the complete QCD Lagrangian density ³ can be expressed as:

$$\mathcal{L}_{\text{QCD}} = \mathcal{L}_{\text{Dirac}} + \mathcal{L}_{\text{YM}} + \mathcal{L}_{\text{GF}} + \mathcal{L}_{\text{FP}}, \quad (2.1)$$

where

- $\mathcal{L}_{\text{Dirac}}$ is the Dirac Lagrangian describing the dynamics of quark spinor fields ψ_q and is given by

$$\mathcal{L}_{\text{Dirac}} = \sum_q \bar{\psi}_q^a (i \not{D} - m_q)_{ab} \psi_q^b \quad (2.2)$$

The sum runs over all quark flavours N_f ⁴, a and b are quark-color indices, \not{D} is a shorthand notation for $\gamma^\mu D_\mu$, γ^μ are the usual Dirac matrices obeying the Clifford algebra $\{\gamma^\mu, \gamma^\nu\} = 2\eta^{\mu\nu}$, $\eta^{\mu\nu}$ is Minkowski's metric with a signature $\{+, -, -, -\}$, m_q is the mass of quark q , and lastly D_μ is the covariant derivative; necessary for local gauge invariance of the Dirac Lagrangian and takes the following forms:

$$(D_\mu)_{ab} = \partial_\mu \delta_{ab} + ig_s (t^C \mathcal{A}_\mu^C)_{ab}, \quad a, b = 1, 2, 3 \quad (2.3a)$$

$$(D_\mu)_{AB} = \partial_\mu \delta_{AB} + ig_s (T^C \mathcal{A}_\mu^C)_{AB}, \quad A, B, C = 1, \dots, 8 \quad (2.3b)$$

when acting on the triplet (quark) states and octet (ghost) states respectively. Here, g_s is the strong coupling constant, \mathcal{A}_μ are the gluon fields and the matrices t^C (T^C) are the algebra generators of SU(3) in the anti/fundamental (adjoint) representation satisfying the following relations:

$$[t^a, t^b] = if^{abc} t^c, \quad [T^A, T^B] = if^{ABC} T^C, \quad T^A \equiv (T^A)_{BC} = -if^{ABC} \quad (2.4)$$

²quadratic at most in the fields in the free Lagrangian and quartic at most in the interaction Lagrangian term.

³From now onward, Lagrangian always refers to Lagrangian density.

⁴Here, N_f denotes all six quark flavours whereas n_f is for light active quark flavours.

where f^{abc} are the structure constants of SU(3) group, which are anti-symmetric in every pair of the three indices and the non-zero ones [47] (and also others related by permutations) are as follows:

$$f^{123} = 1, \quad f^{147} = f^{165} = f^{246} = f^{257} = f^{345} = f^{376} = 1/2, \quad f^{458} = f^{678} = \sqrt{3}/2. \quad (2.5)$$

A possible representation for the generators t^A is given in terms of a set of eight 3×3 traceless and hermitian matrices called Gell-Mann matrices λ^A :

$$t^A = \frac{1}{2}\lambda^A. \quad (2.6)$$

The exact form of λ^A is given in standard QCD textbooks, e.g. [78, 91], while those of T^A are inferred from the third equality of equation(2.4), the SU(3) generators are normalized such that:

$$\text{Tr}[T_R^A T_R^B] = T(R)\delta^{AB} \quad (2.7)$$

where R denotes the representation, $T(R)$ is a trace normalization constant (Dynkin index for the representation R). In SU(3) these become:

$$T(F) \equiv T_F = \frac{1}{2}, \quad T(A) \equiv T_A = 2N_c T_F = 3, \quad (2.8)$$

where $N_c = 3$ is the number of quark colors, and the factor T_F is defined by convention ($T_F = 1/2$ corresponds to Gell-Mann convention) and we further have:

$$(T^a T^a)_{mn} = C(R)\delta_{mn}, \quad m, n = 1, \dots, \dim(R). \quad (2.9)$$

$C(R)$ is known as the Casimir invariant in the representation R . These are operators that commute with all generators of the group, for the case of SU(3) they are given by:

$$C(F) \equiv C_F = \frac{N_c^2 - 1}{2N_c} \stackrel{N_c=3}{=} \frac{4}{3}, \quad C(A) \equiv C_A = N_c \stackrel{N_c=3}{=} 3. \quad (2.10)$$

These color factors (C_F, C_A and T_F) play a central role in QCD, and are associated with the emission of a gluon off a quark, a gluon emission from a gluon and a gluon splitting into a quark-antiquark pair respectively. They also indicate the number of ways that color can flow in Feynman diagrams. Their values indicate that gluons interact and radiate more than a quark even in the large N_c limit. Measurements done at several experiments over wide range of jet/event shape variables found the direct values and ratios to be in agreement with SU(3) predictions. The average over all measurements for C_F and C_A is [108, 109]:

$$C_F = 1.30 \pm 0.09, \quad \text{and} \quad C_A = 2.89 \pm 0.21. \quad (2.11)$$

- \mathcal{L}_{YM} is the Yang-Mills (or gauge) term and is given by:

$$\begin{aligned} \mathcal{L}_{YM} &= -\frac{1}{4} F_{\mu\nu}^a F^{a\mu\nu} \\ &= -\frac{1}{4} (\partial_\mu \mathcal{A}_\nu^a - \partial_\nu \mathcal{A}_\mu^a - g_s f_{abc} \mathcal{A}_\mu^b \mathcal{A}_\nu^c) (\partial^\mu \mathcal{A}^{a\nu} - \partial^\nu \mathcal{A}^{a\mu} - g_s f_{abc} \mathcal{A}^{b\mu} \mathcal{A}^{c\nu}), \end{aligned} \quad (2.12)$$

which describes the dynamics of the gauge field \mathcal{A}_μ^a introduced in the definition of the covariant derivative (equation (2.2)). $F_{\mu\nu}^a$ is the non-abelian field strength tensor and included in its expression is the self-interactions among the gauge fields \mathcal{A}_μ^a themselves ($-g_s$ term). This term which is absent in the abelian case is what gives a triple and quartic gluon vertices.

The combined \mathcal{L}_{Dirac} and \mathcal{L}_{YM} constitute the classical Lagrangian $\mathcal{L}_{Classical}$ which is invariant under the *simultaneous* local SU(3) gauge transformations of the fields in a way such that:

$$\psi \longrightarrow \psi' = U\psi \quad (2.13)$$

$$\mathcal{A} \longrightarrow \mathcal{A}'_\mu = U\mathcal{A}_\mu U^\dagger + \frac{i}{g_s} (\partial_\mu U) U^\dagger, \quad (2.14)$$

where

$$U(x) = \exp(i\theta^a(x) T^a). \quad (2.15)$$

- \mathcal{L}_{GF} gauge-fixing term, introduced to properly quantize the gauge field. It serves the purpose of eliminating the redundant gauge configurations (gauge copies) which are related to each other by a simple gauge transformation (lie on the same gauge orbit) by imposing a constraint on the gauge field in the form of a Lagrange multiplier term. Several choices for such gauge-dependent term can be used, e.g., Coulomb (radiation) gauge $\vec{\nabla} \cdot \vec{\mathbf{A}}^a = 0$, axial gauge $A_3^a = 0$ and temporal gauge $A_0^a = 0$. A popular choice for its manifest relativistic invariance is the Lorenz gauge $\partial_\mu \mathcal{A}^{a\mu} = 0$, and in this particular choice, the gauge-fixing term is written as follows:

$$\mathcal{L}_{GF} = -\frac{1}{2\xi}(\partial_\mu \mathcal{A}^{a\mu})^2 \quad (2.16)$$

where ξ is the gauge parameter [127] ($\xi = 0, 1, 3$ for Landau, Feynman, Yennie gauges respectively). However, a price to pay depending on the choice made, is more/less complex calculations of physical quantities (e.g., S-matrix elements) as well as dis/appearance of non-physical particles in the theory (ghosts).

- \mathcal{L}_{FP} Depending on the choice of the gauge discussed above, one can have additional longitudinal and a scalar (time-like) polarizations on top of the gluon's two physical transverse ones. This can be easily seen by expressing the gluon propagator as a weighted sum of a direct product of its polarization vector states $\epsilon^\mu(p)$. These non-physical spurious components can not only propagate but also interact with the physical parts [91] and contribute to gluon loop diagrams. A remedy for this issue in non-abelian gauge theories is the introduction of a non-physical field (that can only appear as an intermediate state between physical external states) which behaves oppositely to the non-physical gluon states thus canceling their contribution, and one is left only with the physical states of the gluon field and is able to obtain correct physical results. This new field is known as the Faddeev-Popov ghost field⁵ and is most conveniently derived in path integral formalism. These are a complex scalar fields which obey Fermi-Dirac statistics thus represented by Grassmannian variables and contribute with a minus sign in loop diagrams.

⁵In fact, there are as many ghosts as gauge fields.

The ghost field Lagrangian is written in terms of the ghost fields η as:

$$\begin{aligned}\mathcal{L}_{FP} &= \partial_\mu \eta^{a\dagger} D_{ab}^\mu \eta^b \\ &= \partial_\mu \eta^{a\dagger} (\partial^\mu \delta_{ab} + g_s f_{abc} \mathcal{A}^{c\mu}) \eta^b.\end{aligned}\tag{2.17}$$

We thus, for the sake of completeness, rewrite the complete QCD Lagrangian (equation (2.1)) in detail as:

$$\begin{aligned}\mathcal{L}_{QCD} &= \sum_q \bar{\psi}_q^a (i\gamma^\mu (\partial_\mu \delta_{ab} + i g_s t_{ab}^C \mathcal{A}_\mu^C) - m_q \delta_{ab}) \psi_q^b - \frac{1}{4} (\partial_\mu \mathcal{A}_\nu^a - \partial_\nu \mathcal{A}_\mu^a - g_s f_{abc} \mathcal{A}_\mu^b \mathcal{A}_\nu^c)^2 \\ &\quad - \frac{1}{2\xi} (\partial_\mu \mathcal{A}^{a\mu})^2 + \partial_\mu \eta^{a\dagger} (\partial^\mu \delta_{ab} + g_s f_{abc} \mathcal{A}^{c\mu}) \eta^b.\end{aligned}\tag{2.18}$$

Now we can from this expression extract the Feynman rules and build our theory as we shall see in the next section.

2.2 Feynman rules

From the Lagrangian expression (equation (2.18)), we can extract the Feynman rules which are the main ingredient for performing senseful/useful predictions of physical processes.

The standard procedure for this, is that we first separate the Lagrangian into a free and an interaction part. The free (kinetic) part is constructed with terms bilinear in the fields and serves to determine the dynamics of the field through the definition of its corresponding propagator. This term for the quark, gluon and ghost field is given by:

$$\mathcal{L}_{0,Dirac} = \sum_q \bar{\psi}_q^a [(i \not{\partial} - m_q) \delta_{ab}] \psi_q^b,\tag{2.19a}$$

$$\begin{aligned}\mathcal{L}_{0,YM} &= -\frac{1}{4} (\partial_\mu \mathcal{A}_\nu^a - \partial_\nu \mathcal{A}_\mu^a) (\partial^\mu \mathcal{A}^{a\nu} - \partial^\nu \mathcal{A}^{a\mu}) - \frac{1}{2\xi} (\partial_\mu \mathcal{A}^{a\mu})^2 \\ &= \frac{1}{2} \mathcal{A}_\mu^a \left[\left(\eta^{\mu\nu} \partial_\mu \partial^\mu - \left(1 - \frac{1}{\xi} \right) \partial^\mu \partial^\nu \right) \delta_{ab} \right] \mathcal{A}_\nu^b,\end{aligned}\tag{2.19b}$$

$$\mathcal{L}_{0,FP} = \eta^{a\dagger} [\partial_\mu \partial^\mu \delta_{ab}] \eta^b.\tag{2.19c}$$

The “0” subscript denotes “free” fields and by making a Fourier transformation from coordinate space into momentum space, the propagator’s algebraic form is obtained by inverting the square bracketed differential operator (times i).

The interaction part is formed by all terms multiplied by g_s , from which the interaction vertices can be read off directly. All Feynman rules are illustrated in table 2.2. One thing to notice is the form in which the gluon propagator is written in, known as the generalized renormalizable R_ξ -gauge. This choice makes a good check of results in other gauges as well as for checking that the physics does not depend on whether we assign a value to the parameter ξ or leave it unspecified.

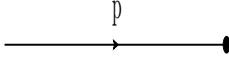
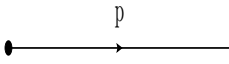
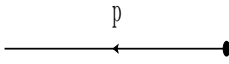
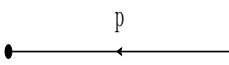
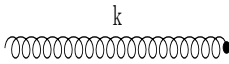
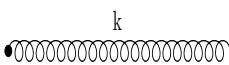
Name	Diagram	Rule
External legs		incoming quark: $u_i(p, s)$
		outgoing quark: $\bar{u}_i(p, s)$
		incoming anti-quark: $\bar{v}_j(p, s)$
		outgoing anti-quark: $v_j(p, s)$
		incoming gluon: $\epsilon_\mu^c(k, \lambda)$
		outgoing gluon: $\epsilon_\mu^{*c}(k, \lambda)$

Table 2.1: QCD Feynman rules for external lines, quarks are represented by straight lines, gluons by curly lines, ghosts are unphysical thus do not appear as an external leg. $k(p)$ are the momenta of the gluon (quark or anti-quark) respectively, i, j, c are the color indices of the quark, anti-quark and the gluon respectively, while s, λ are their spin/polarization states in the same order.

Name	Diagram	Rule
Propagators		$\frac{i}{(\not{p}-m+i\epsilon)_{\mu\nu}}\delta_{ij}$
		$-\frac{i}{(k^2+i\epsilon)}\left(\eta^{\mu\nu} - (1-\xi)\frac{k^\mu k^\nu}{k^2}\right)\delta_{ab}$
		$\frac{i}{p^2+i\epsilon}\delta_{ab}$
Vertices		$g_s(\gamma^\rho)_{\mu\nu}(t^c)_{ji}$
		$-g_s f_{abc}(p')^\rho$
		$-ig_s f_{cde} \begin{cases} +\eta^{\mu\nu}(k_1 - k_2)^\rho \\ +\eta^{\nu\rho}(k_2 - k_3)^\mu \\ +\eta^{\rho\mu}(k_3 - k_1)^\nu \end{cases}$
		$g_s^2 \begin{cases} +f_{gcd}f_{gef}(\eta^{\mu\rho}\eta^{\nu\gamma} - \eta^{\mu\gamma}\eta^{\nu\rho}) \\ +f_{gce}f_{gdf}(\eta^{\mu\nu}\eta^{\rho\gamma} - \eta^{\mu\gamma}\eta^{\nu\rho}) \\ +f_{gcf}f_{gde}(\eta^{\mu\nu}\eta^{\rho\gamma} - \eta^{\mu\rho}\eta^{\nu\gamma}) \end{cases}$

Table 2.2: QCD Feynman rules, quarks are represented by straight lines, gluons by curly lines and the massless Faddeev-Popov ghosts by dotted lines.

2.3 Radiative corrections

The Feynman rules that we obtained in the last section are all one needs for making predictions in QFTs. This is in hindsight true for simple tree-level scattering processes. However, once we try and calculate diagrams with loops, things do not go so well due to the theory being plagued with divergences. The latter appear in the evaluation of unconstrained loop integrands in the very high momenta (short wavelength) limit (hence the name ultraviolet or UV divergences) or in the

very low (long wavelength) limit (infrared or IR divergences for *massless* theories). This issue puzzled the theorists at the time for years until a solution came into existence in the form of two procedures: *regularization* and *renormalization*. These two procedures are of great importance since as it turns out, the full knowledge of a gauge theory is not only about its Lagrangian but also about the regularization and renormalization schemes used on top of it, as ideally one would prefer to work with schemes that try and preserve as much symmetries of the Lagrangian as one can.

2.3.1 Regularization

As an example for the need of these procedures is when one attempts to calculate radiative corrections to Green functions, let us consider the quark self energy diagram, one can see by a simple naive power counting that the integrand in question diverges linearly:

$$\begin{aligned}
 i\Sigma(p) &= \text{---}\overrightarrow{\text{---}}\overbrace{\text{---}\overrightarrow{\text{---}}}^k\text{---}\overrightarrow{\text{---}} \\
 &= -g_s^2 C_F \int \frac{d^4k}{(2\pi)^4} \frac{\gamma_\mu (\not{p} - \not{k} + m) \gamma_\nu}{((p-k)^2 - m^2 + i\epsilon)} \frac{1}{i(k^2 + i\epsilon)} \left(\eta^{\mu\nu} - (1-\xi) \frac{k^\mu k^\nu}{k^2} \right) \delta_{ab} \\
 &\sim d^4k \frac{k}{k^2 k^2} \\
 &\sim \lim_{k \rightarrow \infty} k
 \end{aligned} \tag{2.20}$$

The treatment for such divergences comes in two steps, firstly we try and regulate the integrands in a way that they become mathematically well-defined and manageable. This calls for the use of some sort of a regulator. This step is therefore called regularization. Second, cancellation of the divergences by absorbing divergent terms into redefinitions of theory parameters (couplings, masses, wave function normalization) in such a way that the divergences that arise from original Lagrangian and the new terms cancel between each other order by order and one is left with finite matrix elements provided that these new terms have the same structure as the original.

Let us begin with regulating the integral (equation (2.20)). For that we need to make a choice on the regularization scheme. A few choices worth mentioning are: (a) Pauli-Villars regulator,

which consists of changing the form of the propagator in a way to make it converge faster in the UV limit, (b) analytic regulator, which modifies the power of the propagator's denominator into z where $\Re(z)$ is large enough to ensure convergence when the physical limit $z = 1$ is taken, and (c) higher covariant derivative method which is implemented in two steps, firstly inserting higher covariant derivatives in the Lagrangian and secondly regularizing the theory using a modified Pauli-Villars procedure.

The currently most preferred among all is *dimensional regularization*, based on the idea that 4 dimensional divergent integrals can be made finite⁶ if evaluated at complex $d = 4 - 2\varepsilon < 4$ by means of analytic continuation. This is the standard scheme in many gauge theories for its many advantages [105], preservation of all theory symmetries⁷ (gauge invariance, unitarity, Poincaré invariance), ease of isolation/exposure of divergent parts as they manifest themselves as poles in $1/\varepsilon^n$ when expanded in a Laurent series around $\varepsilon = 0$ with $n = 1, 2, \dots$, the possibility to consistently regulate both IR divergences for $\varepsilon < 0$ as well as UV ones for $\varepsilon > 0$. However, this procedure does come with some inconveniences related to the delicate definition of certain tensors in complex spacetime dimensions (e.g Levi-Civita totally anti-symmetric tensor $\epsilon_{\alpha\beta\gamma\delta}$, Dirac γ^5 matrix) but luckily for us here, those only matter when one delves into the EW sector and considers QCD corrections there.

A consequence of going to d dimensions is that the initially dimensionless coupling constant g_s , now has to carry mass dimension as required by the dimensionlessness of the action. By keeping the coupling without mass dimension, we introduce a scale μ called renormalization scale such that $g_s \rightarrow g_s \mu^\varepsilon$ where $\varepsilon = 2 - D/2$. Furthermore, Dirac γ matrices algebra need to be generalized for arbitrary number of dimensions.

2.3.2 Renormalization

Having decided to use dimensional regularization as a regulator, one needs to perform a check on the renormalizability of the theory before committing to any explicit loop calculation. By using

⁶Just like in equation (2.20), if $d < 3$ then the integral is rendered finite.

⁷This is very important since powerful theorems link a theory's renormalizability to its gauge symmetry.

the expression of index of divergence:

$$r = \frac{d-2}{2}b + \frac{d-1}{2}f + \delta - d, \quad (2.21)$$

for which a theory is said to be renormalizable if $r \leq 0$ and non-renormalizable for $r > 0$. b, f, δ are respectively the number of gauge, fermion fields and spacetime derivatives in \mathcal{L}_I . The interaction part of \mathcal{L}_{QCD} contains 4 fundamental interactions: quark-gluon, ghost-gluon, triple and quartic gluon vertices, we denote them respectively by $r_{\psi A}, r_{\eta A}, r_{3A}$ and r_{4A} . By applying equation (2.21), we find $r_{\psi A} = r_{\eta A} = r_{3A} = \frac{d-4}{2}$ and $r_{4A} = d - 4$, from which alongside the fact $dim[g_s] = 0$, we deduce the renormalizability of QCD in 4 spacetime dimensions. This fact motivates us to proceed with renormalizing the theory.

We define the new ‘‘renormalized’’ fields, mass and coupling in relation to the old ‘‘bare’’ one by making the following changes:

$$\psi_0 = Z_\psi^{1/2}\psi, \quad \mathcal{A}_0 = Z_A^{1/2}\mathcal{A}, \quad \eta_0 = Z_\eta^{1/2}\eta, \quad m_0 = Z_m m, \quad \xi_0 = Z_A \xi, \quad g_{s0} = Z_g g_s, \quad (2.22)$$

such that our QCD Lagrangian becomes:

$$\begin{aligned} \mathcal{L}_{QCD} &= \mathcal{L}_R + \mathcal{L}_{CT} & (2.23) \\ &= \mathcal{L}_0 + \mathcal{L}_I + \mathcal{L}_{CT}, \\ \mathcal{L}_{CT} &= (Z_2 - 1)\bar{\psi}(i\gamma^\mu\partial_\mu - m)\psi - Z_2(Z_m - 1)\bar{\psi}m\psi - \frac{1}{4}(Z_3 - 1)(\partial_\mu\mathcal{A}_\nu^a - \partial_\nu\mathcal{A}_\mu^a)(\partial^\mu\mathcal{A}^{a\nu} - \partial_\nu\mathcal{A}^{a\mu}) \\ &+ i(\tilde{Z}_3 - 1)\partial^\mu\eta^{a\dagger}\partial_\mu\eta^a + (Z_{1F} - 1)g_s\bar{\psi}\gamma^\mu t_{ij}^a\psi\mathcal{A}_\mu^a - \frac{1}{2}(Z_1 - 1)g_s f_{abc}(\partial_\mu\mathcal{A}_\nu^a - \partial_\nu\mathcal{A}_\mu^a)\mathcal{A}^{b\mu}\mathcal{A}^{c\nu} \\ &- \frac{1}{4}(Z_4 - 1)g_s^2 f_{abe}f_{cde}\mathcal{A}_\mu^a\mathcal{A}_\nu^b\mathcal{A}^{c\mu}\mathcal{A}^{d\nu} - i(\tilde{Z}_1 - 1)g_s f_{abc}(\partial^\mu\eta^{a\dagger})\eta^b\mathcal{A}_\mu^c, \end{aligned} \quad (2.24)$$

with

$$Z_{1F} \equiv Z_g Z_\psi Z_A^{1/2}, \quad Z_1 \equiv Z_g Z_3^{3/2}, \quad \tilde{Z}_1 \equiv Z_g \tilde{Z}_3 Z_A^{1/2}, \quad Z_4 \equiv Z_g^2 Z_A^2, \quad (2.25)$$

\mathcal{L}_0 and \mathcal{L}_I have the same structure and Feynman rules as our original Lagrangian (equation (2.18)) with μ^ε attached with each g_s . The new additional term \mathcal{L}_{CT} which is called *counter*

term Lagrangian and is treated as a perturbation, it has the same divergent structure⁸ as our basic Lagrangian, thus the infinities that arose earlier can be compensated by the corresponding counter terms through suitable definitions of renormalization factors Z , thus the infinities do not affect our measured quantities in physical experiments, and this leads to a strong hint of QCD renormalizability to all orders.

We now report the regularized result [124] of radiative corrections for 2-point Green function in d dimensions and in R_ξ gauge, from which one sees the divergent poles when we take the physical limit $\varepsilon \rightarrow 0^+$.

$$\Sigma^{ij}(p) = \delta_{ij}[(Am - B \not{p}) - (Z_\psi Z_m - 1) + (Z_\psi - 1) \not{p}] + \text{finite terms}, \quad (2.26)$$

with

$$\left. \begin{aligned} A &= -\frac{\alpha_s}{4\pi} C_F \frac{1}{\varepsilon} (3 + \xi) \\ B &= -\frac{\alpha_s}{4\pi} C_F \frac{1}{\varepsilon} \xi \end{aligned} \right\} \Rightarrow \left\{ \begin{aligned} Z_\psi &= 1 + B \\ Z_m &= 1 + A - B \end{aligned} \right. \quad (2.27)$$

Now the exact definition of the Z has some arbitrariness to it, more precisely in the exact treatment of the finite terms, different choices correspond to different schemes. A popular scheme is the *minimal subtraction* or MS scheme which naturally goes hand in hand with dimensional regularization and in it, only the $1/\varepsilon$ pole is subtracted, while the subtraction of the always appearing combination $1/\varepsilon - \gamma_E + \ln[4\pi]$ from the expansion of the gamma functions thus improving a bit the convergence of the perturbative series, defines its modified form, the widely adopted $\overline{\text{MS}}$ scheme [138, 139].

Other corrections to gluon, ghost propagators as well as quark-gluon, ghost-gluon, triple and quartic gluon vertices as well as their corresponding renormalization constants in the MS-like schemes are reported in the literature [73, 124].

One interesting fact is that the strong coupling renormalization constant cannot be directly determined by itself, only through other constants. We can deduce that $Z_g Z_3^{3/2} g_s$, $Z_g^2 Z_3^2 g_s$, $Z_g \tilde{Z}_3 Z_3^{1/2} g_s$ and $Z_g Z_2^{3/2} Z_3^{1/2} g_s$ are all related to each other by the BRS invariance leading to Slavnov-Taylor identities (A generalization of Ward-Takahashi identities to the non abelian case) and we therefore

⁸This can be seen by solving $d = 4 - N_B - \frac{3}{2}(N_F + N_{FP}) \geq 0$, from which we find 7 divergent integrals corresponding to diagrams similar to those of QCD vertices.

have four independent but equivalent ways to determine Z_g , usually the least tedious path is by using the ghost-gluon vertex correction

$$\frac{Z_1}{Z_3} = \frac{\tilde{Z}_1}{\tilde{Z}_3} = \frac{Z_{1F}}{Z_2} = \frac{Z_4}{Z_1} = Z_g, \quad (2.28)$$

thus guaranteeing the universality of the renormalized coupling constant g_s across all interactions.

2.3.3 Renormalization group

We have seen in the previous section that we have the freedom of how we attempt regularizing the theory, guided only by the thought of preserving as much symmetries as possible and not only that but also in choosing how much subtraction of the finite terms is done. There is still however some arbitrariness present in this procedure, namely the exact selection of the scale μ , as opposed to the on(off)shell scheme where the subtraction takes place at the physical mass (spacelike value of p of the particle subjected to renormalization), the MS-like schemes do not specify a thing at which value of μ should the subtraction occur at.

The requirement that physics should not depend on a particular choice of this scale, i.e exhibits *scaling*. We shall see how this requirement leads to coupling running, mass running, . . . etc.

As a first idea, let us look at the renormalized coupling as a function of the bare one.

$$g_s(\mu) = Z_g^{-1}(\mu)g_{s0}, \quad (2.29a)$$

$$g_s(\mu') = Z_g^{-1}(\mu')g_{s0}, \quad (2.29b)$$

Clearly, the bare coupling have to be equal, we have:

$$g_s(\mu') = \frac{Z_g(\mu)}{Z_g(\mu')}g_s(\mu) \quad (2.30)$$

$$\equiv Z_g(\mu', \mu)g_s(\mu). \quad (2.31)$$

From equation (2.31), we can find that the set⁹ of finite renormalizations $\{Z_g(\mu', \mu), \dots\}$ caused by a change of scale μ possesses the properties of a group, the *renormalization group*, and when

⁹Note however $Z(\mu_i, \mu_j)Z(\mu_k, \mu_l)$ is not in general a group element.

considering an infinitesimal change of scale μ , i.e continuously varying μ , would give a set of differential equations describing the change in Green function with respect to the said variation of μ , thus compensating each other's change and obtaining unique physical predictions. This set of differential equations is called the *renormalization group equations* or *RGEs*.

On a general note, suppose we have a 1PI diagram¹⁰ representing some generic Green function Γ , we write the renormalized Green function in terms of the bare one as usual:

$$\Gamma(\alpha_{s0}, m_0, \xi_0, Q) = Z_\Gamma \Gamma(\mu, \alpha_s, m, \xi, Q), \quad (2.32)$$

with Z_Γ is the appropriate product of renormalization constants corresponding to that particular Green function. For a scattering of n_A gluon, n_ψ quark and n_η ghost external leg, we have:

$$\Gamma(\alpha_{s0}, m_0, \xi_0, Q) = Z^{-\frac{n_A}{2}} Z^{-\frac{n_\psi}{2}} Z^{-\frac{n_\eta}{2}} \Gamma(\mu, \alpha_s, m, \xi, Q), \quad (2.33)$$

where Q is a scale characterized in terms of external momenta p_i . The L.H.S above clearly does not depend on μ , as it should be. Using the chain rule we therefore can write:

$$\begin{aligned} 0 &= \mu \frac{d}{d\mu} \left[Z^{-\frac{n_A}{2}} Z^{-\frac{n_\psi}{2}} Z^{-\frac{n_\eta}{2}} \Gamma(\mu, \alpha_s, m, \xi, Q) \right] \\ &= \left(\mu \frac{\partial}{\partial \mu} + \beta \frac{\partial}{\partial \mu} + m \gamma_m \frac{\partial}{\partial m} + \xi \delta_\xi \frac{\partial}{\partial \xi} - n_A \gamma_A - n_\psi \gamma_\psi - n_\eta \gamma_\eta \right) \Gamma(\mu, \alpha_s, m, \xi, Q), \end{aligned} \quad (2.34)$$

equation (2.34) is known as renormalization group equation. The first term takes into account direct μ dependence while the rest of terms implicit dependence via $\alpha_s(\mu)$, $m(\mu)$ and $\xi(\mu)$. The coefficient functions β , γ_m , δ_ξ , γ_A , γ_ψ and γ_η are the QCD beta function, mass, gauge fixing and the wave function anomalous dimensions for the gluon, quark and ghost fields respectively.

¹⁰Those that can not be disconnected by cutting any single internal line.

2.3.3.1 Strong coupling running

Despite the rich content offered in equation (2.34)¹¹, we turn our focus solely onto the QCD beta function, which accounts for the running of the effective coupling, we have:

$$\begin{aligned}\mu \frac{d\alpha_s(\mu)}{d\mu} &= 2\beta(\alpha_s(\mu)) \\ &= -2\left(\varepsilon\mu + \mu\alpha_s \frac{1}{Z_g(\mu)} \frac{dZ_g(\mu)}{d\mu}\right).\end{aligned}\tag{2.35}$$

Using explicit expression of Z_g expanded as a Laurent series as $Z_g = 1 + \sum_{n \geq 1} \varepsilon^{-n}$, we can write:

$$\mu^2 \frac{d\alpha_s(\mu)}{d\mu^2} \simeq -\alpha_s^2(\beta_0 + \alpha_s\beta_1 + \alpha_s^2\beta_2 + \dots),\tag{2.36}$$

here β_0, β_1, \dots are the one, two, \dots -loop beta function coefficients and are determined up to β_4 , their expression for the first two is given by

$$\beta_0 = \frac{11C_A - 4n_f T_R}{12\pi} \quad \beta_1 = \frac{17C_A^2 - n_f T_R(10C_A + 6C_F)}{24\pi^2},\tag{2.37}$$

where n_f is the number of *active* quark flavors that contribute to the running of α_s ¹², usually taken to be fixed, i.e., $n_f = 5$ for modern day LHC. The positiveness of the beta coefficients together with the minus sign in equation (2.36) lead to concept of *asymptotic freedom* [93, 129], the fact that strong coupling decreases with increasing scale μ therefore quarks behave as quasi-free states when probed inside hadrons. This phenomenon can be traced back to the triple and quartic gluon interaction terms in the Lagrangian, a property that only non-abelian gauge theories have, it is often said that QED is infrared free whereas QCD is asymptotically free.

Equation (2.36) has a solution when solved iteratively, i.e by truncating the series in α_s order

¹¹Another major consequence of the RGE is the running of quark masses, however we will not touch upon it (just like the other terms) since the quarks are considered massless in this thesis.

¹²The question of how many active quark flavours that enter in calculations relies on the quark's mass relative to the physical scale of the problem Q , for certain quark flavour with $m_q^2 \gg Q^2$, their contribution in QCD dynamics can be removed by suitable choice of counterterms, hence they simply decouple from the theory and one only includes those with $m_q^2 \ll Q^2$ [16].

by order at a time, the solution at 1-loop order is found to be:

$$\alpha_s(\mu_R^2) = \frac{1}{\beta_0 \ln(\frac{\mu_R^2}{\Lambda_{QCD}^2})}, \quad (2.38)$$

where Λ_{QCD} is an integration constant corresponding to the fundamental QCD scale, where non-perturbative dynamics dominate (large α_s) and perturbation theory becoming no longer viable¹³ for describing hard processes, its value depends on the renormalization scheme, the order at which the beta function was truncated, n_f , matching scheme for α_s at flavour thresholds, the current value in the $\overline{\text{MS}}$ scheme and using the 4-loop beta function is:

$$\Lambda_{QCD}^{(5FS)} \approx 205 \text{ MeV} \quad (2.39)$$

A more convenient and commonly used expression for equation (2.38) is¹⁴:

$$\alpha_s(Q^2) = \frac{\alpha_s(\mu_R^2)}{1 + 2\alpha_s(\mu_R^2)\beta_0 \ln(\frac{Q}{\mu_R})} \quad (2.40)$$

Thus obtaining α_s at scale Q^2 as a function of its value at some renormalization scale μ_R^2 , provided that both μ_R and Q are well within the perturbative regime i.e., $\Lambda_{QCD} \ll \mu_R, Q$. The current world average for α_s evaluated at Z pole mass and taken from several measurements is [143]:

$$\alpha_s(M_Z^2) = 0.1179 \pm 0.0010 \quad (2.41)$$

2.3.4 IR safety

We have seen that QCD, just as any gauge theory, suffers in the UV limit and that issue is resolved by the procedure of renormalization. However, at the opposite end of the scale, one is again met with divergences resulting from long-wavelength aspect of Feynman rules. To see how these singularities come into play, we consider a simple electron-positron annihilation into hadrons process i.e., $e^+e^- \rightarrow q\bar{q}$, although at heart is a pure EW process and one of the simplest, the

¹³As can be seen from eq (2.37) when $\mu_R = \Lambda_{QCD}$.

¹⁴For a 2-loop expression see appendix A.

following discussion and ideas can be generalized to any other hard process. The leading order (LO) Born cross section reads¹⁵:

$$\sigma_{e^+e^- \rightarrow q\bar{q}}^{(LO)} = \frac{4\pi N_c \alpha_{QED}^2}{3s} \sum_q e_q^2 \quad (2.42)$$

Corrections to this process at next-to-leading-order (NLO) are represented in figure 2.1, where real contributions are represented in the second row and virtual ones in the third row.

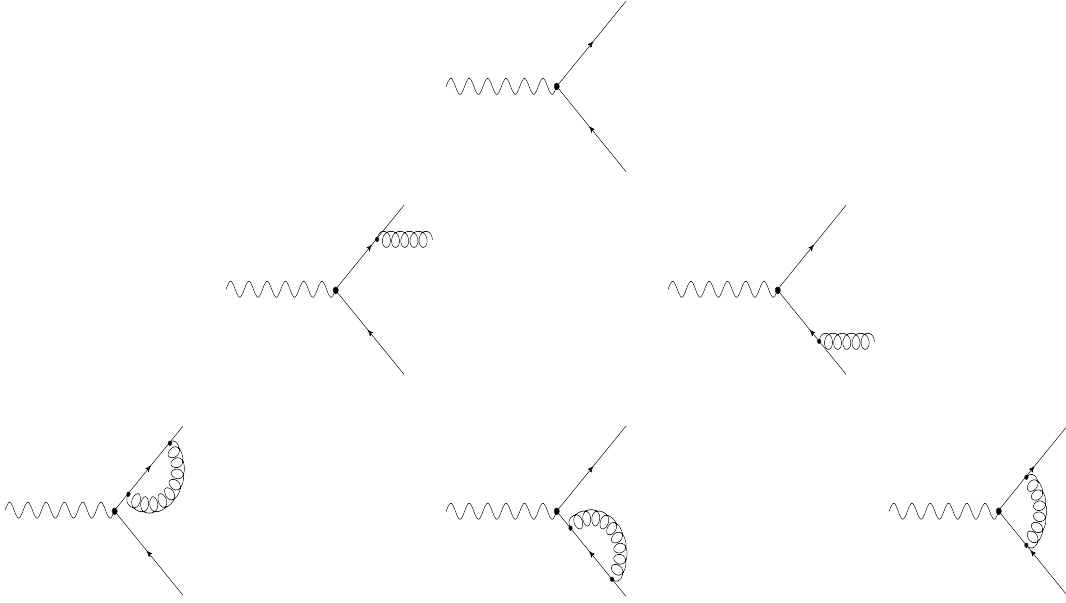


Figure 2.1: Diagrams that contribute to the total (inclusive) cross section of the process $e^+e^- \rightarrow q\bar{q}$

The total (inclusive) cross section for this process becomes:

$$\begin{aligned} \sigma_{total}^{(NLO)} &= \sigma_B + \sigma_R + \sigma_V \\ &= \int d\Phi_0 |\mathcal{M}_B|^2 + \int d\Phi_k |\mathcal{M}_R|^2 + 2 \int d\Phi_0 \Re \epsilon |\mathcal{M}_B^* \mathcal{M}_V| \end{aligned} \quad (2.43)$$

¹⁵This expression takes only the γ^* contribution that dominates at low & very high \sqrt{s} , whereas Z^0 and its interference with γ^* that come into play at intermediate energies is neglected, but again this doesn't affect the following discussion.

We start with real emission diagram (second row of figure 2.1), we have:

$$\begin{aligned}
i\mathcal{M}_R &= \bar{u}_s^i(p_a)[ig_s\gamma^\mu t_{ij}^c]\frac{\not{p}_a + \not{k} + m}{(p_a + k)^2 - m^2 + i\varepsilon}B^\nu v_{s'}^j(p_b)\epsilon_\mu^{*c}(k, \lambda) \\
&+ \bar{u}_s^i(p_a)B^\nu\frac{\not{p}_b + \not{k} + m}{(p_b + k)^2 - m^2 + i\varepsilon}[ig_s\gamma^\mu t_{ij}^c]v_{s'}^j(p_b)\epsilon_\mu^{*c}(k, \lambda),
\end{aligned} \tag{2.44}$$

where B^ν the incoming particles and their QED vertex which again for the purpose of this discussion are irrelevant, the other terms are Feynman rules found in tables 2.2 and 2.1. Using γ matrices algebra and Dirac equation in spinor space, i.e the following relations:

$$\gamma_\mu \not{p}_a = -\not{p}_a \gamma_\mu + 2p_{a\mu}, \tag{2.45}$$

$$\bar{u}(p)(\not{p} + m) = 0, \quad (\not{p} - m)u(p) = 0, \quad \bar{v}(p)(\not{p} - m) = 0, \quad (\not{p} + m)v(p) = 0, \tag{2.46}$$

as well as neglecting any k in front of $p_{a/b}$ in the numerator (this defines the *eikonal* approximation [114]) and using the onshell condition i.e $p_a^2 = p_b^2 = m^2$ and $k^2 = 0$ and Dirac equation satisfied by the spinors u and v , we arrive at:

$$\begin{aligned}
i\mathcal{M}_R &= [ig_s t_{ij}^c][\bar{u}_s^i(p_a)B^\nu v_{s'}^j(p_b)]\left(\frac{p_a^\mu}{p_a \cdot k} - \frac{p_b^\mu}{p_b \cdot k}\right)\epsilon_\mu^{*c}(k, \lambda) \\
&= [ig_s t_{ij}^c]\mathcal{M}_B\left(\frac{p_a^\mu}{p_a \cdot k} - \frac{p_b^\mu}{p_b \cdot k}\right)\epsilon_\mu^{*c}(k, \lambda).
\end{aligned} \tag{2.47}$$

Following similar arguments, we find for $i\mathcal{M}_R^*$:

$$\begin{aligned}
-i\mathcal{M}_R^* &= [ig_s t_{ji}^c][\bar{v}_s^i(p_b)B^\nu u_{s'}^j(p_a)]\left(\frac{p_a^\nu}{p_a \cdot k} - \frac{p_b^\nu}{p_b \cdot k}\right)\epsilon_\nu^c(k, \lambda) \\
&= [ig_s t_{ji}^c]\mathcal{M}_B^*\left(\frac{p_a^\nu}{p_a \cdot k} - \frac{p_b^\nu}{p_b \cdot k}\right)\epsilon_\nu^c(k, \lambda)
\end{aligned} \tag{2.48}$$

Multiplying equation (2.47) with (2.48) and using $\sum_c \epsilon_\mu^c \epsilon_\nu^c = -g_{\mu\nu}$, we have:

$$\begin{aligned}
|\mathcal{M}_R|^2 &= |\mathcal{M}_B|^2 g_s^2 Tr[t_{ij}^c t_{ji}^c] 2 \frac{p_a \cdot p_b}{(p_a \cdot k)(k \cdot p_b)} \\
&= |\mathcal{M}_B|^2 2g_s^2 C_F \frac{p_a \cdot p_b}{(p_a \cdot k)(k \cdot p_b)}.
\end{aligned} \tag{2.49}$$

Using Fermis's golden rule, i.e multiplying equation (2.49) by flux factors & Lorentz invariant phase space for outgoing particles, we obtain the differential cross section for one gluon emission off of the outgoing quark-antiquark pair:

$$\begin{aligned}
d\sigma_R &= \frac{1}{2E_A 2E_B |\vec{v}_A - \vec{v}_B|} (2\pi)^4 \delta^{(4)}(p_{e^+} + p_{e^-} - p_a - p_b) 2g_s^2 C_F \frac{p_a \cdot p_b}{(p_a \cdot k)(k \cdot p_b)} \frac{d^3 \vec{k}}{(2\pi)^3 2\omega_k} \\
&\times |\mathcal{M}_B|^2 \frac{d^3 \vec{p}_a}{(2\pi)^3 2E_a} \frac{d^3 \vec{p}_b}{(2\pi)^3 2E_b} \\
&= \sigma_B 2g_s^2 C_F \frac{p_a \cdot p_b}{(p_a \cdot k)(k \cdot p_b)} \int \frac{d^3 \vec{k}}{(2\pi)^3 2\omega_k}
\end{aligned} \tag{2.50}$$

Taking the outgoing momenta to be:

$$p_a = \frac{Q}{2}(1, 0, 0, 1), \quad p_b = \frac{Q}{2}(1, 0, 0, -1), \quad k = \omega_k(1, \sin(\theta) \cos(\phi), \sin(\theta) \sin(\phi), \cos(\theta)), \tag{2.51}$$

we find:

$$\begin{aligned}
\frac{d\sigma_R}{\sigma_B} &= 2g_s^2 C_F \frac{2}{\omega_k^2 \sin^2(\theta)} \frac{\omega_k^2 d\omega_k \sin(\theta) d\theta d\phi}{(2\pi)^3 2\omega_k} \\
&= 2C_F \frac{g_s^2}{4\pi^2} \frac{d\omega_k}{\omega_k} \frac{d\theta}{\sin(\theta)} \frac{d\phi}{2\pi},
\end{aligned} \tag{2.52}$$

a result which is clearly logarithmically divergent in the soft (i.e $\omega_k \rightarrow 0$) and/or collinear (i.e $\theta \rightarrow 0, \pi$) limits. However this is not the end of the story at this order, as there are still contributions from the virtual diagrams that we shall compute.

The virtual piece is composed of 3 diagrams (third row of figure 2.1), however the first 2 virtual diagrams are zero in the eikonal limit since they go like $\sim p_a^2 = p_b^2 = 0$ and therefore only the third one contributes giving¹⁶:

$$\begin{aligned}
i\mathcal{M}_V &= \int \frac{d^4 k}{(2\pi)^4} \bar{u}_s^i(p_a) [ig_s \gamma^\mu t_{ij}^c] \frac{\not{p}_a + \not{k} + m}{(p_a + k)^2 - m^2 + i\varepsilon} B^\nu \frac{-\not{p}_b - \not{k} + m}{(p_b - k)^2 - m^2 + i\varepsilon} \\
&\times \frac{-i\eta_{\mu\nu} \delta^{cc'}}{k^2 + i\varepsilon} [ig_s \gamma^\mu t_{jk}^{c'}] v_{s'}^k(p_b)
\end{aligned} \tag{2.53}$$

¹⁶In the full correction, the UV singularities of the aforementioned diagrams cancel exactly with that of the third virtual diagram such that no renormalization is required while in the IR regime, the contribution of the first two virtual diagrams is zero in the DR scheme.

following the same manner of calculating \mathcal{M}_R we find:

$$\begin{aligned}
i\mathcal{M}_V &= \int \frac{d^4k}{(2\pi)^4} \bar{u}_s^i(p_a) [ig_s \gamma^\mu t_{ij}^c] \frac{\not{p}_a + \not{k} + m}{(p_a + k)^2 - m^2 + i\varepsilon} B^\nu \frac{-\not{p}_b - \not{k} + m}{(p_b - k)^2 - m^2 + i\varepsilon} \\
&\times \frac{-i\eta_{\mu\nu} \delta^{cc'}}{k^2 + i\varepsilon} [ig_s \gamma^\nu t_{jk}^{c'}] v_{s'}^k(p_b) \\
&= ig_s^2 C_F \int \frac{d^4k}{(2\pi)^4} \bar{u}_s^i(p_a) \frac{2p_a^\mu}{(p_a + k)^2 - m^2 + i\varepsilon} B^\nu \frac{2p_{b\mu}}{(p_b - k)^2 - m^2 + i\varepsilon} \frac{1}{k^2 + i\varepsilon} v_{s'}^k(p_b) \\
&= 4ig_s^2 C_F \mathcal{M}_B \int \frac{d^4k}{(2\pi)^4} \frac{p_a \cdot p_b}{[2p_a \cdot k + k^2 + i\varepsilon][-2p_b \cdot k + k^2 + i\varepsilon][k^2 + i\varepsilon]} \\
&= -ig_s^2 C_F \mathcal{M}_B \int \frac{d^4k}{(2\pi)^4} \frac{p_a \cdot p_b}{[p_a \cdot k + i\varepsilon][p_b \cdot k - i\varepsilon][k^2 + i\varepsilon]} \\
&= -ig_s^2 C_F \mathcal{M}_B \int \frac{d^3\vec{k}}{(2\pi)^3 2k_0} \int_{-\infty}^{\infty} \frac{dk_0}{2\pi} \frac{1}{[k_0 - |\vec{k}| + i\varepsilon][k_0 + |\vec{k}| - i\varepsilon]} \\
&\times \frac{p_a \cdot p_b}{[k_0 \cdot p_{a0} - \vec{k} \cdot \vec{p}_a + i\varepsilon][k_0 \cdot p_{b0} - \vec{k} \cdot \vec{p}_b - i\varepsilon]}
\end{aligned} \tag{2.54}$$

Performing the integral above using the residue theorem¹⁷ and choosing the integration contour to enclose the upper half of the complex plane in an anti clock wise direction, thus encompassing two out of the four poles, one coming from the gluon approaching its mass-shell i.e $k^2 \rightarrow 0$ and the second is attributed to the internal (anti)quark also satisfying its on-shell condition, the latter contributes with a pure imaginary phase dubbed “*Coulomb* or *Glauber*” phase.

We therefore find:

$$\begin{aligned}
i\mathcal{M}_V &= -ig_s^2 C_F \mathcal{M}_B \int \frac{d^3\vec{k}}{(2\pi)^3} \frac{-1}{2|\vec{k}|} \frac{1}{2\pi} 2\pi i \frac{p_a \cdot p_b}{(p_a \cdot k)(k \cdot p_b)} + i\pi \int \frac{dk_t}{(2\pi)^2 k_t} \\
&= -g_s^2 C_F \mathcal{M}_B \int \frac{d^3\vec{k}}{(2\pi)^3 2|\vec{k}|} \frac{p_a \cdot p_b}{(p_a \cdot k)(k \cdot p_b)} + i\pi \int \frac{dk_t}{(2\pi)^2 k_t}
\end{aligned} \tag{2.55}$$

Multiplying equation (2.55) with the Born contribution, we find the virtual correction to our

¹⁷A quick recall to residue theorem: for $f(z)$ a regular function with simple poles at z_0 , then the integral of $f(z)$ in a closed contour is given by: $\oint_C f(z) dz = 2\pi i \sum (\text{enclosed residues})$ where the residues are determined by: $\text{residue} = \lim_{z \rightarrow z_0} (z - z_0) f(z)$ where z_0 is a simple pole.

$e^+e^- \rightarrow q\bar{q}$ process at order $\mathcal{O}(\alpha_s)$ to be:

$$\begin{aligned} 2\Re\epsilon|\mathcal{M}_B^*\mathcal{M}_V| &\equiv |\mathcal{M}_B^*\mathcal{M}_V + \mathcal{M}_V^*\mathcal{M}_B| \\ &= -|\mathcal{M}_B|^2 2g_s^2 C_F \int \frac{d\vec{k}}{(2\pi)^3 2\omega_k} \frac{p_a \cdot p_b}{(p_a \cdot k)(k \cdot p_b)} \end{aligned} \quad (2.56)$$

Including the flux factors and Lorentz invariant phase space, we get:

$$d\sigma_V = -\sigma_B 2g_s^2 C_F \int \frac{d\vec{k}}{(2\pi)^3 2\omega_k} \frac{p_a \cdot p_b}{(p_a \cdot k)(k \cdot p_b)} \quad (2.57)$$

Being an interference type of a contribution, the virtual piece can (and in this case does) have an overall minus sign and an identical kinematic structure to that of the real emission component (equation (2.50)), thus it cancels against the result from the real piece leading into a complete cancellation between the real and virtual contributions to the total cross section, i.e in the eikonal approximation, it receives no corrections at $\mathcal{O}(\alpha_s)$. The full and dimensionally regularized real and virtual pieces are reported to be [73]:

$$\sigma_{q\bar{q}(g)} \equiv \sigma_V = \sigma_B C_F \frac{\alpha_s}{2\pi} H(\epsilon) \left(-\frac{2}{\epsilon^2} - \frac{3}{\epsilon} - \frac{16}{2} + \pi^2 + \mathcal{O}(\epsilon) \right) \quad (2.58a)$$

$$\sigma_{q\bar{q}g} \equiv \sigma_R = \sigma_B C_F \frac{\alpha_s}{2\pi} H(\epsilon) \left(+\frac{2}{\epsilon^2} + \frac{3}{\epsilon} + \frac{19}{2} - \pi^2 + \mathcal{O}(\epsilon) \right) \quad (2.58b)$$

Here one can see the single and double poles in ϵ originating from the soft/collinear divergences and their interference/overlap respectively. $H(\epsilon)$ is a finite function when the physical limit (i.e $\epsilon \rightarrow 0$) is taken and the two expressions give when combined:

$$\sigma_{e^+e^- \rightarrow hadrons}^{(NLO)} = \sigma_B \left(1 + \frac{\alpha_s}{\pi} C_F \frac{3}{4} \right), \quad (2.59)$$

which is finite and well behaved in the $\epsilon \rightarrow 0$ limit as should be for all physical observables. Equation (2.59) is known up to α_s^3 with the higher coefficients as functions of μ_R thus effectively demonstrating order by order the Kinoshita [104], Lee & Nauenberg [113] (KLN) theorem, a generalization from Bloch-Nordsiek [38] (BN) theorem to non-abelian gauge theories due to non-abelian features that QCD has. The KLN theorem states that in massless field theories, total

transition rates are free from IR divergences once the summation over initial/final degenerate states (i.e states characterized by the same energy eigenvalue) has been carried out.

The cancellation of soft and/or collinear divergences or collectively denoted as IR divergences is backed also from an experimental point of view. An ideal collider detector would be able to resolve arbitrarily soft/collinear emissions in the whole 4π solid angle which in truth is limited to a finite granularity and a limited resolution parameter $\lambda \equiv E_0$. Therefore a quark state alone is no different than a quark with arbitrary number of soft/collinear gluons attached to it, i.e are indistinguishable and with same energy eigenvalue. The above requirements (experimental and theoretical) impose that we perform perturbative calculations with a special kind/type of observables, those that cannot be sensitive to IR emissions or long distance physics as long as one only limits him/herself to two classes of observables [36]:

- Infra Red and Collinear safe observables (IRC) for them to be consistently computable in pQCD to all orders and for the KLN theorem to be applicable, they must satisfy:

$$\mathcal{O}(p_a, p_b, \dots, k_i, \dots) = \mathcal{O}(p_a, p_b, \dots, k_j + k_l, \dots) \quad \text{for } k_i \rightarrow k_j + k_l \ \& \ k_j \parallel k_l \quad (2.60a)$$

$$\mathcal{O}(p_a, p_b, \dots, k_i, \dots) = \mathcal{O}(p_a, p_b, \dots, k_{i-1}, k_{i+1}, \dots) \quad \text{for } k_i \text{ vanishingly soft.} \quad (2.60b)$$

- Factorizable quantities where where any IR sensitivity can be pulled/factorized and absorbed by some non-perturbative factor.

It is worth mentioning that for fully or sufficiently inclusive observables, the cancellation is complete but for other less inclusive observables (e.g. those where real emission required to be above some resolution threshold λ or defined in a limited phase space region), the cancellation between real and virtual diagrams is incomplete. This miscancellation is manifested by the appearance of large logarithms with disparate scales (or with dimensionless quantity such as our observable $\delta\phi$) as an argument. These logarithm enhancements (e.g. $\ln(Q/\lambda)$) although finite, can compensate the smallness of α_s and potentially spoil the perturbative series convergence and going to higher orders would not improve the situation since in fact, these logarithmic structures persist to all orders and depending on the observable under study, each power of α_s can be accompanied by up to two powers of these logarithms (i.e $\alpha_s^n L^{2n}$ where L is the large logarithm). This calls for the use of

procedure to reshuffle the troubling terms according to their severity to all orders either by some evolution equation¹⁸ or some analytical technique. This procedure is known as *resummation*.

2.4 Factorization

At particle colliders,¹⁹ whether they were e^+e^- such as LEP or pp like LHC or Tevatron, we observe after each collision bunches of colorless hadrons, i.e states which are far different in terms of what our initial Lagrangian & Feynman rules describe the underlying high energy collisions with. So it seems that we have no predictive power but it proves useful to consider the interaction of elementary quantas from an uncertainty point of view. The physical picture of hard scattering is that it is characterized by a large momentum scale Q that is transferred between elementary quantas, which by Heisenberg's uncertainty principle corresponds to a timescale (or equivalently distance) of order $\sim 1/Q$. The formation of hadrons (by a non-perturbative process called *hadronization*) takes place at a much longer time $\sim 1/\Lambda_{QCD}$ that it cannot alter the probability of the hard process in any way, only leading at most to corrections of the form $\sim \mathcal{O}\left(\left(\frac{\Lambda_{QCD}}{Q}\right)^n\right)$, thus the process can be factorized into a short distance interaction where PT can be safely applied for large enough value of Q , and a long distance process where non-perturbative effects are modeled experimentally.

The picture discussed above is easily seen to be valid only in the simpler e^+e^- environment and neglects the fact that at ep or pp colliders, the incoming beams are made of composite objects; the proton, so how does one account for internal hadron structure?

The answer comes from ideas developed in the parton model [37, 80] for deeply inelastic scattering processes or DIS, where an electron scatters off a nucleus or a nucleon (usually a proton) by emitting a highly virtual photon with a virtuality $Q^2 = -q^2$. In the center of mass (or infinite momentum frame, i.e Breit where all masses and transverse momenta are ignored) frame, the proton is Lorentz contracted along its travel axis (e.g. z -axis) and the lifetime of its constituents (i.e partons) as well as their interactions are time dilated. For the virtual photon with longitudinal momentum $q_z = 2x_B P_z$ (x_B is Bjorken- x variable and P_z is the proton's longitudinal momentum) to interact with a parton from the proton, their (longitudinal) wavelengths must be on the same

¹⁸Examples of such equations: DGLAP [74, 92, 11], BMS [26], ...

¹⁹The discussion in this section is based on that found in [44, 123].

order ($\lambda_z^{\gamma^*} \sim \lambda_z^p \sim 1/q_z$) and that the lifetime of the parton must be much longer than the time it takes for the photon to cross the contracted proton ($\tau_{parton} \sim p_z/p_t^2 \gg \tau_{\gamma^*} \sim 1/q_z$), therefore we can consider that the proton is a definite state (i.e no occurring quantum fluctuations) with definite number of quasi-free partons, each carrying a fraction of the proton's momentum (i.e $p_z = xP_z$ with x satisfying $0 < x < 1$). The assumptions above put kinematical constraints on x , thus the photon is effectively probing for partons inside the proton with such kinematics (i.e $x \sim x_B$ at a scale $Q^2 \sim -q^2$ in a surface $\sim 1/Q^2$), therefore this whole process must be proportional to some sort of a function describing the probability to find such partons, we refer to them as *parton distribution functions* or PDFs.

The PDFs are to a first approximation, regarded as functions of x only and since they involve interaction of almost free quantas, they are considered *universal*, in the sense that when extracted from data in a certain process, they can be systematically used in another process.

The whole picture above and the assumptions behind it form the basis of what is known as *collinear factorization* theorem [61, 123]. Although it was first formulated initially for DIS, it was later pointed firstly by Drell & Yan that the same ideas can be systematically extended to pp processes (eg DY process for lepton pair production [77]), this fact along side the non-interference between long and short distance (i.e effects that occur long before or after the hard scattering) mentioned before enables us to write apart from some flux factors and power-suppressed corrections:

$$\sigma_{AB \rightarrow X} \sim \sum_{a,b} \int dx_a dx_b f_{a/A}(x_a) f_{b/B}(x_b) \hat{\sigma}_{ab \rightarrow X}(\mu_R^2, \alpha_s(\mu_R^2), Q^2) \quad (2.61)$$

This is what is referred to as the *naive parton model formula* where $\sigma_{AB \rightarrow X}$ is the cross-section for hadronic production of X which denotes anything allowed by conservation laws. x_a is the momentum fraction carried by parton a with respect to its mother hadron A . $f_{a/A}(x_a)$ denotes PDF, which at LO has a probabilistic interpretation as the probability to find a parton a with momentum fraction x_a inside its mother hadron A . $\hat{\sigma}_{ab \rightarrow X}$ is the perturbatively computed partonic cross-section, initiated by partons a and b from hadrons A and B respectively. $\hat{\sigma}_{ab \rightarrow X}$ is computable in PT as a series in α_s and where each order coefficient is parameterized in terms of renormalization scale μ_R and external momenta (through Q^2).

It is worth mentioning that renormalizability is not taken for granted for all field theories (e.g.,

Fermi's theory for weak interactions is a prime example for a non-renormalizable theory) but it has been proven for gauge theories to all orders (for QCD case by t' Hooft & Veltmann [139]), however factorization is only proven to all orders in DIS and order by order in DY (even the proofs for these cases are highly non-trivial). For other processes, only their success at making correct predictions is accounted for instead of a justified mathematical proof.²⁰

2.4.1 Collinear splittings

The KLN theorem [104, 113] as stated before, ensures the cancellation of IR singularities between real/virtual diagrams, once the summation over all degenerate states is to be carried out. But for singularities coming from initial state radiation, the KLN theorem alone is insufficient, more specifically the collinear singularities survive the cancellation. This divergence reflects the non-perturbative dynamics present in the nucleon's internal structure. But eventually, these are found to be of universal nature, independent from the hard scattering, and therefore can be safely factorized and absorbed into a non-perturbative factor that turns out to be the parton distribution functions. To see the universal structure of these, let us consider a Feynman diagram where an initial massless parton undergoes a splitting before entering into the hard process $\mathcal{M}^{(n)}$. In evaluating the matrix element, one starts with the expression:

$$\mathcal{M}^{(n+1)} = \mathcal{M}^{(n)}_i \frac{\not{p} + \not{k}}{(p-k)^2 + i\epsilon} [ig_s \gamma^\mu t_{ij}^c] u_s^j(p) \epsilon_\mu^*(k, \sigma) \quad (2.62)$$

and arrives at the result²¹:

$$|\overline{\mathcal{M}^{(n+1)}}|^2 = \frac{\alpha_s}{2\pi} \int \frac{dk_t^2}{k_t^2} dz P_{ij}(z) |\mathcal{M}^{(n)}|^2 \quad (2.63)$$

i.e in the collinear approximation, the $(n+1)$ -body process is factorized into a (n) -body process plus a splitting. The collinear singularity is evident from the $1/k_t^2$ factor when $k_t \rightarrow 0$, $P_{ij}(z)$ is the azimuthally averaged Altarelli-Parisi splitting function [11], describing splitting probabilities $j \rightarrow i+k$ that a parent parton j undergoes a splitting into two other (offspring) partons averaged

²⁰As a matter of fact, there has been some effects signaling the possible breakdown of factorization [81].

²¹For more information over the derivation, intermediary steps can be found in the literature, e.g., [116, 131]

(summed) over polarization and spin [75], where parton i retains a momentum fraction z . Due to QCD flavour and charge conjugation symmetry, the number of independent AP splitting functions is reduced to only four:

$$\begin{aligned}
P_{qq} &\equiv P_{uu} = P_{dd} = \dots = P_{\bar{u}\bar{u}} = P_{\bar{d}\bar{d}} = \dots, \\
P_{qg} &\equiv P_{ug} = P_{dg} = \dots = P_{\bar{u}g} = P_{\bar{d}g} = \dots, \\
P_{gq} &\equiv P_{gu} = P_{gd} = \dots = P_{g\bar{u}} = P_{g\bar{d}} = \dots, \\
P_{gg} &.
\end{aligned} \tag{2.64}$$

Momentum conservation at elementary vertices also implies for $z \neq 1$:

$$P_{kj}(z) = P_{ij}(1 - z). \tag{2.65}$$

The splitting functions themselves admit a perturbative expansion in α_s , i.e:

$$P_{ij} = P_{ij}^{(0)} + \left(\frac{\alpha_s}{2\pi}\right) P_{ij}^{(1)} + \left(\frac{\alpha_s}{2\pi}\right)^2 P_{ij}^{(2)} + \left(\frac{\alpha_s}{2\pi}\right)^3 P_{ij}^{(3)} + \dots, \tag{2.66}$$

where the coefficient functions are the LO, NLO, NNLO splitting functions respectively. The state of the art of the power series above is the partial determination of NNNLO splitting function.

The LO splitting function are represented pictorially in figure 2.2 and their expression given by [11]:

$$P_{qq}(z) = C_F \left[\frac{1+z^2}{(1-z)_+} + \frac{3}{2} \delta(1-z) \right], \tag{2.67a}$$

$$P_{qg}(z) = T_R \left[z^2 - (1+z)^2 \right], \tag{2.67b}$$

$$P_{gq}(z) = C_F \left[\frac{z^2 - (1+z)^2}{z} \right], \tag{2.67c}$$

$$P_{gg}(z) = C_A \left[\frac{2z}{(1-z)_+} + 2 \frac{1-z}{z} + 2z(1-z) \right] + \frac{11C_A - 4n_f T_R}{6} \delta(1-z), \tag{2.67d}$$

here, the + subscript denotes the *plus-prescription*, a regulating technique to render $P_{ij}(z)$ finite in the soft gluon emission region $z \rightarrow 1$. Mathematically it is defined in terms of a smooth function

$f(x)$ by:

$$\int_0^1 f(z)[g(z)]_+ dz = \int_0^1 [f(z) - f(1)]g(z) dz \quad (2.68)$$

The $\delta(1-z)$ term present in $P_{qq}(z)$ and $P_{gg}(z)$ contains both Born contribution and virtual gluon emission effects thus regulating the soft divergence $z \rightarrow 1$. The plus-prescription is equivalent to explicit real and virtual diagrams calculation [103].

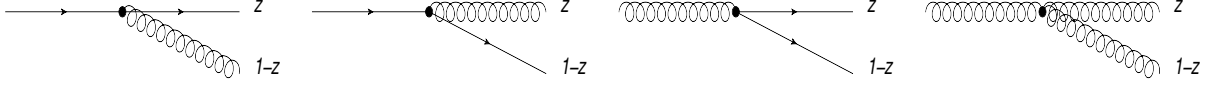


Figure 2.2: The LO Altarelli-Parisi splitting kernels.

2.4.1.1 Divergences factorization in DIS

We stated at the beginning of this section that IR singularities appear also when considering gluon emissions from incoming partons and we also stated that these will be absorbed into a non-perturbative factor. To set the stage for this demonstration, we take the case of hadron-electron deeply inelastic scattering (DIS) $e^\pm(k)h(p) \rightarrow e^\pm(k')X$ via the exchange of a highly virtual photon. The cross section for this process is found to be related to the contraction of two symmetric tensors:

$$d\sigma_{DIS} \sim L_{\mu\nu}W^{\mu\nu}, \quad (2.69)$$

where the cross-section is factored into a leptonic tensor describing the QED vertex and a hadronic tensor describing the interaction of EM current with the hadron target. Their expressions are given by [72]:

$$L_{\mu\nu} = \frac{1}{2}Tr[(\not{k} + m_e)\gamma_\mu(\not{k}' + m_e)\gamma_\nu] = 2(k'_\mu k_\nu + k_\nu k'_\mu - \eta_{\mu\nu}(k \cdot k' - m_e^2)), \quad (2.70a)$$

$$W^{\mu\nu} = \left(-\eta^{\mu\nu} + \frac{q^\mu q^\nu}{q^2}\right)W_1(x, Q^2) + \left(p^\mu + q^\nu \frac{p \cdot q}{Q^2}\right)\left(p^\nu + q^\mu \frac{p \cdot q}{Q^2}\right)W_2(x, Q^2), \quad (2.70b)$$

where the general form of $W^{\mu\nu}$ was deduced from symmetries arguments (Lorentz invariance & current conservation). One usually redefines the real scalar structure functions $W_{1/2}(x, Q^2)$ into

dimensionless ones by:

$$F_1(x, Q^2) \equiv W_1(x, Q^2) \quad F_2(x, Q^2) \equiv p.qW_2(x, Q^2) \quad (2.71)$$

To a first approximation, the structure functions were observed to exhibit “*scaling*”, an independence from Q i.e, $F_{1/2}(x, Q^2) \xrightarrow{Q^2 \gg m_h^2} F_{1/2}(x)$. This behavior can be explained within the parton model as the virtual photon scattering off “point-like” constituents, hence the independence of the resolving power $1/Q$ of the photon.

The doubly differential cross in x and Q is:

$$\frac{d^2\sigma}{dx dQ^2} = \frac{2\pi\alpha^2}{xQ^4} \left([1 + (1-y)^2] F_2(x, Q^2) - y^2 F_L(x, Q^2) \right) \quad (2.72)$$

where the longitudinal structure function related to the scattering of a quark with a longitudinal photon is defined by: $F_L = F_2 - 2xF_1$. The parton model to a leading order predicts $F_2(x) = \sum_i e_i^2 x q_i(x)$ i.e the structure function as a charge weighted sum of parton momentum densities whose sole dependence is on x only, i.e the observed scaling by Bjorken and also $F_L = 0$ thus $F_2 = 2xF_1$ i.e Callan-Gross characteristic relationship to spin 1/2 partons.

Taking NLO corrections in the same manner as was done for e^+e^- annihilation into hadrons, we find for F_2 (for a single quark flavour):

$$F_2(x, Q^2) = xe^2 \int_x^1 \frac{d\xi}{\xi} q(\xi) \left[\delta\left(1 - \frac{x}{\xi}\right) + \frac{\alpha_s}{2\pi} P_{qq}\left(\frac{x}{\xi}\right) \ln\left(\frac{Q^2}{Q_0^2}\right) + C(z) \right] \quad (2.73)$$

where the log term arises from integration over transverse momentum of the emitted gluon (see equation (2.63)) and as a consequence, $F_2(x, Q^2)$ acquires Q -dependence and therefore violating Bjorken scaling, Q_0 is a lower momentum cutoff to regulate the latter integral. Here the collinear singularity is apparent when one takes $Q_0 \rightarrow 0$. This singularity does not cancel against those from other diagrams contributing at this order. To deal with the persistent singularity one resorts in a similar fashion as UV renormalization to redefinition of the bare PDF in equation (2.73) into a renormalizable one at some *factorization* scale μ_F by identifying it with the bare one plus a

divergent term i.e:

$$q(x, \mu_F^2) = xe^2 \int_x^1 \frac{d\xi}{\xi} q(\xi) \left[\delta\left(1 - \frac{x}{\xi}\right) + \frac{\alpha_s}{2\pi} P_{qq}\left(\frac{x}{\xi}\right) \ln\left(\frac{\mu_F^2}{Q_0^2}\right) + C(z) \right] \quad (2.74)$$

Choosing how much of the the finite function $C(z)$ gets absorbed defines the *factorization-scheme* and similar to renormalization scheme there exists also different choices like: DIS scheme, MS-like schemes, \dots , etc. The PDFs at two different scales are related by:

$$q(x, Q^2) = q(x, \mu_F^2) + \frac{\alpha_s}{2\pi} \int_x^1 \frac{d\xi}{\xi} q(\xi, \mu_F^2) P_{qq}\left(\frac{x}{\xi}\right) \ln\left(\frac{Q^2}{\mu_F^2}\right) \quad (2.75)$$

We obtain for F_2 :

$$F_2(x, Q^2) = xe^2 \left[q(x, \mu_F^2) + \frac{\alpha_s}{2\pi} \int_x^1 \frac{d\xi}{\xi} q(\xi, \mu_F^2) P_{qq}\left(\frac{x}{\xi}\right) \ln\left(\frac{Q^2}{\mu_F^2}\right) \right] \quad (2.76)$$

Here μ_F can be thought of as the scale that separates perturbative aspect of our calculation from non-perturbative one, as partons emitted with $k_t < \mu_F$ is considered part of the hadron's internal structure while those emitted with $k_t > \mu_F$ are considered part of the hard interaction.

2.4.2 DGLAP evolution equations

As was the case for the UV renormalization procedure, all physical quantities should not depend on an arbitrary scale. Thus we also should have:

$$\begin{aligned} \frac{\partial F_2(x, Q^2)}{\partial \ln(\mu_F^2)} &= \frac{\partial \sigma}{\partial \ln(\mu_F^2)} = 0 \\ &= \frac{\partial f(x, \mu_F^2)}{\partial \ln(\mu_F^2)} + \frac{\alpha_s}{2\pi} \int_x^1 \frac{d\xi}{\xi} \left[\frac{\partial f(\xi, \mu_F^2)}{\partial \ln(\mu_F^2)} \ln\left(\frac{Q^2}{\mu_F^2}\right) - f(\xi, \mu_F^2) \right] P_{qq}\left(\frac{x}{\xi}\right), \end{aligned} \quad (2.77)$$

where the first term in the integral is discarded since it leads to a $\mathcal{O}(\alpha_s^2)$ term, therefore we have:

$$\frac{\partial f(x, \mu_F^2)}{\partial \ln(\mu_F^2)} = \frac{\alpha_s}{2\pi} \int_x^1 \frac{d\xi}{\xi} f(\xi, \mu_F^2) P_{qq}\left(\frac{x}{\xi}\right). \quad (2.78)$$

The RGE above is none other than the famous DGLAP (after Dokshitzer [74], Gribov, Lipatov [92], Altarelli and Parisi [11]) evolution equation, the analogue to β function, it describes how the quark PDF “*evolves*” as the scale μ_F is varied.

To fully determine the quark PDF dependence, one needs to add to DGLAP equation (2.78) a term corresponding to the splitting shown in figure 2.2 where a gluon fluctuates into a $q\bar{q}$ pair and one of them is destined to interact with γ^* . Another piece to consider is the gluon PDF, since half the nucleon’s momentum is carried by gluons. Taking these considerations into account, we arrive to a set of $2n_f + 1$ coupled integro-differential equations:

$$\frac{\partial q_s(x, \mu_F^2)}{\partial \ln(\mu_F^2)} = \frac{\alpha_s}{2\pi} \left[P_{qq} \otimes q_s + 2n_f P_{qg} \otimes g \right] \quad (2.79)$$

$$\frac{\partial g(x, \mu_F^2)}{\partial \ln(\mu_F^2)} = \frac{\alpha_s}{2\pi} \left[P_{gq} \otimes q_s + P_{gg} \otimes g \right] \quad (2.80)$$

or in compact matrix notation as

$$\frac{\partial}{\partial \ln(\mu_F^2)} \begin{pmatrix} q_s \\ g \end{pmatrix} = \frac{\alpha_s}{2\pi} \begin{pmatrix} P_{qq} & 2n_f P_{qg} \\ P_{gq} & P_{gg} \end{pmatrix} \otimes \begin{pmatrix} q_s \\ g \end{pmatrix} \quad (2.81)$$

The singlet distribution q_s is defined as the sum over all active flavours of quarks and anti-quarks distributions, i.e $q_s = \sum_{i=1}^{n_f} (q_i + \bar{q}_i)$.

The usual strategy to determine PDFs by several groups such as: CTEQ [130], MSTW [119], ... is to measure the PDFs through fits to global data at some low (but still perturbative) reference scale μ_0 and evolve them to higher scale μ using the DGLAP equation. The x dependence is not predicted by DGLAP and so, only determined from said data fits. We show in figure 2.3 an example of PDFs obtained by said groups²².

The solution to DGLAP equation often carried out by brute force numerical integration methods.

Uncertainties related to scale choice can be assessed by varying both of μ_F, μ_R together by a factor of two (i.e a two point variation) or separately from each other (i.e a six point variation) and then the envelope is taken.

²²The plots were all obtained from <https://apfel.mi.infn.it> [46]

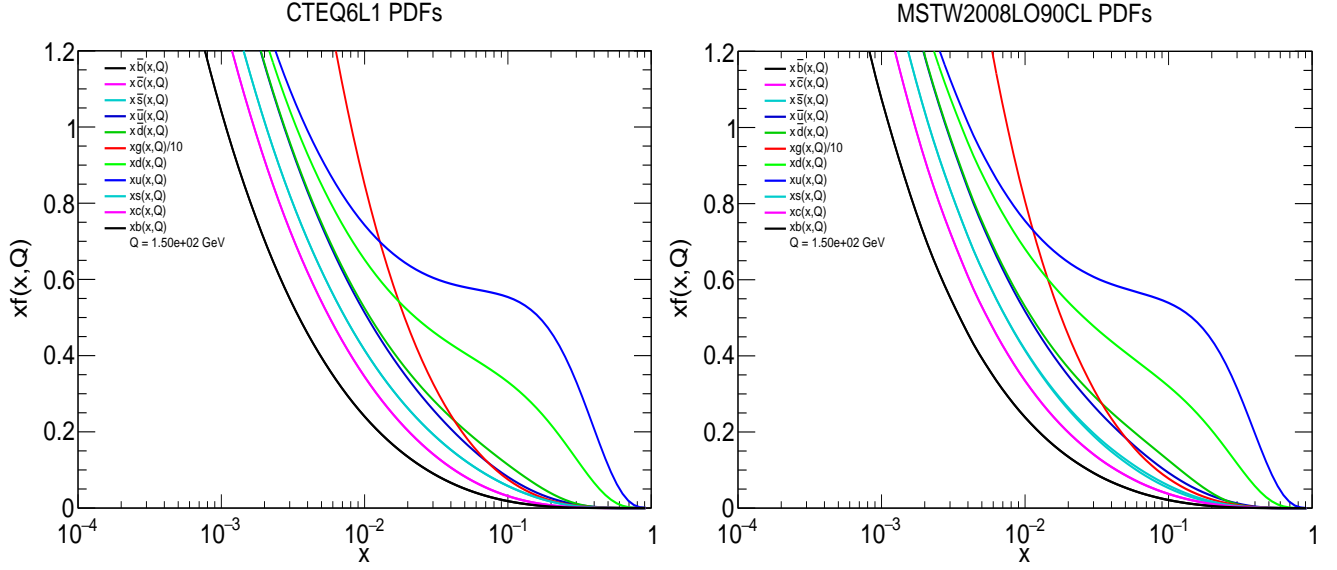


Figure 2.3: The leading order PDF sets from MSTW [119] & CTEQ [130] collaborations.

Taking into account the renormalized PDFs in equation (2.74), we rewrite equation (2.61) as:

$$\sigma_{AB \rightarrow X} \sim \sum_{a,b} \int dx_a dx_b f_{a/A}(x_a, \mu_F^2) f_{b/B}(x_b, \mu_F^2) \hat{\sigma}_{ab \rightarrow X}(\mu_F^2, \mu_R^2, \alpha_s(\mu_R^2), Q^2) \quad (2.82)$$

This is the *QCD-improved parton model formula* or often referred to as *QCD master formula* which is the basis of all perturbative calculations. Now the PDFs are interpreted as probabilities to find partons carrying momentum fraction x inside their respective mother hadrons when resolved at a factorization scale μ_F . Although QCD is scale invariant theory (i.e exhibits no scale dependence), the truncation of the perturbative series at a given order in α_s introduces dependence on the two completely arbitrary scales: μ_R and μ_F . The common choice is to set them both equal to the process hard scale Q in order to reduce the effect of scale logarithms that emerge in PT and therefore improve the convergence of the perturbative series. A poor choice for these scales can lead to unstable perturbative series or even worse to violation of important symmetry (conservation) laws. For a discussion on the scale choice, see [128].

2.4.3 Resummation

In the study of QCD events or jet observable distributions which as stated in the introduction characterize the energy flow in an event or within an individual jet in that event, one usually

proceeds order by order in the framework of PT. This route is often termed “*fixed-order*” approach is sufficient for many energetic and well separated partons, since each parton emission scales and therefore is suppressed by powers of α_s leading into a well behaved perturbation series and reasonable predictions for said distributions. However, since most of QCD radiation resides in the soft/collinear corner of phase space, each emission scales as $\sim \alpha_s L \sim 1$ hence the all-order perturbative series can be generally written as:

$$\frac{1}{\sigma_0} \frac{d\sigma}{dv} = \frac{d}{dv} \left[1 + \sum_{n=1}^{\infty} [\mathcal{A}_n^{(1)} \alpha_s^n L^{2n} + \mathcal{A}_n^{(2)} \alpha_s^n L^{2n-1} + \mathcal{A}_n^{(3)} \alpha_s^n L^{2n-2} + \dots] \right] \quad \text{for } v \ll 1 \quad (2.83)$$

Here $L \equiv \ln[1/v]$ is the large log and \mathcal{A}_n are observable-dependent coefficients from which we can see that these logarithms can potentially spoil the convergence and the fixed-order approach is invalidated.

One often takes the cumulative (integrated) distribution of an event shape v normalized to Born cross-section defined by:

$$\Sigma(v) = \int_0^v \frac{1}{\sigma_0} \frac{d\sigma}{dv'} dv', \quad (2.84)$$

which gives the probability that the observable when measured to have a value less than v . As an example, let us take v to be the hemisphere mass defined as:

$$\rho = \frac{1}{Q^2} \left(\sum_{i \in \mathcal{H}_R} k_i + p_a \right)^2 \simeq 2 \sum_{i \in \mathcal{H}_R} \frac{k_i \cdot p_q}{Q^2} = \sum_{i \in \mathcal{H}_R} \rho_i \quad (2.85)$$

$$\rho_i = \frac{2k_i \cdot p_q}{Q^2} = x_i e^{-\eta_i}, \quad x_i = \frac{k_{ti}}{Q}, \quad \eta_i = \ln(\arctan(\frac{\theta_i}{2})). \quad (2.86)$$

The cumulative distribution for the hemisphere mass to be measured with a value below ρ is:

$$\begin{aligned} \Sigma(\rho) &= \int_0^\rho \frac{1}{\sigma_0} \frac{d\sigma}{d\rho'} d\rho' \\ &= 1 + \Sigma_1(\rho) + \Sigma_2(\rho) + \dots \end{aligned} \quad (2.87)$$

where $\Sigma_1(\rho) = \int d\Phi_1 \hat{u}_1 \mathcal{W}_1$ with the measurement function $\hat{u}_1 = 1 - \Theta_1^\rho \Theta_1^{in} \Theta_1^R$ where $\Theta_1^\rho \equiv \Theta(\rho_1 - \rho)$, $\Theta_1^{in} \equiv \Theta(\eta_1)$ and the last Heaviside function requires that the gluon to be real. The eikonal

amplitude $\mathcal{W}_1 = \mathcal{W}_1^R + \mathcal{W}_1^V$ together give (for details see [102]):

$$\begin{aligned}
\Sigma_1(\rho) &= - \int d\Phi_1 \Theta_1^\rho \Theta_1^{in} \mathcal{W}_1^R \\
&= -2C_F \frac{\alpha_s}{\pi} \int_0^L d\eta_1 \int_{\rho e^{\eta_1}}^1 \frac{dx_1}{x_1} \int_0^{2\pi} \frac{d\phi_1}{2\pi} \\
&= -C_F \bar{\alpha}_s L^2
\end{aligned} \tag{2.88}$$

Here $\bar{\alpha}_s = \alpha_s/\pi$, and L is the large log, i.e $L \equiv \ln(1/\rho)$ and the leading logarithmic contribution is doubly logarithmic, originating from soft and collinear singularities. Several other logarithmic enhancements which come from other kinematical configurations contribute to $\Sigma(\rho)$. Luckily, for large number of observables of phenomenological interest, these logs are said to exponentiate, and we can therefore write $\Sigma(v)$ as:

$$\Sigma(v) = \left(1 + \left(\frac{\alpha_s}{2\pi} \right) C_1 + \left(\frac{\alpha_s}{2\pi} \right)^2 C_2 + \dots \right) e^{Lg_1(\alpha_s L) + g_2(\alpha_s L) + \alpha_s g_3(\alpha_s L) + \dots} + D(v), \tag{2.89}$$

where the remainder function $D(v)$ vanishes when $v \rightarrow 0$. The function $Lg_1(\alpha_s L)$ resums leading (double) logarithms (LL) $\alpha_s^n L^{n+1}$, $g_2(\alpha_s L)$ resums next to leading (single) logarithms (NLL) $\alpha_s^n L^n$, $\alpha_s g_3(\alpha_s L)$ resums next to next to leading (subleading) logarithms (NNLL) $\alpha_s^n L^{n-1}$ and so on. In the case when the observable is dominated by single logs, the function $g_1(\alpha_s L)$ vanishes. Finally, the C_n terms are out of reach of the resummation procedure and are determined with the help of fixed-order approach either analytical or numerical (by use of MC codes).

Overall, to say that one is performing a resummation procedure, it has to be characterized by three main things:

- The kind of logarithms to be controlled at hand, eg: $\ln[1/v]$, $\ln[m_Z/p_T]$, $\ln[R]$, $\ln[b]$, ...
- The accuracy one wants to achieve: LL, NLL, NNLL, ...
- A prescription for handling possible ambiguities.

2.5 Jets & jet algorithms

At any given event at particle colliders, the detector receives entries from tens or even hundreds of colorless particles, a point of view of this picture can be seen in figure 1.2. The transition from elementary to composite objects can be understood through models to hadronization process, the question now becomes how one quantifies the complex picture seen at almost all event in terms of well-defined and behaved objects? And how can one relate the observed particles to the quark & gluon partonic language of PT?

The answer comes in terms of the concept *jets* which by definition are a collimated sprays/clusters of final state particles traveling along the same direction. The basic idea in defining a jet given a set of final state momenta consists of two steps: first one is to determine how and when particles are clustered together. This defines the jet algorithm used. Several algorithms were proposed throughout the years starting from Weinberg-Sterman's original jet definition [136] all the way to present day LHC²³. Today, all jet algorithms fall under two categories: the sequential recombination algorithms and cone type. For more information on the subject of jets, Salam's comprehensive and extensive review [132] is a must read.

2.5.1 Sequential recombination algorithms

First appearing during initial years of running the LHC, sequential recombination scheme algorithms were the first choice at hand for theorists and experimentalists alike. One such algorithm of this kind is the generalized k_t family [48, 79, 76, 142, 42] for which we define two distance measures:

$$d_{ij} = \min(k_{ti}^{2p}, k_{tj}^{2p}) \Delta R_{ij}^2 \quad d_{iB} = k_{ti}^{2p} R^2 \quad (2.90)$$

d_{ij} is the distance measure between pair of particles i and j while d_{iB} is distance between particle i and the axis of travel of colliding beams, k_{ti} is the transverse momentum of particle i wrt beam direction. $\Delta R_{ij}^2 = (\phi_i - \phi_j)^2 - (\eta_i - \eta_j)^2$ is the separation between i and j in the (ϕ, η) plane, R is the jet radius parameter, usually taken to be $R \leq 1.0$ and p is a parameter that defines the algorithm to use. For instance, the choice $p = 0$ corresponds to Cambridge-Aachen (CA) algorithm [76, 142]

²³The jet definition was formalized in the snow mass accord [95] where jet algorithms have to fulfill criteria such as IRC, ease of implementation on theoretical & experimental side, minimal sensitivity to non-perturbative effects.

where particles are clustered based on purely geometrical measures, the choice $p = +1(-1)$ defines k_t [48, 79] (anti- k_t [42]) algorithm where the clustering of particles starts with the softest (hardest) first leading into irregular (regular) round jets in the (ϕ, η) plane. The second step is to find the minimum between all pairwise measures d_{ij} and d_{iB} . If $d_{min} = d_{iB}$ then particle i is promoted to jet status and consequently removed from the list of particles. On the other hand, if $d_{min} = d_{ij}$ then particle i and j are recombined into a proto/pseudojet with total four momentum defined according to some recombination scheme (e.g., E-scheme where the resultant momentum is just the sum of the two constituent momenta i.e $p_{tot}^\mu = p_i^\mu + p_j^\mu$).

2.5.2 Cone algorithms

Due to questions of IR safety and performance issues, many of the algorithms of this kind were discarded during LHC runs. One exception is the **Seedless Infrared Safe Cone** or **SISCone** algorithm [133]. The old cone type algorithms relied on finding a stable cones centered around N particles which can be a CPU-expensive operation, a quick solution to this issue is to set the starting point for the algorithm from a seed particle and cluster nearby particles within the cone radius however failure to find all stable cones can lead to instability in results due to the algorithm becoming IR sensitive. The SISCone algorithm employs a geometric procedure to find all stable cones as well as reducing the number of iterative operations from $\mathcal{O}(N2^N)$ to $\mathcal{O}(N^2 \ln N)$.

Chapter 3

Monte Carlo tools & methods.

Since the establishment of QCD as a theory of strong interactions, the field has known rapid growth/advancement over the consequent years. However, the methods and rules of the last chapter are both time and effort consuming beyond a handful simple $2 \rightarrow 2$ processes. As the complexity grows with each additional parton in the final state since the number of Feynman diagrams grows factorially rendering the standard textbook method of calculating matrix elements and squaring them tedious at best. Furthermore, with each additional emission, the integration over final state phase space becomes over $(3n - 4) + 2$ where n is the number of final state partons. For high multiplicities it becomes useless for analytical or even conventional numerical quadrature methods and the need for MC methods use for their efficiency becomes critical.

The previous points show the necessity of some kind of a dedicated computer code for the simulation of some or all aspects of high energy particle collisions whether they were perturbative or non-perturbative and whether describe them exactly by means of exact analytical expressions or approximately by modeling them through semi-empirical models is best suited for said computer code.

In this chapter, we first begin by giving a review of Monte-Carlo methods and show why they are best suited for event simulations and how they excel at this task better than any other numerical method. Then we talk how the overall simulation of events takes place. After that, we take advantage of the factorization theorem to discuss each aspect of the simulation separately. Finally,

we conclude by mentioning some of the widely used Monte-Carlo tools and a brief description.¹

3.1 Random number generation

A main/important ingredient that Monte-Carlo methods relied on is random numbers. Being a method based on probabilistic approach to solve mathematical issues or model undeterministic processes whenever the deterministic approaches fail, it is then natural to look for a way to obtain/generate such numbers. One way is to observe and study random processes occurring in nature such as a simple coin flip, unstable nuclei decays, the motion of a double pendulum system beyond a certain point in time, brownian motion of pollen particles on the surface of a fluid, ..., etc.

However, these are hard to come by and not many can be obtained and on top of that, biases can be hard to remove in the collection. Therefore, we turn our attention into generating them numerically with the aid of some algorithm. Although, these are at heart deterministic but after subjecting them to some statistical test on the randomness of the sequence of numbers they produce, they can be considered as a good source.

The algorithms that supply us with such numbers are called *pseudo random numbers generators* or PRNGs. One working principle behind PRNGs is the *linear congruential generators* (LCG) where a sequence of PRNs is generated according to the recurrence relation:

$$r_{n+1} = (ar_n + b) \text{ mod } m \tag{3.1}$$

provided the user initializes the sequence with a seed number r_0 . The *mod* stands for the modulo operation (i.e it returns the remainder of $(ar_n + b) \div m$) and the choice for a, b and m defines the algorithm to use. And then, the random number within $[0; 1)$ ² is found to be $\xi_i = r_i/m$.

This kind of algorithms is preferable for debugging, testing, reproducibility of results. Good qualities that PRNGs should have are [96]: large period (i.e at which the sequence repeats itself), efficiency, good distribution of points, absence of correlations between numbers in a sequence

¹The reader is reminded that this by no means a comprehensive review but a brief one only. For a comprehensive review see [40] and references therein.

²And within $[a; b]$, the random number is: $\xi_i = \frac{r_i}{m}(b - a + 1)$ for $a, b \ll m$

and to be system or machine independent. Two good algorithms that satisfy the statistical tests mentioned are Mersenne Twister [120] & RngStreams [112].

Today, LCGs fell in popularity (due to bad correlations between successive/consecutive numbers) in favour to new algorithms based on the theory of mixing in classical dynamical systems. For a recent review of high quality RNGs, see [97].

3.2 Monte Carlo methods

Event simulations or commonly termed event generation are revolved around MC methods for integration. To gain an understanding at it, let us consider the following 1D integral over a domain $[a, b]$:

$$I = \int_a^b f(x)dx \quad (3.2)$$

the mean value of f over the range $[a, b]$ is:

$$\langle f(x) \rangle = \frac{1}{b-a} \int_a^b f(x)dx \quad (3.3)$$

and the integral is then expressed as:

$$I = (b-a) \langle f(x) \rangle \quad (3.4)$$

The mean value of f can be estimated by summing over $f(x)$ evaluated at some sampled points x_i of a uniformly distributed (i.e sampled with equal probability) set x_i and divided over the set size N i.e:

$$\langle f(x) \rangle \simeq \frac{1}{N} \sum_{i=1}^N f(x_i) \quad (3.5)$$

hence the integral becomes estimated by $I_N \simeq \frac{b-a}{N} \sum_{i=1}^N f(x_i)$ and converges to the true I value for large enough number of set points as per the law of large numbers (LLN) states.

The above formulas can be systematically extended to higher number of dimensions d , it gives then:

$$I = \int f(x_1, \dots, x_d)dV \simeq V \langle f(x_1, \dots, x_d) \rangle \quad (3.6)$$

here V is the hyper-dimensional volume enclosed by the function $f(x_1, \dots, x_d)$ in d dimensions.

The next question arises as how one quantifies the accuracy of a MC method given a finite number of points N ? because the estimation of the error of the measurement is as important as the measurement itself. The error (or its estimation) can be shown to be

$$I = I_N \pm \sqrt{\frac{\sigma^2}{N}} \quad (3.7)$$

Where σ^2 is the variance of the estimate I_N . Its square root is the standard deviation which is written as:

$$\sigma = \sqrt{\langle f(x)^2 \rangle - \langle f(x) \rangle^2} \quad (3.8)$$

From the two equations above, we see that the error will decrease as the inverse squared root of the number of sample points $\sim 1/\sqrt{N}$ and is independent of the dimensionality of the integral. This makes MC methods for integration in high dimensions far more appealing than the traditional methods. For example, the error in MC method will always scale as $1/\sqrt{N}$ while other methods such as Trapezoidal or Simpson rule will scale as $1/N^{d/2}$ and $1/N^{d/4}$ respectively.

Another room for improvement in MC methods comes from the variance, which measures the fluctuation from the mean value of the integral. So, the overall error can be reduced by taking a larger number of sampled points and not only that but also by reducing the variance which can be achieved by a better sampling than the flat or uniform one. Other sampling is based on generating points according to some probability distribution function (pdf) rather than unity (i.e uniformly).

3.2.1 Sampling

We have seen the idea of expressing the idea of integrating a one or multi-dimensional function expressed as mean value of $f(x)$ over a set of x values, but how one generates such set to begin evaluating the integral at hand with? a few methods exist and be reviewed in the next section[96, 141, 40].

3.2.1.1 Sampling by inversion

A first method to generate a set of points for use in equation (3.5), is to sample them according to some probability distribution function (pdf) $p(x)$, whether this pdf was uniform, exponential, or Gaussian or whatever. The pdf $p(x)$ is a positive function $p(x) \geq 0$ for all $x \in [a, b]$ and is normalized to unity over the extent of its domain, i.e $\int_{-\infty}^{+\infty} p(x) dx = 1$ as should be for a probability function.

We define the cumulative distribution function (cdf) $F(x)$ as:

$$F(x) = \int_{-\infty}^x p(x') dx' \equiv \mathcal{P}(X \leq x) \quad (3.9)$$

Here $F(x)$ represents the probability that the random variable X takes a value less than or equal to x and therefore we have:

$$\mathcal{P}(a \leq X \leq b) = \int_a^b p(x) dx = F(b) - F(a) \quad (3.10)$$

This method of sampling random numbers according to some pdf $p(x)$ begins with determining the corresponding cdf $F(x)$ to $p(x)$ and also its inverse $F^{-1}(y)$ and then with the help of a uniform random number variable ξ , we obtain our non-uniform (again, according to $p(x)$) number η by solving $F^{-1}(\xi) = \eta$. As an example, we take the case of two probability distribution functions, a uniform and an exponential one.

- a uniform distribution $p_u(x)$ which is defined as:

$$p_u(x) = \begin{cases} \frac{1}{b-a} & a \leq x \leq b \\ 0 & \text{otherwise} \end{cases} \quad (3.11)$$

its corresponding cdf is: $F(x) = (x - a)/(b - a)$ which by inversion and then solving for $F^{-1}(\xi) = \eta$, we get our uniformly distributed number as: $\eta = a + (b - a)\xi$

- an exponential distribution $p_{exp}(x)$ which is defined as:

$$p_{exp}(x) = \begin{cases} \lambda \exp^{-\lambda x} & x \geq 0 \\ 0 & x < 0 \end{cases} \quad (3.12)$$

its corresponding cdf is: $F(x) = 1 - \exp^{-\frac{x}{\lambda}}$ which by inversion, we get our random number as: $\eta = -\lambda \ln(1 - \xi) = -\lambda \ln(\xi)$, since ξ is a random number, so is $1 - \xi$.

3.2.1.2 Sampling by rejection

When $F^{-1}(x)$ is hard to obtain since for other more complicated pdfs, the inversion is not possible (or at least not in a closed form). The basic idea of acceptance-rejection (sometimes called hit-or-miss) method is that $p(x)$ can be fully enclosed by another easily integrable distribution $k h(x)$. This means that for all x in integration range, we have $p(x) \leq k h(x)$ and $k \geq 1$ since both of $p(x)$ and $h(x)$ are normalized to unit area. Then one generates a uniformly distributed random number ξ in $[0; 1]$. If $\xi \leq p(x)/k h(x)$ then ξ is accepted, otherwise it is rejected and another random number is generated and the check is once again performed. For efficiency issues, $h(x)$ needs to be as tightly close to $p(x)$ as possible, such that the efficiency of this sampling method becomes $1/k$.

3.2.2 Variance reduction

The method of MC integration as we have seen proves its worth against other standard methods in the high dimensional calculations. A situation where in particle physics is quickly attained/reached even in the simple $2 \rightarrow 2$ or $2 \rightarrow 3$ processes. The error on the estimate of the integrals is found to be related to the square root of the variance over number of sampled points. Hence, an optimization for MC integration can be achieved by using a large set of points and also by reducing the variance. In this section we'll briefly give an idea on how the latter is achieved using methods designed to improve over simple/crude/naive MC method.

3.2.2.1 Importance sampling

Originated from studies in classical statistical mechanics [122], the method known as *importance sampling* is based on the idea to take the original integral of equation (3.2) and make a change in

integration variables:

$$I = \int f(x)dx \quad \rightarrow \quad I = \int \frac{f(x)}{g(x)}g(x)dx \quad (3.13)$$

mathematically speaking this change of variables amounts to evaluating the integral of $f(x)/g(x)$ according to the non-uniform distribution of points governed by $g(x)$ (i.e it is an application of the inverse transform, see section 3.2.1.1). The now estimator I_N for the integral I and its corresponding error is:

$$I = \left\langle \frac{f}{g} \right\rangle \pm \sqrt{\frac{\langle (f/g)^2 \rangle - \langle f/g \rangle^2}{N}} \quad (3.14)$$

For a better efficiency and as little variance as possible, one needs to choose $g(x)$ to mimic $f(x)$ fairly well and be easily integrable, i.e to be easy to integrate approximation to $f(x)$ such that in the end we generate more often points in regions where $f(x)$ has peaks or rather is *important* (and hence the name) and less often where it is not. A good approximation of $f(x)$ will lead to $\sigma_{f/g} \ll \sigma_f$. In practice, the knowledge of $g(x)$ is required apriori and is obtained either when constructing the relevant MEs (by exploiting the structure of Feynman rules and propagators) or numerically determine the structure/properties of the integrand by probing it *on the fly* with a set of PS points during an initial run (i.e adaptive sampling).

3.2.2.2 Stratified sampling

The second method to reduce the variance is *stratified sampling* is to divide the entirety of the available PS into a number n of non-overlapping sub-volumes (*strata* or *stratum*) and $f(x)$ is evaluated in each sub-volume independently. For a phase space of d dimension and where each dimension is segmented into h pieces, the number of sub-volumes is h^d . At first this seems that it doesn't lead to any improvement but it can be shown that the sum of variances in each sub-volume (or sub-variance) is at most equal to the variance of $f(x)$ when evaluated in the whole PS. We write:

$$S_{PS} \geq S_{tot} = \frac{1}{n} \sum_{i=1}^n S_i \quad (3.15)$$

The estimator for I and the associated error is written then:

$$I = \sum_{j=1}^n \frac{V_j}{N_j} \sum_{i=1}^{N_j} f(x_i) \pm \sum_{j=1}^n \frac{V_j^2}{N_j} \left[\left(\frac{1}{V_j} \langle f(x_j)^2 \rangle \right) - \left(\frac{1}{V_j} \langle f(x_j) \rangle \right)^2 \right] \quad (3.16)$$

here V_j is the volume of the sub-volume j and N_j is the number of points distributed inside V_j more space for improvement is when one distributes or samples the points in each sub-volume according to its corresponding square root sub-variance.

3.2.2.3 Multi-channel sampling

When the integrand (equation (3.2)) represented by MEs squared in our case has several/multiple peaks (stemming from eg: enhanced regions in PS, resonances production, ...), the previous methods cannot handle this complexity. The multi-channel method [107] offers a solution. As it is often extremely difficult to make a transformation that flattens the integrand across all peaks simultaneously. The divide and conquer strategy employed by the multi-channel method makes a transformation for each separate peak structure. Each peak transformation is called a channel and each channel is associated with an appropriate pdf $p_i(x)$, such that each $p_i(x)$ is normalized $\int p_i(x)dx = 1$ for $i = 1, \dots, n$. n is the number of channels. In the evaluation, each channel is selected with a probability α_i where α_i are non-negative numbers and $\sum_{i=1}^n \alpha_i = 1$. Each channel is evaluated approximately/roughly by $N_i \sim \alpha_i N$ so the estimate of the integral is:

$$\begin{aligned} \int f(x)dx \sim I_N &= \sum_{i=1}^n \alpha_i \int \frac{f(x)}{p(x)} dF_i \\ &= \frac{1}{N} \sum_{i=1}^n \sum_{j=1}^{N_i} \frac{f_i(x_j)}{p_i(x_j)} \quad / \quad p(x) = \sum_{i=1}^n \alpha_i p_i(x) \end{aligned} \quad (3.17)$$

3.3 Hard processes simulation

The machinery developed so far represented on one side by the theory of fields and quantas as the physical picture of hard interactions supplemented by mathematical tools and techniques to be able to provide a solid picture of hard interactions and thus making the full description of collisions a highly sophisticated endeavor. Despite each interaction can involve hundreds of

particles across a wide range of energies, nature exhibited its fundamental simplicity once again through the theorem of factorization. In a similar manner to what was described in section 2.4, hard interactions at particle colliders proceed first by a hard collision between not the hadrons in each beam themselves but between two partons from each incoming hadron, being a composite object itself, the identity (of flavor) of the collision initiating partons is determined in a probabilistic manner governed by the non-perturbative quantities known as the parton distribution functions. Then the hard scattering can be described by summing over all diagrams that contain the set of all initial/final particles and applying Feynman rules to a certain order in PT. The objects at this level can be partons, leptons, gauge bosons, ..., etc. If the outgoing final state particle were unstable resonances, then they themselves would undergo into decay according to some branching ration. These outgoing states are usually color/electrically charged, they are eventually start emitting a succession of soft/collinear QED/QCD bremsstrahlung marking the beginning of the parton shower phase. This phase can also take place before (after) the hard collision leading to the initial (final)-state radiation ISR(FSR). The shower can be simulated as a Markov chain starting from the high momentum transfer scale Q emitting all kinds of possible particles down to the order of a few GeVs of the order of Λ_{QCD} where PT ceases to be valid. The plethora of these produced particles then enter the hadronization³ phase which currently only described by models tuned from experiments. An example of these models is Cluster and String fragmentation models used in Herwig [29] and Pythia8 [35] respectively. The now produced hadrons are decayed using a combination of basic MEs or models and then the final piece in the simulation of hard events is the emulation of detector response with the help of tools such as GEANT4 [8], DELPHES [68],

Putting all this together defines the framework of general purpose monte carlo event generators. It simulates events as close as possible to what they appear in real-life colliders. The simulation starts by first constructing the corresponding matrix element squared. The GPMCs of today possess a huge library of these MEs for many processes and in fact for others, the determination of MEs is fully automated even @ NLO (and for handful other processes @ NNLO). The second step is to sample a phase space point (assigning randomly momenta, spin, color for initial-final

³It can be described at calculation by Fragmentation functions (FF) which as the PDFs obey the DGLAP equation but have different boundary conditions.

particles) therefore generating a candidate event with an associated weight $\omega \equiv d\sigma = 1/2\hat{s}|\mathcal{M}|^2d\Phi$. This weight plays a crucial role in determining the type of computation we are doing (either FO in which the simulation is only limited to only parton level or unweighted events for later stages of simulation) but also in including corrections such as the assessment of systematic scale uncertainties (by keeping track of the weights and their squares in each bin) without redoing the whole simulation once again using a re-weighting technique [83]. As the cross section is related to the number of events that pass the cuts, using each event weight to a certain bin in some histogram describing a differential distribution of some observables and in the limit of large sample, the average/sum of weights is a direct estimator for the integral $\langle d\sigma \rangle = \int d\sigma$ i.e corresponds to the (total) cross section of the process under study.

Other aspects of events that were mainly skipped were the non-perturbative aspects mainly the fact that hadrons are mainly a collection of comoving⁴ that multiple pairs that can take part in the interaction alongside the main hard process, this is know as *multiple parton interaction* (MPI). The same idea but at hadrons level can occur since each beam contains several bunches which in turn are made up of several millions of hadrons each and which can also lead to several pairs of hadrons to collide at the same time, a consequence of high luminosities attained by present and future colliders, this phenomenon is known as *Pile-up* (PU). Since the hadron is a composite object and the hard interaction only involves one parton from each colliding hadron, the hadron remainder or fragments may also interact with each other leading to what is known as *Underlying events* (UE). All these fall under the category of non-perturbative effects. Their estimation for the moment only relies on fully-experimental or QCD inspired models.

3.4 Tree level matrix element generators

Whether we seek to simulate an entire event, or be satisfied with only cross section calculation and fill some histograms, the starting point for both approaches is the same. As both depart from a ME describing the underlying hard process in question to a certain order in PT.

Much effort has been put to determine these MEs to all SM processes. The tools that provide

⁴In fact, they are more or less comoving, as it was found that they have a transverse component, the non-perturbative effect/aspect stemming Heisenberg's uncertainty principle known as the *primordial k_T*

these MEs are called *Matrix element generators*. They contain all the necessary tools/ingredient to provide and supply with MEs squared summed/averaged over relevant quantum numbers of final/initial states.

MEs generators fall under two categories:

- Specific ones where they only specialize in simulating only certain process and the MEs therein are implemented/hard-coded manually by hands of respective authors. Thus, the desired process is selected among the many ones available. Examples of such codes are: Alpgen [118], Vecbos-W/Z+n jets [32], ...
- General ones where the desired MEs are fully generated in an automated fashion, such that the user only need to specify the initial and final states only. Other possible BSM models or effective theories can be easily implemented by using a UFO [69] (Universal Feynrules Output) model. The only limiting factor for automated tools is the computer-power and the number of final states (usually between 6-10 depending on the process complexity). Example of such automated ME providers are: Madgraph [12], Comix [90], CalcHEP [30], ...

In both cases and after specifying a certain process to be simulated, the code determines all relevant LO Feynman diagrams (and their corresponding topologies $s - t - u$ channels) that lead to a non-trivial and non-zero contributions to the cross section. For example, the LO DY process proceeds through γ^*/Z^0 in s-channel thus contributes @ $\mathcal{O}(\alpha^2)$ whereas LO Z+jets production proceeds through a t and s-channel thus contributing @ $\mathcal{O}(\alpha_s\alpha)$ (i.e the expansion parameter can be pure α_s , α or mixed).

Now having specified how MEs are generated, we now talk about how they are evaluated. Firstly, MEs implemented by hand are usually expressed as $\hat{s}, \hat{t}, \hat{u}$ to be later sampled with phase space. For automated codes & more complicated processes, the method of *helicity amplitudes* [106, 140] is more suitable. The basic idea in the transition from Feynman amplitudes to helicity amplitudes is to write each Feynman amplitude (*not* amplitude squared!) in terms of spinor products, for example the basic objects in any Feynman amplitude like Dirac spinor can be easily decomposed into its helicity states by the action of the projection operator. The fermionic propagator (or more

precisely its numerator) can be identified as:

$$\not{p} + m = \frac{1}{2} \sum_{\lambda} \left[\left(1 + \frac{m}{\sqrt{p^2}}\right) u(p, \lambda) \bar{u}(p, \lambda) + \left(1 - \frac{m}{\sqrt{p^2}}\right) v(p, \lambda) \bar{v}(p, \lambda) \right], \quad (3.18)$$

also for the polarization vector of a massless boson with momentum $p + q$ is written as⁵:

$$\epsilon_{\mu}(p + q) = \frac{1}{\sqrt{4p \cdot q}} \bar{u}(q, \lambda) \gamma_{\mu} u(p, \lambda) \quad (3.19)$$

The polarization vector for a massive boson follows in a similar manner with the caveat of non-zero mass and the presence of the third longitudinal polarization state.

Each amplitude \mathcal{M} is evaluated to yield a simple complex number c and is then multiplied with c^* from \mathcal{M}^* and the operation is repeated over all possible helicity combinations. Furthermore, this method can be improved upon even more to lead to faster amplitude evaluation by identifying diagrams with certain helicity configurations, for which a helicity flip is not allowed due to conservation of angular momentum thus leading to such diagrams to vanish, this is known as *helicity filtering* [121]. The identification of common sub-expressions of amplitudes across a wide number of diagrams, thus storing the common pieces to be only evaluated only once i.e the so-called *helicity recycling* [121]. Such techniques reduce the number of diagrams M containing N external particles and iterations to evaluate them. For regular methods based on Feynman diagrams, the evaluation takes M^2 diagrams to evaluate and $(N!)^2$ steps while the improved helicity methods only considers M diagrams and $(N - 1)!2^{N-1}$ steps.

Diagrams with even higher number of particles are better evaluated by recursive methods. In the high N particle they lead to efficient amplitude construction and evaluation. One such method is Berends-Giele recursive relation [31].

⁵This choice for the polarization vector is compliant with one in the axial gauge and satisfies the following completeness relation:

$$\sum_{\lambda=\pm} \epsilon_{\mu}(p, \lambda) \epsilon_{\mu}^*(p, \lambda) = -\eta_{\mu\nu} + \frac{p_{\mu} q_{\nu} + p_{\nu} q_{\mu}}{p \cdot q}$$

where q is a light-like vector not aligned with p .

3.5 Higher order corrections

Often times the LO computation of some desired observable is not enough (the observable can contribute in a non-trivial way only at higher orders, high theoretical uncertainties, ...). For a better quantitative/qualitative study and for obtaining results to compare to data at the percent or even sub-percent level, one has to include higher order corrections into the calculations.

An example is the cross section of some process to NLO accuracy which comprises of three parts: Born, real & virtual contributions and is expressed as:

$$\begin{aligned} d\sigma^{(NLO)} &= d\Phi_n \mathcal{B}(\Phi_n) + \alpha_s [d\Phi_{n+1} \mathcal{R}(\Phi_{n+1}) + d\Phi_n \mathcal{V}(\Phi_n)] \\ &= d\Phi_n [\mathcal{B}(\Phi_n) + \alpha_s \mathcal{V}(\Phi_n)] + d\Phi_{n+1} \alpha_s \mathcal{R}(\Phi_{n+1}) \end{aligned} \quad (3.20)$$

As we have seen, the individual real \mathcal{R} and virtual \mathcal{V} pieces each have IR singularities. In analytical calculations they are mutually canceled to give finite result as per guaranties of KLN theorem. However, in numerical calculations the situation cannot be implemented as straightforward due to the said individual pieces residing in different dimensional phase space. One therefore needs to address the divergences of each piece before moving on to their numerical evaluation.

The solution to this comes in two approaches: IR subtraction [51, 55, 110, 64, 85, 84] & phase space slicing [87, 88].

In the subtractive method, one adds (subtracts) a function that behaves as the singular cross section to the virtual (real) pieces in equation (3.20). This function encodes the universal IR behavior of the cross section and therefore can be constructed by exploiting the factorization of emissions in the IR regime. It also needs to be simple enough such that it is MC integrable. Thus, the NLO cross section now reads:

$$\begin{aligned} d\sigma^{(NLO)} &= d\Phi_n \mathcal{B}(\Phi_n) + \alpha_s d\Phi_n [\mathcal{V}(\Phi_n) + d\Phi_1 \mathcal{S}(\Phi_{n+1})] \\ &\quad + \alpha_s d\Phi_{n+1} [\mathcal{R}(\Phi_{n+1}) - \mathcal{S}(\Phi_{n+1})] \end{aligned} \quad (3.21)$$

where the bracketed terms i.e the virtual integrated (VI) & real subtracted (RS) are now separately finite and the numerical integration can be safely carried out. Examples of subtractive methods

are the Catani-Seymour dipole subtraction [51, 55], antenna subtraction [110, 64], FKS algorithm [85, 84].

The phase space slicing relies as the name suggests, on cutting the phase space into slices or strips. The divergent strips are evaluated analytically and added to the divergent virtual piece. The well-behaved strips are straightforward MC evaluated and the overall result is finite.

One thing to point out is that usually the IR singularities in RS term are vulnerable to what is known as *catastrophic cancellation* of the form when one subtracts almost very equal two numbers from each other. A remedy to this depends on the numerical accuracy of the code and for the difference if below a certain very low cutoff, the difference is set directly to zero.

3.6 Parton showers

As was described in the jet section 2.5, the detector cells and tracking system receive entries from up to hundreds of particles at once. It was later realized that the partons emerging from the hard interaction can emit other secondary partons and the latter themselves can do the same and so on. The description of this multi-parton picture as we have seen in chapter 2 in terms of Feynman rules would get not only extremely complicated beyond a few emissions but also largely contributing to the related cross section, however after analyzing the energy spectrum of these emitted quanta, we observe that they are emitted relatively soft and collinear w.r.t to the hard partons and for these types of emissions, we have seen that they factorize and hence can be systematically approximated to all orders by invoking a simulation of a consecutive cascade of soft/collinear emissions in a probabilistic manner, i.e performing a *parton shower* (PS).

The basic building block of a parton shower is the factorization formula (2.52) and (2.63), where in the collinear limit equation (2.63) becomes:

$$d\sigma_{n+1} \approx d\sigma_n \frac{\alpha_s}{2\pi} \frac{d\tilde{q}^2}{\tilde{q}^2} dz P_{ij}(z), \quad (3.22)$$

here we only replaced k_i^2 with a general energy scale \tilde{q}^2 . The equation above was universal in the sense that it does not depend on the underlying hard process, only on the branching in question. The above equation represents the probability for collinear splitting $i \rightarrow j + k$, between two scales

\tilde{q}^2 and $\tilde{q}^2 + d\tilde{q}^2$ i.e:

$$d\mathcal{P} \equiv \frac{d\sigma_{n+1}}{d\sigma_n} = \frac{\alpha_s d\tilde{q}^2}{2\pi \tilde{q}^2} \int dz P_{ij}(z), \quad (3.23)$$

the scale $d\tilde{q}^2/\tilde{q}^2$ can be substituted with any kinematical observable in relation with it (since they are equivalent soft/collinear limit but not otherwise, one choice is the virtuality of the internal particle line q^2 , the transverse momentum w.r.t its emitter k_t^2 or its emission angle weighted by its energy $E^2\theta^2$). Nevertheless, this choice corresponds to choosing the *ordering variable* for said PS. The splitting functions we are working in equation (3.23) are the un-regularized ones (singular in the soft limit $z \rightarrow 1$), so we are forced to set a lower cutoff on the z integration in order to simulate only resolvable emissions (a similar argument for arbitrarily collinear emissions). Usually we set it to be $q_0 \sim 1\text{GeV}$ and we therefore have:

$$d\mathcal{P} \equiv \frac{d\sigma_{n+1}}{d\sigma_n} = \frac{\alpha_s dQ^2}{2\pi Q^2} \int_{\frac{q_0^2}{Q^2}}^{1-\frac{q_0^2}{Q^2}} dz P_{ij}(z). \quad (3.24)$$

On the other hand, the no-emission probability is found by invoking unitarity arguments:

$$\mathcal{P}(q^2 < \tilde{q}^2 \leq Q^2) + \bar{\mathcal{P}}(q^2 < \tilde{q}^2 \leq Q^2) = 1, \quad (3.25)$$

$\bar{\mathcal{P}}(q^2 < \tilde{q}^2 \leq Q^2)$ obeys a multiplication rule, i.e:

$$\bar{\mathcal{P}}(q^2 < \tilde{q}^2 \leq Q^2) = \bar{\mathcal{P}}(q^2 < \tilde{q}^2 \leq \tilde{q}_1^2) \bar{\mathcal{P}}(\tilde{q}_1^2 < \tilde{q}^2 \leq Q^2) \quad (3.26)$$

In the limit where the emission scale is descretized in smaller steps, equation (3.26) becomes:

$$\begin{aligned}
\overline{\mathcal{P}}(q^2 < \tilde{q}^2 \leq Q^2) &= \lim_{n \rightarrow \infty} \prod_{i=0}^{n-1} \overline{\mathcal{P}}(\tilde{q}_i^2 < \tilde{q}^2 \leq \tilde{q}_{i+1}^2) \\
&= \lim_{n \rightarrow \infty} \prod_{i=0}^{n-1} 1 - \mathcal{P}(\tilde{q}_i^2 < \tilde{q}^2 \leq \tilde{q}_{i+1}^2) \\
&= \exp \left[- \lim_{n \rightarrow \infty} \sum_{i=0}^{n-1} \mathcal{P}(\tilde{q}_i^2 < \tilde{q}^2 \leq \tilde{q}_{i+1}^2) \right] \\
&= \exp \left[- \int_{q^2}^{Q^2} \frac{d\mathcal{P}}{d\tilde{q}^2} d\tilde{q}^2 \right] \\
\Delta(Q^2, q^2) &= \exp \left[- \frac{\alpha_s}{2\pi} \int_{q^2}^{Q^2} \frac{dQ^2}{Q^2} \int_{\frac{q_0^2}{Q^2}}^{1-\frac{q_0^2}{Q^2}} dz P_{ij}(z) \right] \tag{3.27}
\end{aligned}$$

$\Delta(Q^2, q^2)$ is known as Sudakov form factor and is used to successively branch final state partons. The usual strategy initializes by randomly selecting a final state parton. Then a random number ξ is generated between 0 and 1 and the probability for the parton emission at scale q^2 is obtained by solving $\Delta(Q^2, q^2) = \xi$ for q^2 . If q^2 is above the cutoff q_0^2 , the branching is performed otherwise the sequence of branchings for this particular parton is terminated. Once the branching is permitted, the kinematics of the shower need to be constructed, so a z value is sampled according to $P_{ij}(z)$ and ϕ either uniformly or according to some algorithm to include spin correlation effects. The cascade of FSR is kept running over the growing set of partons until the cutoff scale q_0 is reached. The same ideas are applied for ISR, but the partons need to be distributed according to their respective PDFs, and the branching is started with the incoming parton in the backward direction since otherwise we can not guarantee that we end up with the same parton flavor and momentum fraction as in the partonic level,⁶ we therefor modify the Sudakov factor as:

$$\Delta(Q^2, q^2, x) = \exp \left[- \frac{\alpha_s}{2\pi} \int_{q^2}^{Q^2} \frac{d\tilde{q}^2}{\tilde{q}^2} \int_{\frac{q_0^2}{Q^2}}^{1-\frac{q_0^2}{Q^2}} dz P_{ij}(z) \frac{x/z f(x/z, \tilde{q}^2)}{x f(x, \tilde{q})} \right], \tag{3.28}$$

here x is the usual momentum fraction while x/z is momentum fraction attained via a branching.

The shower description given in the beginning of this section forms the classical picture of

⁶Another reason is the efficiency in simulation since it would be extremely CPU expensive to simulate ISR as a forward branching.

successive emissions off an outgoing/incoming parton at a time from a high scale Q down to the fundamental scale Λ_{QCD} . Now, other descriptions are developed. So instead of a certain parton that emits by its own, we have a (color-connected) parton dipole (an emitter and a spectator) that coherently emits a cascade of partons as a series of $1 \rightarrow 2$ or $2 \rightarrow 3$.

3.6.1 Large N_c

One often used approximation both in theory and MC codes is the *large- N_c* limit [94], in which we consider a generalization of SU(3) to a theory with N_c colors, i.e SU(N_c) for N_c large. For this approximation, any fundamental color N_c (associated with a quark) can be combined with an anti-color \bar{N}_c (associated with an anti-quark) and produce a adjoint color and singlet such that, we can think of the gluon color charge being composed of one of the quark and anti-quark up to corrections whereas that of the quark is half of it, i.e $C_F \xrightarrow{N_c \rightarrow \infty} N_c/2$. Also, only Feynman diagrams whose lines are on the plane (i.e planar) contribute to a certain process with their color structure decomposed as a set of delta functions between color connected initial/final partons while those with lines which protrude from the plane are suppressed (by powers of $1/N_c$). This decomposition denotes explicitly the color flow of each diagram. Being a powerful organizing and simplifying principle as well as corrections are of $\sim 10\%$ or less, the large- N_c is nowadays implemented almost in every MC code.

3.7 Matching/merging

While for an n particle process, fNLO corrections give description to $n + 1$ particle final state, the parton shower through its successive branching would contribute to $n + m$ with $n \ll m$. The cascade spectrum being mostly in the soft/collinear region thus it offers a better description at lower bins a kinematical distributions. A combination of the two approaches directly to obtain a good description across all of phase space is highly desirable and therefore one resorts to some sort of procedure to match both approaches as a direct naive sum of the two would produce a double counting and we therefore we resort to what is known as *matching*.

Different techniques and schemes exist to match MEs with PS. At LO, we have MLM [118], CKKW-(L) [50, 115] methods where a comparative study done in [15] determined the equivalence of their output to a good level of agreement. For the NLO case, the first method that appeared in the literature is the MC@NLO [86] although it depends on the exact PS in order to construct the appropriate counter terms and as a side effect it yields a fraction of events with negative weights that need to be included in the analysis (hence large statistics to obtain sensible distributions). Another method that remedies the previous issues is the POWHEG formalism [125] (**PO**sitive **W**eight **H**ardest **E**mission **G**enerator) which works in a PS independent way and alleviates altogether the issue of negative weights.

For a more inclusive description of any process and a better data description especially at the tail of the distribution, a sequence of (N)LO MEs with an increasing final state multiplicities is generated and combined or *merged* according to some scheme to produce a sample with no double counting and is correct to LL accuracy. A first merging scheme at LO is the CKKW [50, 111] and in the NLO case we have the FxFx scheme [82].

3.8 Monte Carlo tools

We have seen how all MC tools use Monte Carlo methods and techniques as well as rules of quantum field theory to put a physical picture of particle collisions, as these tools are split into simulation, cross-section integrators, analysis tools, ... etc. An example of these tools⁷:

- MG5_aMC@NLO [12] A modular framework for SM phenomenology and beyond. Originally written in Fortran and later supplemented with a command line interface in Python for ease of use. It employs several addons for MEs construction and cross section integration for any process of interest in a fully automated fashion. Events can be generated and matched (after interfacing with a parton shower) up to NLO accuracy and can then be forwarded for analysis.
- Herwig [18, 29] **H**adron **E**mission **R**eactions **W**ith **I**nterfering **G**luons is general purpose event generator, it describes all aspects of a typical SM or BSM event. A library of the most

⁷The list given above is non exhaustive. Other MC tools (also non-complete list) can be found with associated documentation at: <https://hepforge.org/projects>

interesting MEs is available for full simulation from the hard interaction down to hadron decays. It employs angular ordered parton shower for ISR or FSR (other options exist) and the cluster hadronization model.

- **Pythia** [35] One of the oldest MC codes with knowledge from constant development that carried over 30 years. It simulates all aspects of high energy events at all particle colliders, from perturbative to non-perturbative ones. It uses a k_t ordered parton shower for initial and final state radiation, the string hadronization model.
- **Sherpa** [39] **S**imulation of **H**igh energy **R**eactions of **P**Aarticles is a general purpose event generator. From a library of processes, events are generated and then showered using a variety of formalisms.
- **MCFM** [45] **M**onte **C**arlo for **F**e**M**tobarn processes is a MC code for parton-level physics studies. with a library containing various MEs at hadron colliders, the cross section can be calculated for such processes up to NNLO accuracy for certain processes and certain kinematical histograms can be filled on the fly using weighted events.
- **Rivet** [34] **R**obust **I**ndependent **V**alidation of **E**xperiment and **T**heory is the go to toolkit for experiment data as well as MC generators analysis and validation. With a large collection of analyses (over 900), the validation and tuning of any SM (or BSM) prediction is made efficient.
- **MadAnalysis5** [63] A widely used and flexible analysis tool. With a growing database for data reinterpretation and validation, signal discrimination and setting exclusion limits on models by using confidence level (CL) prescription.

Chapter 4

Azimuthal decorrelation in Z +jet process @ LHC.

The process of production of a Z boson in association with a high- p_t jet in proton-proton collisions is of great importance for LHC physics. It has been used in various ways to test the Standard Model and make precision measurements. It is also a significant background to many important processes for LHC physics such as top quark and Higgs boson production. Precise phenomenological calculations as well as experimental measurements of observables related to this process can therefore be very valuable in the identification of signal events from larger background ones.

In the transverse plane to the beam, the jet and Z boson are produced back-to-back at the partonic Born order with an azimuthal angle between them equal to π . A deviation from this back-to-back configuration due to additional radiation from the incoming or outgoing partons causes a decorrelation $\delta\phi$ of the azimuthal angle between the Z boson and the jet. The quantity $\delta\phi$ has been studied extensively (both phenomenologically and experimentally) in various processes and between different particles and/or jets at several colliders. It has been considered between di-jets produced in deep-inelastic $e-p$ scattering (DIS) [9, 23] as a probe of small-Bjorken- x BFKL dynamics, and in hadron-hadron [7, 4, 100, 99, 2, 134, 3] and ion-hadron [3] collisions. Using this quantity the ATLAS collaboration measured the strong coupling α_s and its running at high energy scales [2]. Azimuthal decorrelation between hadrons (instead of jets) has also been studied in di-jet production in DIS and in e^+e^- annihilation [21, 98]. The observable of interest in this thesis, i.e.,

the azimuthal decorrelation between a Z boson and a jet produced in hadron-hadron collisions, has been studied in refs. [5, 58, 137, 59, 144, 60, 1].

When the jets are reconstructed with the p_t -weighted scheme in sequential recombination algorithms such as the k_t [49, 79] or anti- k_t [42] clustering algorithms, the resummation of the azimuthal decorrelation is relatively straightforward. For instance, in ref. [23] the di-jet azimuthal decorrelation in DIS was fully resummed at NLL accuracy. Additionally, the resummation of the Z -jet azimuthal decorrelation has been achieved in the transverse-momentum-dependent factorisation formalism [137], and in the soft-collinear effective theory formalism up to NNLL accuracy [59, 60], where in the latter the axis of the jet is defined by the direction of the highest- p_t particle in the jet (known as the winner-take-all recombination scheme [33]).

In this chapter we consider the azimuthal decorrelation distribution when the jets are clustered with the E -scheme in the k_t or anti- k_t algorithms. We perform an NLL resummation of this distribution in the Fourier space conjugate to $\delta\phi$. We also improve the accuracy of the fixed-order expansion of our distribution up to NNLL accuracy, i.e., controlling up to $\alpha_s^n L^{2n-2}$ at all orders. We additionally verify the validity of our resummation by comparing its one-loop expansion with a fixed-order MC distribution obtained with MadGraph5_aMC@NLO [12] and MCFM [45]. This confirms that our resummation correctly captures the double and single logarithms, at least at one loop.

This chapter is organised as follows. In the next section we give the kinematic definitions involved in the azimuthal decorrelation observable between the Z boson and the leading jet and show how this definition changes over different recombination schemes of the jet algorithm, and the impact of this on the resummation. In section 3 we perform the resummation of the large global logarithms up to NLL accuracy in the Fourier space of the azimuthal decorrelation variable. We conclude this chapter by inverting the resummed result from Fourier space back to $\delta\phi$ space. We also include the fixed-order NLO corrections in our distribution and show that our resummation correctly reproduces all the large logarithms at $\mathcal{O}(\alpha_s)$ by comparing to the NLO distribution of $\delta\phi$ obtained with MadGraph5_aMC@NLO and MCFM.

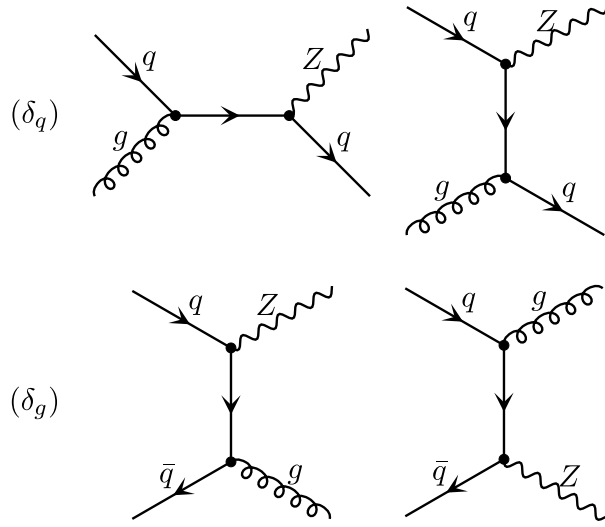


Figure 4.1: Leading order Feynman diagrams contributing to Z +jet process at Born level.

4.1 Kinematics and observable definition

In this chapter we consider the process of production of a Z boson and a jet J at hadron colliders. There are two partonic channels contributing to the Born process, as shown in figure 4.1, specifically $(\delta_g) : q\bar{q} \rightarrow Zg$ and $(\delta_q) : qg \rightarrow Zq$.¹ Beyond the Born level this process is showered by soft/collinear emissions from both initial-state and final-state hard partons. For the purpose of this chapter, and in order to achieve NLL accuracy, it suffices to assume the eikonal approximation in which the emissions are strongly ordered such that at order n we have $k_{tn} \ll \dots \ll k_{t2} \ll k_{t1} \ll p_t$. The transverse momenta of the outgoing particles in the plane perpendicular to the beam axis are given by

$$\vec{\mathbf{p}}_{tZ} = \tilde{p}_t (1, 0), \quad (4.1a)$$

$$\vec{\mathbf{p}}_{tJ} = p_t (\cos(\pi - \epsilon), \sin(\pi - \epsilon)), \quad (4.1b)$$

$$\vec{\mathbf{k}}_{ti} = k_{ti} (\cos \phi_i, \sin \phi_i), \quad (4.1c)$$

with \tilde{p}_t , p_t , and k_{ti} being, respectively, the transverse momenta of the Z boson, the hard parton initiating the jet J , and the emitted soft gluon (i). Moreover, ϕ_i is the azimuthal angle of the soft emission (i) measured with respect to the beam axis. At the Born level the J and Z are exactly back-to-back in the transverse plane, that is, the azimuthal angle between them is exactly

¹The channel (δ_q) also includes incoming anti-quarks, i.e. $\bar{q}g \rightarrow Z\bar{q}$.

π . At higher orders, when there are accompanying soft emissions, a small “decorrelation” $|\epsilon| \ll 1$ between them occurs. Without loss of generality we fixed the azimuthal angle of the Z boson to be 0 and that of the hard parton J to be $\pi - \epsilon$. From conservation of momentum, specifically the y component, we infer that ϵ is expressed at order n in terms of the transverse momenta k_{ti} at NLL accuracy as

$$\epsilon = - \sum_i^n \frac{k_{ti}}{p_t} \sin \phi_i. \quad (4.2)$$

When clustering the jets with a given jet algorithm, there are three commonly-used recombination schemes. In the E -scheme, which is the most common one, the four-momentum of the jet is simply defined to be the sum of the four-momenta of its particle constituents, $p_J = \sum_{i \in J} p_i$. The jet transverse momentum p_{tJ} , rapidity η_J , and azimuthal angle ϕ_J are then deduced from the resulting four-momentum. In the p_t -weighted scheme, the p_{tJ} , η_J , and ϕ_J of the jet are defined by

$$p_{tJ} = \sum_{i \in J} p_{ti}, \quad (4.3a)$$

$$\eta_J = \frac{1}{p_{tJ}} \sum_{i \in J} p_{ti} \eta_i, \quad (4.3b)$$

$$\phi_J = \frac{1}{p_{tJ}} \sum_{i \in J} p_{ti} \phi_i. \quad (4.3c)$$

Additionally there is the “Winner-Take-All” (WTA) scheme [33] in which the direction of the jet axis (and thus the jet rapidity and azimuth) is defined to be that of the hardest parton within it, and its transverse momentum is the scalar sum of its constituent transverse momenta as in eq. (4.3a).² The ATLAS and CMS collaborations at the LHC and the DØ collaboration at the Tevatron employ the E -scheme, while the H1 collaboration at HERA uses the p_t -weighted scheme.

In the p_t -weighted scheme, the Z -jet azimuthal decorrelation observable $\delta\phi$ may be shown to depend on the emission of the soft gluons at order n as

$$\delta\phi^{p_t\text{-weighted}} = \left| \sum_i^n \frac{k_{ti}}{p_t} (\sin \phi_i - \Theta_{iJ}(\pi - \phi_i)) \right|. \quad (4.4)$$

²In all cases, the recombination scheme is applied at each intermediate iteration step to define pseudo-jets during the clustering.

Furthermore, in the WTA scheme, the observable becomes

$$\delta\phi^{\text{WTA}} = \left| \sum_i^n \frac{k_{ti}}{p_t} \sin\phi_i \right|. \quad (4.5)$$

In the above two definitions, the sum over i extends over *all* emissions in the event, and $\Theta_{iJ} = 1$ if gluon i is clustered into the jet J and 0 otherwise. Being inclusive over emissions in the entire angular phase space, the definitions above make the observable *continuously* global,³ as has been established in the literature [23, 59, 60, 27]. Consequently, the resummation of this observable in these two cases is relatively straightforward since it does not require the non-trivial treatment of NGLs and/or CLs.

Employing the E -scheme, on the other hand, the decorrelation is caused only by the emitted soft gluons that do not get clustered to the jet. We thus define the observable to be studied in this thesis as

$$\delta\phi = \left| \sum_{i \notin J}^n \frac{k_{ti}}{p_t} \sin\phi_i \right|, \quad (4.6)$$

where the sum excludes all emissions that end up inside the jet after applying the jet algorithm. This situation is similar to gap-energy observables which are sensitive to emissions in the rapidity gap between two jets. Therefore the observable under consideration is non-global [65, 67], and to achieve NLL accuracy one is forced to properly address the resummation of NGLs and/or CLs.

4.2 Global resummation

At small values of $\delta\phi$ one may expect the distribution to behave like a Sudakov form factor. While this is correct for a wide range of values of $\delta\phi$ this observation actually fails at very small $\delta\phi$. To explain this, we note that the azimuthal decorrelation $\delta\phi$ as defined in eq. (4.6) is the *algebraic* sum of the y components of momenta of emitted gluons, normalised to p_t . This implies that the small values of $\delta\phi$ may well be obtained by cancellation of hard emissions instead of suppression of soft emissions. This observation is similar to that made by Parisi and Petronzio in ref. [126] for transverse momentum distributions. The implication of this fact is the failure of

³In the p_t -weighted scheme, although the dependence of $\delta\phi$ on emissions inside and outside the jet are different, the observable is still global because its dependence on k_t is linear in both cases.

the strong hierarchy of the logarithmic accuracy, $LL \gg NLL \gg NNLL \dots$, in the distribution at very small values of $\delta\phi$. Nevertheless, as we shall show, at small and intermediate values of $\delta\phi$ the resummation based on the soft gluon suppression, and combined with fixed-order NLO effects, provides a good description of the distribution obtained with MC parton showers.

To achieve NLL resummation we need to treat three types of gluon emissions off the three primary hard partons, namely

- primary soft and/or collinear emissions outside the jet, resulting in global logarithms,
- primary soft wide-angle emissions inside or outside the jet, resulting in CLs,
- secondary non-Abelian soft emissions, resulting in NGLs.

In this section we address the former contribution and leave the discussion of the other two contributions to the next chapter. To compute the differential cross-section $1/\sigma d\sigma/d\delta\phi$ we first evaluate the integrated distribution defined by the cross-section $\sigma(\Delta)$ for events with azimuthal decorrelation $\delta\phi$ being less than some value Δ . To this end we compute the integrated cross-section (following the notation adopted in refs. [27, 145, 66])

$$\sigma_{\text{sc}}^{\text{R}}(\Delta) = \sum_{\delta} \int d\mathcal{B}_{\delta} \frac{d\sigma_{0\delta}}{d\mathcal{B}_{\delta}} \Xi_{\mathcal{B}} \sum_{n=1}^{\infty} \int dP_n \Theta \left(\Delta - \left| \sum_{i \notin J}^n \frac{k_{ti}}{p_t} \sin \phi_i \right| \right), \quad (4.7)$$

where the subscript “sc” indicates that we have only considered soft-collinear emissions, and the superscript “R” indicates real-emission contributions. Virtual corrections and hard collinear contributions will be included later. Here $d\sigma_{0\delta}/d\mathcal{B}_{\delta}$ is the differential Born cross-section for the process channel δ and $\Xi_{\mathcal{B}}$ denotes kinematical cuts. The explicit expression for $d\sigma_{0\delta}/d\mathcal{B}_{\delta}$ together with the differential Born configuration $d\mathcal{B}_{\delta}$ are presented in detail in ref. [145]. In the eikonal approximation, one can write the probability of independent emission of n primary soft gluons off the three hard partons (q, \tilde{q}, g) outside the jet as [101, 19]

$$dP_n = \frac{1}{n!} \prod_{i=1}^n \sum_{(\alpha\beta)} \mathcal{C}_{\alpha\beta} \frac{\alpha_s(\kappa_{ti,\alpha\beta}^2)}{\pi} \frac{dk_{ti}}{k_{ti}} d\eta_i \frac{d\phi_i}{2\pi} w_{\alpha\beta}^i \Theta_{\text{out}}(k_i), \quad (4.8)$$

where $\sum_{(\alpha\beta)}$ is the sum over the three dipoles formed by the three hard legs (q, \tilde{q}, g) , and $\mathcal{C}_{\alpha\beta}$ is the colour factor associated with the dipole $(\alpha\beta)$. We have $\mathcal{C}_{q\tilde{q}} = -1/N_c$ for dipoles involving quarks

only and $\mathcal{C}_{qg} = N_c = 3$ for dipoles involving a quark and a gluon. Here α_s is the strong coupling defined in the bremsstrahlung Catani-Marchesini-Webber (CMW) scheme [54], and its argument is the invariant transverse momentum of the emission (i) with respect to the dipole emitting it [52, 53, 56], $\kappa_{ti,\alpha\beta}^2 = k_{ti}^2/\omega_{\alpha\beta}^i$, where the antenna function is defined by

$$w_{\alpha\beta}^i = \frac{k_{ti}^2}{2} \frac{p_\alpha \cdot p_\beta}{(p_\alpha \cdot k_i)(p_\beta \cdot k_i)}. \quad (4.9)$$

We restrict all emissions to be outside the hard jet with the step function

$$\Theta_{\text{out}}(k_i) = \Theta \left[(\eta_i - y)^2 + (\phi_i - \pi)^2 - R^2 \right], \quad (4.10)$$

with R the jet radius and η_i and y the rapidities of gluon (i) and the outgoing hard parton initiating the jet, respectively. While this correctly captures all logarithms originating from primary emissions in the anti- k_t clustering algorithm, it still needs corrections from CLs contributing at the NLL level when employing the k_t algorithm, as we shall explain in the next section.

To proceed we factorise the step function using its Fourier representation by writing

$$\Theta \left(\Delta - \left| \sum_{i \notin J}^n \frac{k_{ti}}{p_t} \sin \phi_i \right| \right) = \int_{-\infty}^{\infty} \frac{db}{\pi b} \sin(b \Delta) \prod_{i \notin J}^n e^{i b k_{ti} \sin \phi_i / p_t}. \quad (4.11)$$

This factorised form, together with the factorised emission amplitude squared and phase space, allows us to exponentiate the integrated distribution as follows

$$\sigma_{\text{sc}}(\Delta) = \sum_{\delta} \int d\mathcal{B}_{\delta} \frac{d\sigma_{0\delta}}{d\mathcal{B}_{\delta}} \Xi_{\mathcal{B}} \int_{-\infty}^{\infty} \frac{db}{\pi b} \sin(b \Delta) \exp[-\mathcal{R}_{\delta}(b)], \quad (4.12)$$

where the radiator for channel δ is given by

$$\mathcal{R}_{\delta}(b) = - \sum_{(\alpha\beta)} \mathcal{C}_{\alpha\beta} \int \frac{\alpha_s(\kappa_{t,\alpha\beta}^2)}{\pi} \frac{dk_t}{k_t} d\eta \frac{d\phi}{2\pi} \Theta_{\text{out}}(k) w_{\alpha\beta}^k (e^{i b k_t \sin \phi / p_t} - 1). \quad (4.13)$$

The integration over k_t extends from 0 to the hard scale p_t . Notice that our resummed formula (4.12) now includes virtual corrections at all orders through the last term (-1) that appears in the radiator (4.13).

The next step is to employ the following approximation, which is valid at NLL accuracy,

$$- \left(e^{i b k_t \sin \phi / p_t} - 1 \right) \approx \Theta \left(k_t |\sin \phi| - p_t / \bar{b} \right), \quad (4.14)$$

where $\bar{b} = b e^{\gamma_E}$ and $\gamma_E \approx 0.577$ is the Euler-Mascheroni constant. This enables us to reduce the range of integration over b by making the replacement $\int_{-\infty}^{\infty} db \rightarrow 2 \int_0^{\infty} db$ since the integrand becomes an even function in b .

In appendix A we perform at NLL accuracy the integrations over k_t , η and ϕ for the three dipole contributions to the radiator, and present its expression in b space in the standard form. Note that including *hard-collinear* emissions (as we do in the appendix) involves evolving the scale of the parton distribution functions (PDFs) from the factorisation scale μ_f to μ_f / \bar{b} [22]. Further details about this and about how to perform the b integration will be discussed in section 5. In the next section, we consider corrections to the radiator due to CLs and NGLs at two loops and to all orders.

4.3 Results in Δ space

4.3.1 Evaluation of the b integral

One approach that can be employed to evaluate the b integral analytically in order to obtain the resummed distribution in Δ space is to expand the radiator as a Taylor series around the saddle point $\bar{b}_0 = 1/\Delta$

$$\mathcal{R}_\delta(\bar{b}) = \mathcal{R}_\delta(1/\Delta) + \mathcal{R}'_\delta(1/\Delta) (\ln \bar{b} - \ln \bar{b}_0), \quad (4.15)$$

with

$$\mathcal{R}'_\delta(\bar{b}) = \frac{\partial \mathcal{R}_\delta(\bar{b})}{\partial \ln \bar{b}}. \quad (4.16)$$

In the non-global and clustering logarithmic functions as well as in PDFs one simply makes the substitution $\bar{b} \rightarrow 1/\Delta$. One can then perform the integration over b in eq. (4.12) using

$$\int_0^\infty \frac{db}{b} \sin(b \Delta) \exp[-\mathcal{R}'_\delta \ln \bar{b}] = \exp[(-\gamma_E + \ln(1/\Delta)) \mathcal{R}'_\delta] \Gamma[-\mathcal{R}'_\delta] \sin\left(-\frac{\pi}{2} \mathcal{R}'_\delta\right). \quad (4.17)$$

Hence the integrated distribution is given by

$$\begin{aligned} \sigma(\Delta) = & \sum_{\delta} \int d\mathcal{B}_{\delta} \frac{d\sigma_{0\delta}}{d\mathcal{B}_{\delta}} \Xi_{\mathcal{B}} \frac{f_a(x_a, \Delta^2 \mu_f^2) f_b(x_b, \Delta^2 \mu_f^2)}{f_a(x_a, \mu_f^2) f_b(x_b, \mu_f^2)} \mathcal{S}_{\delta}(1/\Delta) \mathcal{C}_{\delta}(1/\Delta) \times \\ & \times \exp[-\mathcal{R}_{\delta}(1/\Delta) - \gamma_E \mathcal{R}'_{\delta}(1/\Delta)] \frac{2}{\pi} \Gamma[-\mathcal{R}'_{\delta}] \sin\left(-\frac{\pi}{2} \mathcal{R}'_{\delta}\right), \end{aligned} \quad (4.18)$$

with f_i being the PDF of the incoming parton $i = \{a, b\}$, x_i the momentum fraction carried by it, and μ_f the factorisation scale.

The above expression for the integrated cross-section has a divergence when $\mathcal{R}'_{\delta}(1/\Delta) = 1$. The divergence reaches values of Δ up to 0.3 depending on the value of the jet p_t , and is always above 0.12 for the quark channel contribution. This means that this approach is not well suited for phenomenological studies since the impact of the divergence on the distribution is quite severe.

In order to be able to avoid this divergence and other ambiguities we follow a commonly used approach in which we perform the b integral numerically. We proceed in the following way:

- We avoid the Landau-pole singularity in the radiator at $\bar{b}_{\max} = \exp[1/(2\alpha_s\beta_0)]$ by cutting off the b integral at $\bar{b} = \bar{b}_{\max}$ setting the radiator to ∞ (and thus the integrand to zero) above this value.
- We avoid low scales in the PDFs (which correspond to large values of b) by making the replacement $b \rightarrow b^* = b/\sqrt{1+b^2/b_{\text{lim}}^2}$ in the radiator and PDFs [62], where we choose $b_{\text{lim}} = \mu_f^2/Q_0^2$ and $Q_0 \sim 1 \text{ GeV}$ is a cutoff scale for PDFs.
- At small b the real and virtual contributions cancel each other and therefore the radiator should be equal to zero in the limit $b \rightarrow 0$. We thus freeze both the radiator and the scale of PDFs for values of b that are less than 1.

Hence the expression for the cross-section to be numerically integrated is written as follows

$$\begin{aligned} \sigma(\Delta) = & \sum_{\delta} \int d\mathcal{B}_{\delta} \frac{d\sigma_{0\delta}}{d\mathcal{B}_{\delta}} \Xi_{\mathcal{B}} \left[\frac{2}{\pi} \text{Si}(\bar{\Delta}) + \frac{2}{\pi} \int_1^{\bar{b}_{\max}} \frac{db}{b} \sin(b\bar{\Delta}) \times \right. \\ & \left. \times \frac{f_a(x_a, \mu_f^2/b^{*2}) f_b(x_b, \mu_f^2/b^{*2})}{f_a(x_a, \mu_f^2) f_b(x_b, \mu_f^2)} \mathcal{S}_{\delta}(b^*) \mathcal{C}_{\delta}(b^*) \exp[-\mathcal{R}_{\delta}(b^*)] \right], \end{aligned} \quad (4.19)$$

with Si standing for the Sine-integral function (i.e) and $\bar{\Delta} = \Delta e^{-\gamma_E}$.

4.3.2 Convolution with the Born cross-section

To obtain the integrated distribution we generate a sample of parton-level Born events for the process of production of a Z boson⁴ and a jet in proton-proton collisions, at centre-of-mass energy $\sqrt{s} = 7 \text{ TeV}$, using MadGraph5 [117, 12] in the “Les Houches Event File” format [14]. We use CTEQ6L PDFs [130] interfaced to MadGraph5 through LHAPDF6 [41] with fixed renormalisation and factorisation scales $\mu_f = \mu_r = 150 \text{ GeV}$. In the event generation we use the same experimental cuts $\Xi_{\mathcal{B}}$ as those employed by the CMS collaboration in ref. [58]. Specifically, the Z boson is required to have $\tilde{p}_t > 150 \text{ GeV}$ and we require at least one jet with transverse momentum $p_t > 50 \text{ GeV}$ and rapidity $|y| < 2.5$. The jets have radius $R = 0.5$ and we use both k_t and anti- k_t clustering.

The generated events are then analysed using MadAnalysis 5 [63], where each Born event $d\mathcal{B}_{\delta}$ is weighed by the integrand shown in the square brackets in eq. (4.19) after performing the b integration numerically using the GSL-GNU Scientific Library. The integrated distribution is then obtained by summing all the event weights and dividing by the effective luminosity $\mathcal{L} = N_{\text{tot}}/\sigma_0$, with N_{tot} the total number of events and σ_0 the cross-section for the generated parton-level Born events. The differential distribution is then easily obtained by straightforward numerical differentiation.

4.3.3 NNLL corrections at two loops

At $\mathcal{O}(\alpha_s^n)$ in the perturbative expansion, the logarithm $\alpha_s^n L^{2n-2}$ is not fully accounted for by the resummation. We can incorporate such an NNLL term⁵ by computing the NLO fixed-order correction term $\alpha_s C_1^{(\delta)}(\mathcal{B}_{\delta})$ for the channel δ and the differential Born configuration \mathcal{B}_{δ} . To see this we note that the sub-leading logarithms $\alpha_s^n L^{n-1}$, not accounted for in the exponent of the resummed result, produce at most an $\mathcal{O}(\alpha_s^n L^{2n-3})$ term when expanded at fixed order, which means they contribute at NNNLL accuracy. On the other hand, the cross-talk of the constant term $\alpha_s C_1^{(\delta)}(\mathcal{B}_{\delta})$ with the expansion of the controlled double logarithms in the exponent $\alpha_s^n L^{2n}$ produce the NNLL terms $\alpha_s^{n+1} L^{2n} \sim \alpha_s^n L^{2n-2}$ [28].

⁴The Z boson is chosen not to decay. This only affects the total cross-section and does not impact the resummed distribution when it is normalised to the Born cross-section.

⁵In the *perturbative expansion*, LL refers to $\alpha_s^n L^{2n}$, NLL refers to $\alpha_s^n L^{2n-1}$, and NNLL refers to $\alpha_s^n L^{2n-2}$. This hierarchy is different from the logarithmic accuracy in the *exponent* of the resummed distribution.

This constant term may be computed by fully subtracting the large single ($\alpha_s \ln(1/\Delta)$) and double ($\alpha_s \ln^2(1/\Delta)$) logarithms from the full NLO Born-differential distribution [28]

$$\alpha_s C_1^{(\delta)}(\mathcal{B}_\delta) = \frac{1}{d\sigma_{0\delta}/d\mathcal{B}_\delta} \lim_{\Delta \rightarrow 0} \left[\int_0^\Delta \frac{d^2\sigma_{\text{NLO}}^{(\delta)}}{d\mathcal{B}_\delta d\delta\phi} d\delta\phi - \frac{d\sigma_1^{(\delta)}(\Delta)}{d\mathcal{B}_\delta} \right], \quad (4.20)$$

where $d^2\sigma_{\text{NLO}}^{(\delta)}/d\mathcal{B}_\delta d\delta\phi$ is the NLO differential cross-section in both $\delta\phi$ and the Born configuration \mathcal{B}_δ for channel δ , and $d\sigma_1^{(\delta)}/d\mathcal{B}_\delta$ is the contribution of the channel δ to the expansion of the differential (in \mathcal{B}_δ) resummed distribution up to $\mathcal{O}(\alpha_s)$. The corrected integrated resummed distribution (in its formal form) is then written as

$$\begin{aligned} \sigma(\Delta) &= \sum_\delta \int d\mathcal{B}_\delta \frac{d\sigma_{0\delta}}{d\mathcal{B}_\delta} \Xi_{\mathcal{B}} \left(1 + \alpha_s C_1^{(\delta)}(\mathcal{B}_\delta) \right) \times \\ &\times \frac{2}{\pi} \int_0^\infty \frac{db}{b} \sin(b\Delta) \frac{f_a(x_a, \mu_f^2/\bar{b}^2) f_b(x_b, \mu_f^2/\bar{b}^2)}{f_a(x_a, \mu_f^2) f_b(x_b, \mu_f^2)} \mathcal{S}_\delta(\bar{b}) \mathcal{C}_\delta(\bar{b}) \exp[-\mathcal{R}_\delta(\bar{b})]. \end{aligned} \quad (4.21)$$

The computation of the Born-differential NLO cross-section (either numerically or analytically) is complicated. For the purpose of this work, we define $\alpha_s C_1^{(\delta)}$ to be the average value over the Born configuration \mathcal{B}_δ

$$\langle \alpha_s C_1^{(\delta)} \rangle = \frac{1}{\sigma_{0\delta}} \int d\mathcal{B}_\delta \frac{d\sigma_{0\delta}}{d\mathcal{B}_\delta} \Xi_{\mathcal{B}} \alpha_s C_1^{(\delta)}(\mathcal{B}), \quad (4.22)$$

and replace $\alpha_s C_1^{(\delta)}(\mathcal{B})$ by its average value $\langle \alpha_s C_1^{(\delta)} \rangle \equiv \alpha_s C_1^{(\delta)}$ for each channel.

4.3.4 Comparison to MC results at fixed order

One can verify that the resummed distribution correctly captures the large single and double logarithms when expanded at $\mathcal{O}(\alpha_s)$ by comparing it with the results obtained from fixed-order programs such as MadGraph5_aMC@NLO and MCFM. The expanded distribution at $\mathcal{O}(\alpha_s)$ is given by

$$\sigma_1(\Delta) = \sum_\delta \int d\mathcal{B}_\delta \frac{d\sigma_{0\delta}}{d\mathcal{B}_\delta} \Xi_{\mathcal{B}} \left(1 + G_{11}^{(\delta)} \frac{\alpha_s}{\pi} \ln \frac{1}{\Delta} + G_{12}^{(\delta)} \frac{\alpha_s}{\pi} \ln^2 \frac{1}{\Delta} \right). \quad (4.23)$$

The expressions of the coefficients $G_{11}^{(\delta)}$ and $G_{12}^{(\delta)}$ are given in appendix B. We perform the integration over the Born configuration $d\mathcal{B}_\delta$ exactly as described in the previous subsections.

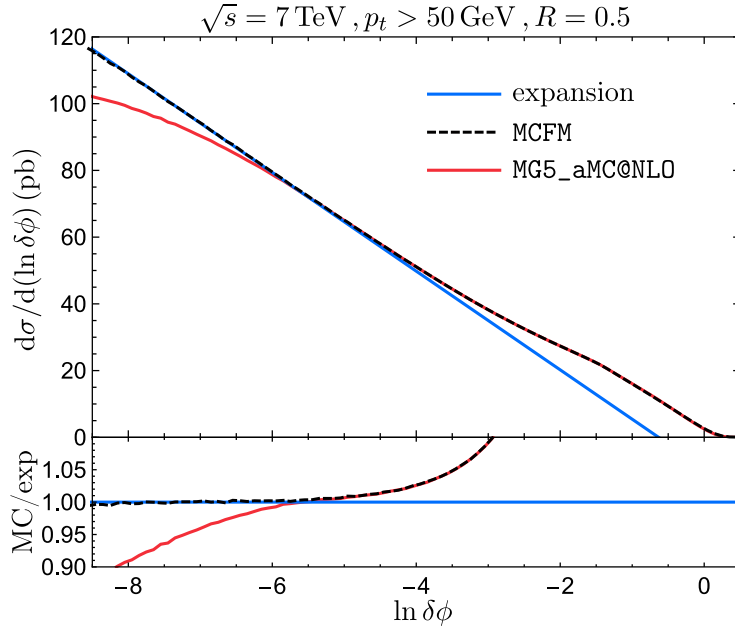


Figure 4.2: Comparison of the differential distributions $d\sigma/d(\ln \delta\phi)$ obtained by expanding the resummed distribution up to $\mathcal{O}(\alpha_s)$ and output from fixed-order programs `MadGraph5_aMC@NLO` and `MCFM`.

We show in figure 4.2 a comparison between the differential expanded distribution (obtained by differentiating eq. (4.23) with respect to Δ) and the fixed-order MC distribution obtained with `MadGraph5_aMC@NLO` and `MCFM`. At NLO the channel separation becomes non-trivial due to the presence of other sub-processes, such as $qq \rightarrow qq$.

Three things to observe in the plots. First, the `MCFM` and expansion results agree up to values of $\delta\phi$ around 0.01. At larger values of $\delta\phi$ the logarithms are not enhanced and NLO effects, not accounted for by resummation, dominate the MC distribution. Second, the `MadGraph5_aMC@NLO` distribution agrees with `MCFM` result over the entire range of $\delta\phi$ down to $\delta\phi$ around 0.003, where we deviations due to integration precision are expected to affect the distribution. Third, there is a kinematical cutoff in the exact NLO MC distribution at around $\delta\phi = 1.54$ (slightly less than $\pi/2$). This cutoff depends on the value of the cut on \tilde{p}_t of the Z boson, and may be shown to be given by the expression

$$\cos \delta\phi^{\max} = \frac{\tilde{p}_{t,\text{cut}}}{\sqrt{s} - \sqrt{\tilde{p}_{t,\text{cut}}^2 + m_Z^2}} \approx \frac{\tilde{p}_{t,\text{cut}}}{\sqrt{s}}, \quad (4.24)$$

where m_Z is the Z boson mass. For $\sqrt{s} = 7 \text{ TeV}$ and $\tilde{p}_{t,\text{cut}} = 150 \text{ GeV}$ this yields $\delta\phi^{\max} = 1.549$.

Chapter 5

Non-global and clustering logarithms in Z+jet process

5.1 Non-global logarithms at 2-loops

At $\mathcal{O}(\alpha_s^2)$, NGLs [65, 67] originate when a soft gluon k_1 is emitted inside the jet, which itself coherently emits another softer gluon k_2 outside of it without being clustered back to the jet [17]. When the softer emission is real it causes a small decorrelation of the azimuthal angle between the jet and the Z boson, and when it is virtual the decorrelation is zero, leading to a real-virtual mismatch in the contribution to the integrated distribution. This configuration is opposite to the jet mass observable where NGLs originate when the harder emission is outside the jet while the softer is inside [66, 145].

The non-global logarithmic contribution to the integrated distribution at $\mathcal{O}(\alpha_s^2)$ may be written as follows [66]

$$\frac{1}{\sigma_{0,\delta}} \sigma_{2,\delta}^{\text{NG}}(\Delta) = -\frac{1}{2!} \frac{\alpha_s^2}{\pi^2} \ln^2 \frac{1}{\Delta} \mathcal{G}_2^\delta(R), \quad (5.1)$$

where $\sigma_{0,\delta}$ denotes the Born cross-section for channel δ . In the anti- k_t algorithm the radius-

dependent function $\mathcal{G}_2^\delta(R)$ is expressed as

$$\begin{aligned}\mathcal{G}_2^{\delta,\text{akt}}(R) &= C_A \sum_{(ij)} \mathcal{C}_{ij} R^4 \int_0^1 r_1 dr_1 \frac{d\theta_1}{2\pi} \int_1^{\pi/(R|\sin\theta_2|)} r_2 dr_2 \frac{d\theta_2}{2\pi} \mathcal{A}_{ij}^{12} \\ &\equiv C_A \sum_{(ij)} \mathcal{C}_{ij} \mathcal{G}_2^{(ij),\text{akt}}(R)\end{aligned}\quad (5.2)$$

where $C_A = N_c$ is the colour factor for the secondary gluon emission, r_i and θ_i are polar variables in the $(\eta_i - \phi_i)$ plane defined by $\eta_i = y + R r_i \cos \theta_i$ and $\phi_i = \pi + R r_i \sin \theta_i$, and \mathcal{A}_{ij}^{12} is the irreducible antenna function for the correlated emission of the two gluons k_1 and k_2 off the hard dipole (ij)

$$\mathcal{A}_{ij}^{12} = w_{ij}^1 (w_{i1}^2 + w_{1j}^2 - w_{ij}^2). \quad (5.3)$$

Notice that \mathcal{A}_{ij}^{12} is symmetric under the exchange $k_1 \leftrightarrow k_2$. This means that the integral (5.2) is exactly identical to that for the jet mass observable in refs. [66, 145], with the change of variable $k_1 \leftrightarrow k_2$. Hence, at two loops, the coefficient of NGLs in the anti- k_t algorithm is identical for both observables. We expect, however, NGLs to be different at higher orders since the phase space is not symmetric under the exchange of the gluons and, at finite N_c , the squared amplitudes too are not symmetric.

The expressions for the dipole functions $\mathcal{G}_2^{(ij)}(R)$ have been computed in refs. [66, 145] and the reported results are as follows

$$\mathcal{G}_2^{(ab),\text{akt}} = -R^2 \ln R + 0.500 R^2 + 0.125 R^4 - 0.003 R^6 + \mathcal{O}(R^8), \quad (5.4a)$$

$$\mathcal{G}_2^{(aj),\text{akt}} = \mathcal{G}_2^{(bj),\text{akt}} = 0.822 + 0.003 R^4 + \mathcal{O}(R^8). \quad (5.4b)$$

Combining the results for the different channels one has

$$\begin{aligned}\mathcal{G}_2^{\delta g,\text{akt}} &= C_F C_A [-2 R^2 \ln R + R^2 + 0.250 R^4 - 0.007 R^6 + \mathcal{O}(R^8)] + \\ &+ C_A^2 [1.645 + R^2 \ln R - 0.500 R^2 - 0.118 R^4 + 0.003 R^6 + \mathcal{O}(R^8)],\end{aligned}\quad (5.5a)$$

$$\begin{aligned}\mathcal{G}_2^{\delta q,\text{akt}} &= C_F C_A [1.645 + 0.007 R^4 + \mathcal{O}(R^8)] + \\ &+ C_A^2 [-R^2 \ln R + 0.500 R^2 + 0.125 R^4 - 0.003 R^6 + \mathcal{O}(R^8)],\end{aligned}\quad (5.5b)$$

where $C_F = (N_c^2 - 1)/(2 N_c)$.

In the k_t algorithm, the clustering of particles starts with the softest emissions. Thus the coefficient of NGLs at two loops reads

$$\begin{aligned} \mathcal{G}_2^{\delta, k_t}(R) &= C_A \sum_{(ij)} \mathcal{C}_{ij} R^4 \int_0^1 r_1 dr_1 \frac{d\theta_1}{2\pi} \int_1^{\pi/(R|\sin\theta_2|)} r_2 dr_2 \frac{d\theta_2}{2\pi} \Theta(d_{12} - d_2) \mathcal{A}_{ij}^{12} \\ &= C_A \sum_{(ij)} \mathcal{C}_{ij} \mathcal{G}_2^{(ij), k_t}(R), \end{aligned} \quad (5.6)$$

where the distance measures are defined by $d_i = k_{ti}^2 R^2$ and $d_{ij} = \min(k_{ti}^2, k_{tj}^2) (\delta\eta_{ij}^2 + \delta\phi_{ij}^2)$. The step function $\Theta(d_{12} - d_2)$ forbids the emission k_2 from being clustered to the harder one k_1 , and subsequently to the jet, resulting in the large NGLs as explained above. Here, the clustering step function is not related by symmetry to that for the jet mass observable [145] (given by $\Theta(d_{12} - d_{2j})$), and thus the result is going to be different. In terms of the polar variables, this step function is given by

$$\Theta(d_{12} - d_2) = \Theta[r_1^2 + r_2^2 - 2r_1 r_2 \cos(\theta_1 - \theta_2) - 1]. \quad (5.7)$$

In analogy to the anti- k_t clustering case, we perform the integrations by expanding the antenna function as a power series in the jet radius. We obtain the following results for the various dipole contributions

$$\mathcal{G}_2^{(ab), k_t} = -R^2 \ln R - 0.128 R^2 + 0.177 R^4 - 0.004 R^6 + \mathcal{O}(R^8), \quad (5.8a)$$

$$\mathcal{G}_2^{(aj), k_t} = \mathcal{G}_2^{(bj), \text{akt}} = 0.183 - 0.121 R^2 + 0.007 R^4 + 0.0003 R^6 + \mathcal{O}(R^8). \quad (5.8b)$$

In terms of channels we may write

$$\begin{aligned} \mathcal{G}_2^{\delta_g, k_t} &= C_F C_A [-2 R^2 \ln R - 0.255 R^2 + 0.353 R^4 - 0.009 R^6 + \mathcal{O}(R^8)] + \\ &+ C_A^2 [0.366 + R^2 \ln R - 0.115 R^2 - 0.163 R^4 + 0.005 R^6 + \mathcal{O}(R^8)], \end{aligned} \quad (5.9a)$$

$$\begin{aligned} \mathcal{G}_2^{\delta_q, k_t} &= C_F C_A [0.366 - 0.243 R^2 + 0.014 R^4 + 0.001 R^6 + \mathcal{O}(R^8)] + \\ &+ C_A^2 [-R^2 \ln R - 0.128 R^2 + 0.177 R^4 - 0.004 R^6 + \mathcal{O}(R^8)]. \end{aligned} \quad (5.9b)$$

Note here that, as opposed to the jet mass variable, the small- R limit of this result is half that

reported for the jet mass distribution in $e^+e^- \rightarrow$ di-jet events. We show in figure 5.1 a plot of the overall coefficient of NGLs, $\frac{1}{2} \mathcal{G}_2$, as a function of the jet radius R for the two algorithms and for the two channels. We observe here the sizable coefficient of NGLs in the case of anti- k_t clustering compared to k_t clustering. This observation has been made in previous studies of NGLs with k_t clustering [17, 70]. The latter algorithm tends to reduce the size of NGLs while resulting in another tower of large logarithms known as CLs. This observation implies that using k_t clustering is in fact phenomenologically favoured over anti- k_t since the all-orders resummation of NGLs is in general less accurate than that of CLs, as one has to employ an approximation such as the large- N_c limit.

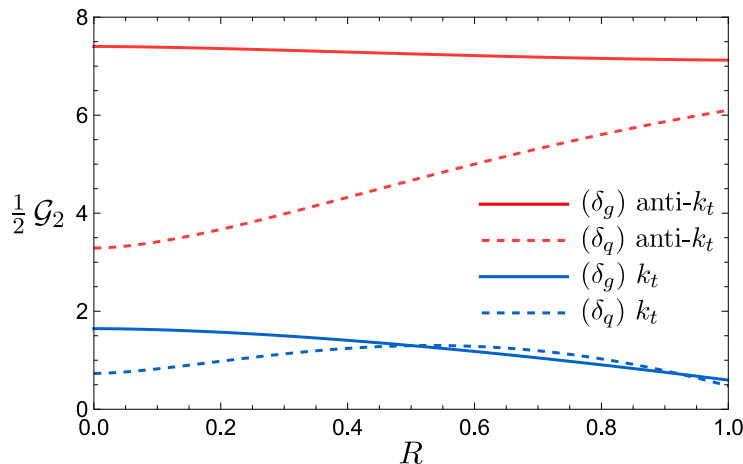


Figure 5.1: The two loops NGL coefficients in k_t and anti- k_t algorithms for the two partonic Born channels $(\delta_{q,g})$.

5.2 Clustering logarithms at 2-loops

As NGLs do, CLs first appear at $\mathcal{O}(\alpha_s^2)$ when two soft gluons are emitted directly from the hard partons (i.e., primary emissions) and when the k_t algorithm is applied on the final-state partons. The phase space that gives rise to CLs is such that the harder emission k_1 is initially inside the jet, $d_{1j} < d_1$,¹ while the softer one k_2 is initially (before clustering) outside, $d_{2j} > d_2$, with the distance between them d_{12} being less than d_2 . Applying the k_t algorithm, when both emissions are real, the softer particle k_2 is clustered to the harder one k_1 and the recombined pseudo-jet is (at NLL accuracy) along the direction of k_1 , and ultimately both partons end up inside the jet

¹The distances d_i and d_{ij} for the k_t algorithm are defined in the previous subsection.

leading to a zero Z -jet azimuthal decorrelation. However, when the particle k_1 is virtual there is no particle to drag the softer real emission k_2 into the jet, and a non-zero decorrelation occurs. Thus we obtain a real-virtual miscancellation which translates into the following contribution to the integrated cross-section at $\mathcal{O}(\alpha_s^2)$

$$\frac{1}{\sigma_{0,\delta}} \sigma_{2,\delta}^{\text{CL}}(\Delta) = \frac{1}{2!} \frac{\alpha_s^2}{\pi^2} \ln^2 \frac{1}{\Delta} \mathcal{F}_2^\delta(R), \quad (5.10)$$

where

$$\mathcal{F}_2^\delta(R) = \sum_{(ij)(\ell m)} \mathcal{C}_{ij} \mathcal{C}_{\ell m} R^4 \int_0^1 r_1 dr_1 \frac{d\theta_1}{2\pi} \int_1^2 r_2 dr_2 \frac{d\theta_2}{2\pi} \Theta(d_2 - d_{12}) w_{ij}^1 w_{\ell m}^2, \quad (5.11)$$

and the sum extends over all 9 dipole pairs (ij) and (ℓm) . The coefficients of CLs for the various channels are given by

$$\begin{aligned} \mathcal{F}_2^{\delta_g}(R) &= C_F^2 0.413 R^4 + C_F C_A [1.510 R^2 - 0.207 R^4 + 0.007 R^6 + \mathcal{O}(R^{10})] + \\ &+ C_A^2 [0.914 - 0.378 R^2 + 0.043 R^4 - 0.002 R^6 + \mathcal{O}(R^8)], \end{aligned} \quad (5.12a)$$

for channel (δ_g) ,

$$\begin{aligned} \mathcal{F}_2^{\delta_q}(R) &= C_A^2 [0.214 R^2 + 0.141 R^4 + 0.001 R^6 + \mathcal{O}(R^{10})] + \\ &+ C_F C_A [0.327 R^2 + 0.027 R^4 + 0.001 R^6 + \mathcal{O}(R^{10})] + \\ &+ C_F^2 [0.914 + 0.592 R^2 + 0.081 R^4 + 0.003 R^6 + \mathcal{O}(R^8)], \end{aligned} \quad (5.12b)$$

for channel (δ_q) .

Figure 5.2 shows a plot of the coefficient of CLs at two loops as a function of the jet radius R for the two channels (δ_q) and (δ_g) . We observe that the gluon channel has quite a large CLs coefficient, even larger than NGLs coefficient in k_t clustering by more than a factor of 2, while the quark channel has a somewhat smaller coefficient. Both coefficients seem to be increasing with R . The overall coefficient of the single logarithm $\alpha_s^2/\pi^2 \ln^2(1/\Delta)$ due to both NGLs and CLs, $\frac{1}{2}(\mathcal{F}_2 - \mathcal{G}_2^{\text{kt}})$, is shown in figure 5.3. For the quark channel NGLs and CLs tend to cancel each other

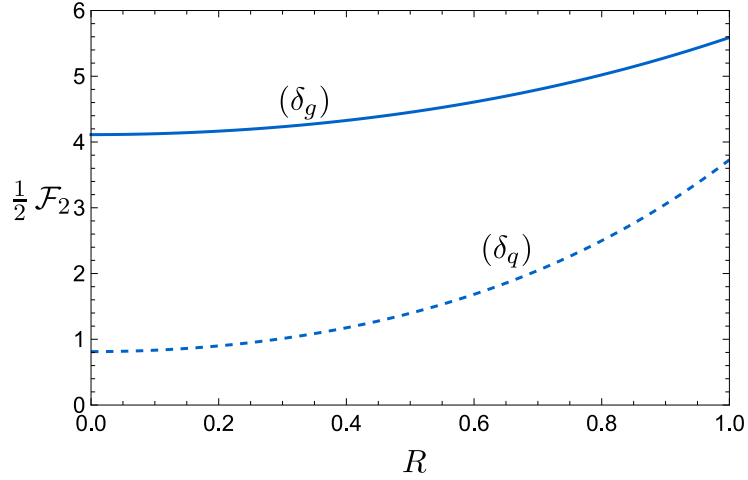


Figure 5.2: The two loops coefficients of CLs for the two partonic Born channels $(\delta_{q,g})$.

for jet radii smaller than about 0.6, while their combination is large for all values of R in the gluon channel. This signifies the importance of the contributions of NGLs and CLs in our distribution for all values of R , as apposed to the jet mass observable where the combined NGLs and CLs are significant only for small values of R , and tend to cancel each other out at larger values of R for both channels [145].

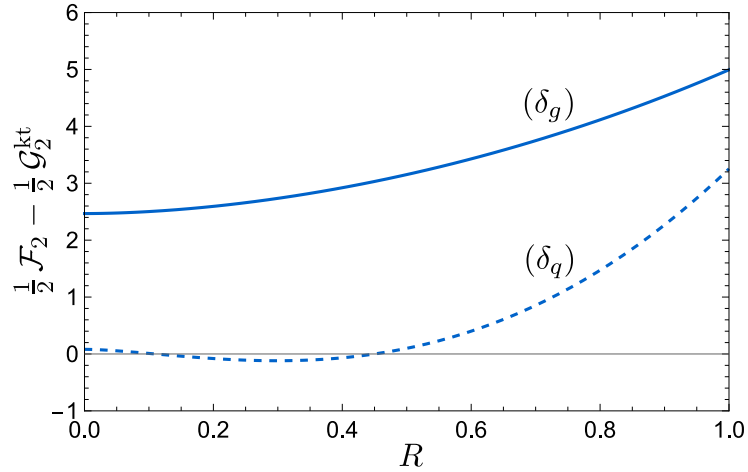


Figure 5.3: The two loops combined NGL and CL coefficients for the two partonic Born channels $(\delta_{q,g})$.

In the next subsection we discuss the all-orders numerical resummation of NGLs and CLs in the large- N_c approximation.

5.3 Non-global & clustering logarithms to all orders

The calculation of NGLs and CLs beyond $\mathcal{O}(\alpha_s^2)$ is difficult due to the complexity of higher-order amplitudes of emission and phase space. NGLs originate from the coherent emission of a single soft gluon clustered outside the hard jet from a group of harder ones which are clustered into the jet. One usually uses a numerical MC approach which employs the large- N_c limit to approximate the all-orders resummation of these emissions.

Recently, a dipole-evolution program (**Gnole**) that resums NGLs at NLL and NNLL accuracy in the large- N_c limit was published [24, 25]. In its current version it is only possible to perform this resummation for observables in single-dipole processes and where NGLs are leading logarithms, i.e., observables defined in regions away from all hard partons, such as rapidity-gap observables and di-jet azimuthal decorrelation in e^+e^- annihilation. Future releases of this program may extend to the resummation of quantities such as the one considered here. In this work we perform the all-orders resummation of NGLs using the code upon which **Gnole** is based, and which was first developed in ref. [65] and adapted in ref. [66]. In the large- N_c limit, one can treat the resummation of NGLs based on the independent evolution of the three hard dipoles in the process [20, 66].

We parameterise the numerical results for the all-orders resummed NGLs obtained for the channel δ in the anti- k_t algorithm by the function [65, 66]²

$$\mathcal{S}_\delta^{\text{ak}_t}(t) = \exp \left(-\frac{t^2}{8} C_A \sum_{(ij)} \mathcal{C}_{ij} \mathcal{G}_2^{(ij), \text{ak}_t} \frac{1 + (a_{ij} C_A t/4)^2}{1 + (b_{ij} C_A t/4)^{c_{ij}}} \right), \quad (5.13)$$

where the evolution parameter is given by

$$t(1/\Delta) = -\frac{1}{\pi\beta_0} \ln(1 - 2\alpha_s\beta_0 \ln(1/\Delta)), \quad (5.14)$$

with β_0 the one-loop coefficient of the QCD beta function (see appendix). Fitting the numerical data to this parametrisation yields the results shown in table 5.1 for the chosen jet radius $R = 0.5$. Notice that the expansion of the parametrisation function at two loops reproduces the results

²Since the program works in the large- N_c limit, and only works with quark dipoles, we set all the colour factors $\mathcal{C}_{ij} = 2C_F = N_c$ during the parametrisation. However, we use the actual colour factors in the resummed form factor.

	(ab)	(aj) and (bj)
a_{ij}	0.446	0.301
b_{ij}	1.882	0.377
c_{ij}	1.33	1.33

Table 5.1: Fit parameters from numerically resummed NGLs for anti- k_t algorithm ($R = 0.5$).

obtained in the previous subsections.

Performing a similar resummation in the k_t algorithm is not straightforward. In order to obtain NGLs and CLs, one has to run the program to compute the overall distribution, and then divide away the global factor that is obtained by allowing only primary emissions directly off the hard Born partons. While this is straightforward in the anti- k_t algorithm, the subtraction is quite difficult in *multi-dipole* processes in the presence of CLs, as was mentioned in ref. [25]. We have verified that the exponential of the two-loops result of NGLs in the anti- k_t algorithm does not produce noticeable differences compared to the numerical all-orders resummed result. Furthermore, the numerical all-orders resummed CLs have been shown to be well approximated by the exponential of the two-loops result in the case of jet mass distribution in di-jet production in e^+e^- annihilation process [71]. We thus adopt for the k_t algorithm this two-loops exponential to approximate the all-orders resummed result for both CLs

$$\mathcal{C}_\delta^{\text{k}_t}(t) = \exp\left(\frac{t^2}{8} \mathcal{F}_2^\delta\right), \quad (5.15)$$

and similarly for the NGLs

$$\mathcal{S}_\delta^{\text{k}_t}(t) = \exp\left(-\frac{t^2}{8} \mathcal{G}_2^\delta\right), \quad (5.16)$$

and where we note that $\mathcal{C}_\delta^{\text{ak}_t}(t) = 1$ in the anti- k_t algorithm.

5.4 Comparison to parton showers and experimental data

In this section we present our results for the resummed distribution $1/\sigma \, d\sigma/d\delta\phi$ and compare our findings with parton shower results obtained with various MC event generators and with experimental data from the CMS collaboration [58]. In the remainder of this section we restrict ourselves to showing preliminary results and comparisons, while we leave other phenomenological studies,

namely matching to fixed order, non-perturbative effects, and uncertainties of the distribution, to our forthcoming work.

We show in figure 5.4 plots of the resummed global distribution (without NGLs/CLs), the resummed distribution in the k_t and anti- k_t algorithms (with CLs/NGLs), and the corrected resummed distribution for NNLL effects at fixed order (including the C_1 constant). We also show, in the same figure, a plot of the fixed-order MC distribution obtained with MadGraph5_aMC@NLO. For small values of $\delta\phi$ the resummed distribution tends towards a constant. This observation may

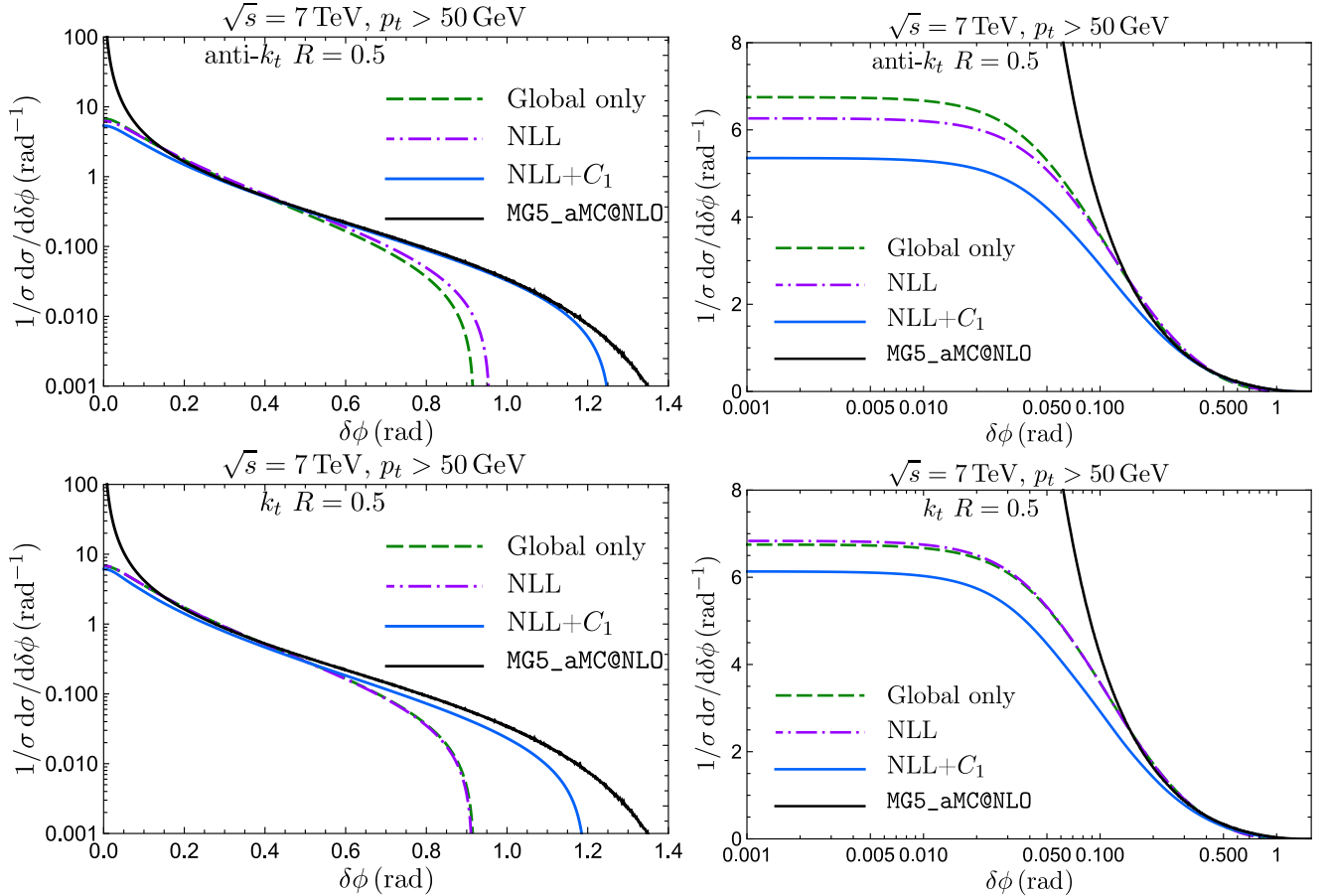


Figure 5.4: The differential distribution $1/\sigma d\sigma/d\delta\phi$ with anti- k_t clustering (top) and k_t clustering (bottom). We show here the global resummed distribution without NGLs/CLs, the full NLL resummed distribution (including NGLs/CLs), and the corrected NLL distribution including the constant C_1 . Also shown is the fixed-order MC result at NLO.

be interpreted, as mentioned earlier, by the fact that the very small values of $\delta\phi$ may be generated by vectorial cancellation of hard emissions which takes over from Sudakov suppression of soft emissions.

In the anti- k_t algorithm and for the value of the jet radius $R = 0.5$ we see that the impact of

NGLs on the distribution is important at small and moderate values of $\delta\phi$. Additionally, including the constant C_1 impacts the distribution both in the small- $\delta\phi$ region as well as in the tail of the distribution, bringing it to a better matching with the fixed-order MC result for values of $\delta\phi$ up to order 1. As for k_t clustering, we note that the impact of NGLs and CLs is not significant for all values of $\delta\phi$, and that including the C_1 constant improves the distribution both at small and large $\delta\phi$, but one still needs the matching in order to obtain a better behaviour at the tail of the distribution. The fixed-order MC distribution behaves reasonably well down to values of $\delta\phi$ of order 0.1, where it starts to behave in a logarithmically divergent way.

As mentioned earlier, at NLO the MC distribution has a kinematical cutoff on the observable around $\pi/2$, when there is only one extra hard emission not clustered to the “measured” jet. However, beyond NLO the distribution receives contributions from two or more extra hard emissions giving possible values of $\delta\phi$ up to π . It therefore makes no sense to perform a matching of the resummed distribution to NLO without including effects of higher jet multiplicities. The matching procedure itself is complicated by the fact that the resummation is performed in b space and we have no analytical form of the resummed distribution in $\delta\phi$ space.

We show in figure 5.5 a comparison of our resummed distribution with parton shower results obtained with Pythia 8 [135, 13], Herwig++ [18, 29] and Sherpa [39]. The Pythia 8 and Herwig++ results are obtained by showering MadGraph5_aMC@NLO events, while the Sherpa results are obtained using the stand-alone version. In all cases the jets are clustered with FastJet [43]. We also include in the plots the NLO results from MadGraph5_aMC@NLO.

We note that the parton-shower results are in agreement with the resummed result for intermediate values of $\delta\phi$ and with fixed-order NLO results from MadGraph5_aMC@NLO. In the parton shower results the observable continues to have a distribution for values of $\delta\phi$ up to π as explained above, and deviation from our NLL-resummed result starts at around 1.0 at the tail of the distribution, where also fixed-order NLO results start to make no sense.

At small values of $\delta\phi$ our resummed distribution in the anti- k_t algorithm has a lower value than the parton shower results. It would seem that the global result is performing better than the NLL+ C_1 result in this region when compared with these parton shower results. On the contrary, one can make the observation that Pythia 8 results in the small- $\delta\phi$ region are quite

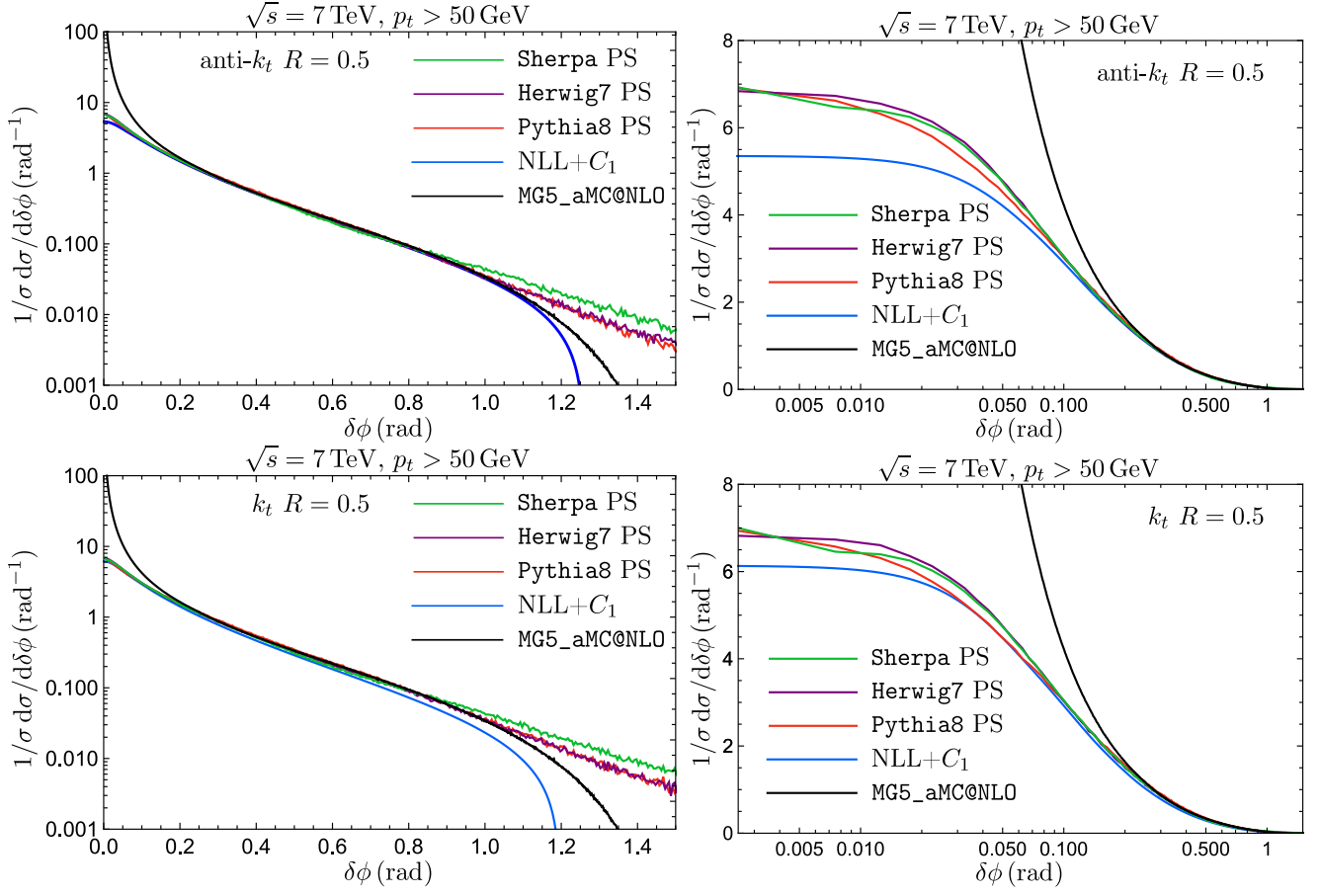


Figure 5.5: The differential distributions $1/\sigma d\sigma/d\delta\phi$ with anti- k_t clustering (top) and k_t clustering (bottom). Results are shown for the resummed distribution NLL+ C_1 and parton showers (PS) obtained with various MC event generators. Also shown is the fixed-order NLO MC result.

high compared to other results obtained in previous works. For instance, in ref. [59] it was noted that the parton shower result, obtained with Pythia 8 stand-alone and multiplied by an NLO K factor of 1.6 in the WTA recombination scheme, is also slightly larger than the resummed result at NLL+NLO and NNLL+NLO accuracy for small azimuthal decorrelation. A similar observation may be noted in the work of the CMS collaboration in ref. [58], where the Pythia 8 stand-alone result (which includes non-perturbative effects) has a higher value than the experimental data in the last bin corresponding to small azimuthal decorrelation. We have verified that this is not due to non-perturbative hadronisation and underlying-event effects, which have a small impact on the distribution as was too observed in ref. [59].

The discrepancy is explained by the fact that the parton shower results do not include effects of higher jet multiplicities. If one includes such effects, the tail of the distribution becomes higher due to contributions from 2 and 3 jet events, and at the same time the small- $\delta\phi$ region gets lower

due to the normalisation of the distribution.³ One can include such effects in `MadGraph5_aMC@NLO` by merging the process of production of $Z + 2$ jets (and also possibly $Z + 3$ jets) with the Born process $Z + \text{jet}$, and performing the showering of events with the said MC parton showers. Doing so gives a reasonable agreement with our resummed distribution and with experimental data in the last bin (corresponding to small $\delta\phi$), as observed from figure 5.6.

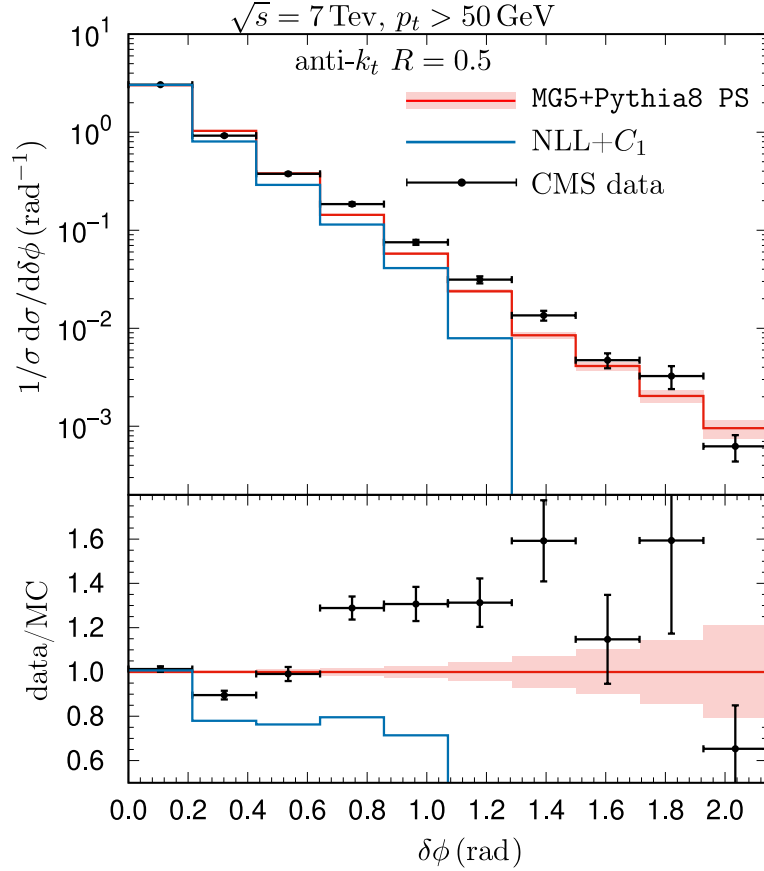


Figure 5.6: Comparison between the NLL-resummed distribution, the Pythia 8 parton shower result (including $Z + 2$ jet process), and the CMS data.

³The parton shower and experimental distributions are normalised such that the area under the curve is equal to 1. As the distribution raises in the tail it gets lower at small $\delta\phi$ to preserve the area under the distribution.

Chapter 6

General conclusion.

In this work, we have taken upon us the study concerning the resummation of logarithms associated to non-global observables. As a case study, the azimuthal decorrelation observable $\delta\phi$ between a Z -boson and the leading associated hard jet at hadron-hadron colliders was taken under consideration. This observable received much attention from an experimental side as it was studied by both of CMS & ATLAS collaborations as well as from a phenomenological/theoretical aspect employing different approaches to the said resummation question.

The azimuthal decorrelation is a doubly logarithmic observable which implies that performing a NLL resummation for this it means taking into consideration the emission effects of soft/collinear gluons as well as including soft/wide-angle from secondary primary and correlated emissions in the presence of a jet clustering algorithms. This leads to the inclusion of CLs & NGLs. In chapter 4, logarithms of the first kind were resummed up to NLL accuracy at the exponent, i.e resumming soft/collinear gluon emissions outside the outgoing region. The integrated cross-section expression is identified alongside the radiator function. The integral expression is evaluated with the help of general purpose Monte Carlo event generators, where the integral in question is convoluted using a sample of unweighted events generated with MG5_aMC@NLO ultimately leading into an integrated and a differential distribution of our observable.

The achievement of NNLL accuracy in the expansion is once again made possible with the help of fixed-order Monte Carlo codes such as MG5_aMC@NLO & MCFM where the C_1 term is extracted to reach such accuracy. As a double check, the resummed result was expanded to order α_s^2 and compared

to fixed-order MC codes and the result shows a clear agreement indicating that resummed formula correctly captures the leading and next to leading logarithms.

Chapter 5 deals with logarithms of the second kind, i.e CLs and NGLs. In the presence of a jet clustering algorithm, the clustering logarithms manifest themselves when considering primary emissions off hard legs into boundary jet regions. the non-global logarithms on the other hand originate from secondary correlated emissions characterized by complicated analytical structure and non-trivial color correlations. Hence a fixed-order approach is in order here in this thesis. We first calculated the leading CLs & NGLs coefficients at two loops in the k_t , anti- k_t and C/A algorithms (due to their sensitivity to the said jet algorithms as well as the recombination scheme employed). For a suitable choice of the jet radius parameter R , the CLs an NGLs coefficients were found to cancel each other thus mitigating their effects on the observable. The all-order result proves challenging to obtain, thus the two loop result obtained was exponentiated as to approximate the all-order result. Comparisons with the output of a private MC code reveals that this exponentiation is to a good degree, an adequate approximation. Finally, this chapter is concluded by putting together the results obtained and a comparison against the output of several GPMCEGs (Herwig++, Sherpa, Pythia8) and data from CMS is made in which we find good agreement over intermediary values of $\delta\phi$. differences in the lower values were attributed to fixed-order effects not captured by the resummation procedure while at the tail of the distribution the difference is related to missing higher order corrections (since as was shown in 4, NLO effect are depleted around the middle values) due to the lack of technology to tackle this process at NNLO. In this study, statistical & systematic error estimation and matching procedure to fixed-order MC codes output and non-perturbative effects were not taken into account. This makes for a future work to include these steps in order to make a full phenomenological study.

Appendix A

Radiator.

A.1 In-in dipole

We begin by evaluating the integral for the (ab) -dipole contribution to the radiator, given by

$$\mathcal{R}_\delta^{(ab)}(\bar{b}) = \mathcal{C}_{ab} \int \frac{\alpha_s(\kappa_{t,ab}^2)}{\pi} \frac{dk_t}{k_t} d\eta \frac{d\phi}{2\pi} \Theta_{\text{out}}(k) w_{ab}^k \Theta(k_t |\sin \phi| - p_t/\bar{b}). \quad (\text{A.1})$$

For this dipole we simply have $w_{ab}^k = 1$ and $\kappa_{t,ab}^2 = k_t^2$. To achieve the evaluation of this integral we write the step function $\Theta_{\text{out}}(k) = 1 - \Theta_{\text{in}}(k)$, and perform the integration over each term separately.

A.1.1 Integrating the whole phase space

We evaluate the integral

$$\mathcal{R}_\delta^{(ab)\text{-all}}(\bar{b}) = \mathcal{C}_{ab} \int \frac{\alpha_s(k_t^2)}{\pi} \frac{dk_t}{k_t} d\eta \frac{d\phi}{2\pi} \Theta(k_t |\sin \phi| - p_t/\bar{b}). \quad (\text{A.2})$$

The rapidity integration has a cutoff originating from the requirement that the emitted gluon when collinear to one of the incoming legs must have an energy less than that of the emitting parent hard parton, i.e. $k_t \cosh \eta < x_a \sqrt{s}/2$ and $k_t \cosh \eta < x_b \sqrt{s}/2$. When the emission is collinear to the leg (a) we have $k_t \cosh \eta \approx k_t e^\eta/2 < x_a \sqrt{s}/2$, and similarly when the emission is collinear to the leg (b) we obtain $k_t e^{-\eta}/2 < x_b \sqrt{s}/2$. Including contributions from hard-collinear emissions to the corresponding hard leg is simply achieved by making the replacement $x_a \sqrt{s} \rightarrow x_a \sqrt{s} e^{B_a}$ and

$x_b\sqrt{s} \rightarrow x_b\sqrt{s} e^{B_b}$, where

$$\begin{aligned} B_q &= -\frac{3}{4} && \text{for quark legs,} \\ B_g &= -\frac{11 C_A - 4 T_R n_f}{12 C_A} = -\frac{\pi\beta_0}{C_A} && \text{for gluon legs,} \end{aligned} \quad (\text{A.3})$$

where $T_R = 1/2$ is the normalisation constant for the $SU(N_c)$ generators, $n_f = 5$ is the number of active quark flavours, and β_0 is the one-loop coefficient of the QCD beta function (defined below). Additionally, the scale of the PDFs is changed from $\mu_f^2 \rightarrow \mu_f^2/\bar{b}^2$. We thus deduce that

$$-\ln\left(\frac{x_b}{k_t}\sqrt{s} e^{B_b}\right) < \eta < \ln\left(\frac{x_a}{k_t}\sqrt{s} e^{B_a}\right). \quad (\text{A.4})$$

Performing the integration over η we obtain

$$\int d\eta = \ln\frac{x_a x_b s}{k_t^2} + B_a + B_b = \ln\frac{Q_{ab}^2}{k_t^2} + B_a + B_b, \quad (\text{A.5})$$

where we define $Q_{ij}^2 = (p_i + p_j)^2 = 2p_i \cdot p_j$. The latter quantities are related to the partonic Mandelstam variables, $Q_{ab}^2 = \hat{s} = x_a x_b s$, $Q_{aj}^2 = -\hat{t} = x_a\sqrt{s} p_t e^{-y}$, and $Q_{bj}^2 = -\hat{u} = x_b\sqrt{s} p_t e^y$.

Next, we perform the integration over k_t . Using the two-loops QCD beta function we have

$$\alpha_s(k_t^2) = \alpha_s \left[\frac{1}{1 + 2\alpha_s\beta_0 \ln(k_t/p_t)} - \frac{\beta_1}{\beta_0} \alpha_s \frac{\ln[1 + 2\alpha_s\beta_0 \ln(k_t/p_t)]}{[1 + 2\alpha_s\beta_0 \ln(k_t/p_t)]^2} \right], \quad (\text{A.6})$$

where α_s in the right-hand-side is evaluated at the renormalisation scale $\mu_r = p_t$, and β_0 and β_1 are the one and two-loops coefficients of the QCD beta function given by

$$\begin{aligned} \beta_0 &= \frac{11 C_A - 2 n_f}{12 \pi}, \\ \beta_1 &= \frac{17 C_A^2 - 5 C_A n_f - 3 C_F n_f}{24 \pi^2}. \end{aligned} \quad (\text{A.7})$$

Integrating over k_t keeping only up to single-logarithmic terms we arrive at

$$\begin{aligned}
& \int_{p_t/(\bar{b}|\sin\phi)}^{p_t} \frac{\alpha_s(k_t^2)}{\pi} \frac{dk_t}{k_t} \left(B_a + B_b + \ln \frac{Q_{ab}^2}{p_t^2} - \ln \frac{k_t^2}{p_t^2} \right) = \\
& = -L \frac{1}{2\pi\beta_0\Lambda} [2\Lambda + \ln(1-2\Lambda)] - \frac{\beta_1}{2\pi\beta_0^3} \left[\frac{1}{2} \ln^2(1-2\Lambda) + \frac{\ln(1-2\Lambda) + 2\Lambda}{1-2\Lambda} \right] + \\
& + \frac{1}{\pi\beta_0} \ln|\sin\phi| \frac{2\Lambda}{1-2\Lambda} - \frac{1}{2\pi\beta_0} \left[\ln \frac{Q_{ab}^2}{p_t^2} + B_a + B_b \right] \ln(1-2\Lambda), \tag{A.8}
\end{aligned}$$

with $L = \ln \bar{b}$ and $\Lambda = \alpha_s \beta_0 L$.

Finally, we perform the azimuthal averaging using $\frac{1}{2\pi} \int_0^{2\pi} \ln|\sin\phi| d\phi = -\ln 2$, which simply results in changing $\ln|\sin\phi| \rightarrow -\ln 2$.

A.1.2 Subtracting the jet region

Here we introduce the change of variables

$$\eta - y = R r \cos \theta, \tag{A.9a}$$

$$\phi - \pi = R r \sin \theta. \tag{A.9b}$$

The step function restricting the gluon to be in the jet is $\Theta[R^2 - (\eta - y)^2 - (\phi - \pi)^2] = \Theta(1 - r^2)$.

The angular phase space becomes $d\eta d\phi = R^2 r dr d\theta$. We thus evaluate the integral

$$\mathcal{R}_\delta^{(ab)-\text{in}}(\bar{b}) = C_{ab} R^2 \int \frac{\alpha_s(k_t^2)}{\pi} \frac{dk_t}{k_t} r dr \frac{d\theta}{2\pi} \Theta(1 - r^2) \Theta(k_t |\sin(R r \sin \theta)| - p_t/\bar{b}). \tag{A.10}$$

This term is free from collinear logarithms since it integrates only over emissions inside the outgoing jet away from the emitting incoming dipole. We thus use just the one-loop running of the coupling and expand at single logarithmic accuracy $\Theta(k_t |\sin(R r \sin \theta)| - p_t/\bar{b}) = \Theta(k_t - p_t/\bar{b})$. It is then straightforward to obtain the result

$$\int_{p_t/\bar{b}}^{p_t} \frac{\alpha_s(k_t^2)}{\pi} \frac{dk_t}{k_t} = \int_{p_t/\bar{b}}^{p_t} \frac{\alpha_s}{\pi} \frac{dk_t}{k_t} \frac{1}{1 + 2\alpha_s \beta_0 \ln(k_t/p_t)} = -\frac{1}{2\pi\beta_0} \ln[1 - 2\Lambda], \tag{A.11}$$

where we discard sub-leading terms. The remaining angular integrations are straightforward and we obtain

$$\mathcal{R}_\delta^{(ab)\text{-in}}(\bar{b}) = -\mathcal{C}_{ab} \frac{1}{2} R^2 \frac{1}{2\pi\beta_0} \ln[1 - 2\Lambda]. \quad (\text{A.12})$$

The overall contribution of the in-in dipole to the radiator is then given by

$$\begin{aligned} \mathcal{R}_\delta^{(ab)}(\bar{b}) &= -\mathcal{C}_{ab} L \frac{1}{2\pi\beta_0 \Lambda} [2\Lambda + \ln(1 - 2\Lambda)] + \mathcal{C}_{ab} \frac{K}{4\pi^2\beta_0^2} \left[\ln(1 - 2\Lambda) + \frac{2\Lambda}{1 - 2\Lambda} \right] - \\ &- \mathcal{C}_{ab} \frac{\beta_1}{2\pi\beta_0^3} \left[\frac{1}{2} \ln^2(1 - 2\Lambda) + \frac{\ln(1 - 2\Lambda) + 2\Lambda}{1 - 2\Lambda} \right] - \mathcal{C}_{ab} \ln 2 \frac{1}{\pi\beta_0} \frac{2\Lambda}{1 - 2\Lambda} - \\ &- \mathcal{C}_{ab} \frac{1}{2\pi\beta_0} \left[\ln \frac{Q_{ab}^2}{p_t^2} + B_a + B_b \right] \ln(1 - 2\Lambda) + \mathcal{C}_{ab} \frac{1}{2} R^2 \frac{1}{2\pi\beta_0} \ln(1 - 2\Lambda), \end{aligned} \quad (\text{A.13})$$

where we changed the coupling from the CMW [54] to the $\overline{\text{MS}}$ renormalisation scheme by making the replacement

$$\alpha_{s,\text{CMW}} = \alpha_{s,\overline{\text{MS}}} + \alpha_{s,\overline{\text{MS}}}^2 \frac{K}{2\pi}, \quad (\text{A.14})$$

with

$$K = C_A \left(\frac{67}{18} - \frac{\pi^2}{6} \right) - \frac{5}{9} n_f. \quad (\text{A.15})$$

A.2 In-jet dipole

Next we evaluate the integral for the contribution of the dipole (aj) to the radiator

$$\mathcal{R}_\delta^{(aj)}(\bar{b}) = \mathcal{C}_{aj} \int \frac{\alpha_s(\kappa_t^2)}{\pi} \frac{dk_t}{k_t} d\eta \frac{d\phi}{2\pi} \Theta_{\text{out}}(k) w_{aj}^k \Theta(k_t |\sin \phi| - p_t/\bar{b}), \quad (\text{A.16})$$

where we have for this dipole $\kappa_t = k_t/\sqrt{w_{aj}^k}$, with

$$w_{aj}^k = \frac{1}{2} \frac{\exp(\eta - y)}{\cosh(\eta - y) - \cos(\phi - \pi)}. \quad (\text{A.17})$$

We make the change of variable $k_t \rightarrow \kappa_t$, where now the integration over κ_t is restricted in the range

$$\frac{p_t}{\bar{b} |\sin \phi| \sqrt{w_{aj}^k}} < \kappa_t < \frac{p_t}{\sqrt{w_{aj}^k}}. \quad (\text{A.18})$$

We expose the singularities resulting from collinear emissions to the dipole legs by writing

$$w_{aj}^k \Theta_{\text{out}}(k) = \left[\omega_{aj}^k - \frac{1}{R^2 r^2} \right] + \left[\frac{1}{R^2 r^2} - \omega_{aj}^k \right] \Theta_{\text{in}}(k) + \frac{1}{R^2 r^2} \Theta_{\text{out}}(k), \quad (\text{A.19})$$

where the variable r has been introduced in eq. (A.9). In the first term the collinear pole to the outgoing jet ($r \rightarrow 0$) is subtracted from the antenna function and the integration is performed in the entire angular phase space, and thus this term results in soft-collinear double logarithms and hard-collinear single logarithms from the incoming leg (a),¹ as well as soft wide-angle single logarithms from the whole dipole (aj). The second term is similar to the first one (contains no collinear pole to the outgoing jet) but the integration is restricted to the interior of the outgoing hard jet, meaning that it results purely in soft wide-angle single logarithms from the dipole (aj). The last term has a pure collinear pole to the outgoing jet, but contains a step function that restricts the gluon to be outside of it. This terms will thus result in a soft wide-angle single logarithm. In what follows we show how to integrate each term separately.

A.2.1 First term

We start with the integration

$$\begin{aligned} \mathcal{R}_\delta^{(aj)-1}(\bar{b}) &= \mathcal{C}_{aj} \int \frac{\alpha_s(\kappa_t^2)}{\pi} \frac{d\kappa_t}{\kappa_t} d\eta \frac{d\phi}{2\pi} \Theta\left(\kappa_t \sqrt{\omega_{aj}^k} |\sin \phi| - p_t/\bar{b}\right) \Theta\left(p_t - \sqrt{w_{aj}^k} \kappa_t\right) \times \\ &\times \left[\frac{1}{2} \frac{\exp(\eta - y)}{\cosh(\eta - y) - \cos(\phi - \pi)} - \frac{1}{(\eta - y)^2 + (\phi - \pi)^2} \right] \Theta\left[-\eta + y + B_a + \ln \frac{Q_{aj}^2}{k_t p_t}\right], \end{aligned} \quad (\text{A.20})$$

where we restored the η and ϕ variables here for convenience and included hard-collinear emissions to the incoming leg (a) via the last step function.

This contribution has both double and single logarithms, and is free from collinear logarithms to the outgoing jet. The double logarithms originate from soft-collinear emissions to the incoming leg (a) corresponding to $\eta \rightarrow +\infty$, where we can approximate $\omega_{aj}^k \rightarrow 1$ and thus replace $k_t \rightarrow \kappa_t$ in the step function $\Theta(-\eta + y + B_a + \ln[Q_{aj}^2/\kappa_t p_t])$. Furthermore, for the single-logarithmic part, the coefficients that multiply κ_t in the two step functions $\Theta\left(\kappa_t \sqrt{\omega_{aj}^k} |\sin \phi| - p_t/\bar{b}\right)$ (i.e. the

¹The collinear singularity to the incoming leg (a) is at $\eta \rightarrow +\infty$.

coefficient $\sqrt{\omega_{aj}^k} |\sin \phi|$) and $\Theta(p_t - \sqrt{\omega_{aj}^k} \kappa_t)$ (i.e. the coefficient $\sqrt{\omega_{aj}^k}$) only contribute at sub-leading accuracy, and can thus be substituted for any constant. We thus set $\omega_{aj}^k \rightarrow 1$ in all the step functions, and additionally take the average contribution of ϕ in the step function (in the region $\eta \rightarrow +\infty$) exploiting $\int_0^{2\pi} \ln |\sin \phi| d\phi/2\pi = -\ln 2$ as we observed in the previous subsection. Hence we may write at single-logarithmic accuracy

$$\begin{aligned} \mathcal{R}_\delta^{(aj)-1}(\bar{b}) &= \mathcal{C}_{aj} \int \frac{\alpha_s(\kappa_t^2)}{\pi} \frac{d\kappa_t}{\kappa_t} d\eta \frac{d\phi}{2\pi} \Theta\left(\frac{1}{2}\kappa_t - p_t/\bar{b}\right) \Theta(p_t - \kappa_t) \times \\ &\times \left[\frac{1}{2} \frac{\exp(\eta - y)}{\cosh(\eta - y) - \cos(\phi - \pi)} - \frac{1}{(\eta - y)^2 + (\phi - \pi)^2} \right] \Theta\left[-\eta + y + B_a + \ln \frac{Q_{aj}^2}{\kappa_t p_t}\right]. \end{aligned} \quad (\text{A.21})$$

We can then integrate over η and ϕ up to single logarithmic accuracy obtaining

$$\begin{aligned} &\int_{-\infty}^{B_a + y + \ln(Q_{aj}^2/\kappa_t p_t)} d\eta \frac{d\phi}{2\pi} \left[\frac{1}{2} \frac{\exp(\eta - y)}{\cosh(\eta - y) - \cos(\phi - \pi)} - \frac{1}{(\eta - y)^2 + (\phi - \pi)^2} \right] = \\ &= B_a + \ln \frac{Q_{aj}^2}{p_t^2} - \ln \frac{\kappa_t}{p_t} - \ln(2\pi). \end{aligned} \quad (\text{A.22})$$

Notice that the integration over ω_{aj}^k and $1/(R^2 r^2)$ separately diverge when $r \rightarrow 0$, but the overall integration is finite. One can avoid this divergence by simply placing a cutoff ϵ on $\eta - y$ around 0, and setting $\epsilon \rightarrow 0$ at the end. Now we perform the integration over κ_t , which is very similar to that performed in subsection A.1.1, to obtain the following result

$$\begin{aligned} \mathcal{R}_\delta^{(aj)-1}(\bar{b}) &= \mathcal{C}_{aj} \int \frac{\alpha_s(\kappa_t^2)}{\pi} \frac{d\kappa_t}{\kappa_t} \Theta\left(\frac{\kappa_t}{2} - \frac{p_t}{\bar{b}}\right) \Theta(p_t - \kappa_t) \left(B_a + \ln \frac{Q_{aj}^2}{p_t^2} - \ln \frac{\kappa_t}{p_t} - \ln(2\pi) \right) \\ &= -\frac{\mathcal{C}_{aj}}{2} L \frac{1}{2\pi\beta_0\Lambda} [2\Lambda + \ln(1 - 2\Lambda)] + \frac{\mathcal{C}_{aj}}{2} \frac{K}{4\pi^2\beta_0^2} \left[\ln(1 - 2\Lambda) + \frac{2\Lambda}{1 - 2\Lambda} \right] - \\ &- \frac{\mathcal{C}_{aj}}{2} \frac{\beta_1}{2\pi\beta_0^3} \left[\frac{1}{2} \ln^2(1 - 2\Lambda) + \frac{\ln(1 - 2\Lambda) + 2\Lambda}{1 - 2\Lambda} \right] - \frac{\mathcal{C}_{aj}}{2} \ln 2 \frac{1}{\pi\beta_0} \frac{2\Lambda}{1 - 2\Lambda} - \\ &- \mathcal{C}_{aj} \frac{1}{2\pi\beta_0} \left[\ln \frac{Q_{aj}^2}{p_t^2} + B_a - \ln(2\pi) \right] \ln(1 - 2\Lambda). \end{aligned} \quad (\text{A.23})$$

A.2.2 Second term

The second term to integrate is

$$\begin{aligned} \mathcal{R}_\delta^{(aj)-2}(\bar{b}) &= \mathcal{C}_{aj} \int \frac{\alpha_s(\kappa_t^2)}{\pi} \frac{d\kappa_t}{\kappa_t} R^2 r dr \frac{d\theta}{2\pi} \left(\frac{1}{R^2 r^2} - w_{aj}^k \right) \Theta_{\text{in}}(k) \Theta \left(\sqrt{w_{aj}^k} \kappa_t |\sin \phi| - p_t/\bar{b} \right) \\ &\times \Theta \left(p_t/\sqrt{w_{aj}^k} - \kappa_t \right). \end{aligned} \quad (\text{A.24})$$

This term produces only single logarithms as explained earlier, so we integrate over κ_t using the one-loop QCD beta function. The three step functions in the integrand reduce to

$$\Theta(1 - r^2) \Theta(\kappa_t - p_t/\bar{b}) \Theta(p_t - \kappa_t).$$

Performing the integrations over κ_t , r and θ we obtain the result

$$\mathcal{R}_\delta^{(aj)-2}(\bar{b}) = \mathcal{C}_{aj} \frac{1}{2\pi\beta_0} \ln(1 - 2\Lambda) \left(\frac{1}{8} R^2 + \frac{1}{576} R^4 + \mathcal{O}(R^8) \right). \quad (\text{A.25})$$

A.2.2.1 Third term

The last term to integrate is

$$\begin{aligned} \mathcal{R}_\delta^{(aj)-3}(\bar{b}) &= \mathcal{C}_{aj} \int \frac{\alpha_s(\kappa_t^2)}{\pi} \frac{d\kappa_t}{\kappa_t} R^2 r dr \frac{d\theta}{2\pi} \frac{1}{R^2 r^2} \Theta_{\text{out}}(k) \Theta \left(\sqrt{w_{aj}^k} \kappa_t |\sin \phi| - p_t/\bar{b} \right) \times \\ &\times \Theta \left(p_t/\sqrt{w_{aj}^k} - \kappa_t \right). \end{aligned} \quad (\text{A.26})$$

Performing the integration over κ_t , r and θ at single logarithmic accuracy gives

$$\mathcal{R}_\delta^{(aj)-3}(\bar{b}) = \mathcal{C}_{aj} \frac{1}{2\pi\beta_0} \ln \frac{R}{2\pi} \ln(1 - 2\Lambda). \quad (\text{A.27})$$

The overall contribution of the dipole (aj) to the radiator is

$$\begin{aligned}
\mathcal{R}_\delta^{(aj)}(\bar{b}) &= -\frac{\mathcal{C}_{aj}}{2} L \frac{1}{2\pi\beta_0\Lambda} [2\Lambda + \ln(1-2\Lambda)] + \frac{\mathcal{C}_{aj}}{2} \frac{K}{4\pi^2\beta_0^2} \left[\ln(1-2\Lambda) + \frac{2\Lambda}{1-2\Lambda} \right] - \\
&\quad - \frac{\mathcal{C}_{aj}}{2} \frac{\beta_1}{2\pi\beta_0^3} \left[\frac{1}{2} \ln^2(1-2\Lambda) + \frac{\ln(1-2\Lambda) + 2\Lambda}{1-2\Lambda} \right] - \frac{\mathcal{C}_{aj}}{2} \ln 2 \frac{1}{\pi\beta_0} \frac{2\Lambda}{1-2\Lambda} - \\
&\quad - \mathcal{C}_{aj} \frac{1}{2\pi\beta_0} \left[\ln \frac{Q_{aj}^2}{p_t^2} + B_a \right] \ln(1-2\Lambda) + \\
&\quad + \mathcal{C}_{aj} \frac{1}{2\pi\beta_0} \ln(1-2\Lambda) \left(\ln R + \frac{1}{8} R^2 + \frac{1}{576} R^4 + \mathcal{O}(R^8) \right). \tag{A.28}
\end{aligned}$$

We finally note that the contribution of the dipole (bj) to the radiator is identical to that of the dipole (aj), with the substitution $a \rightarrow b$.

A.2.3 Assembled expression for the radiator

The final expression for the total radiator is given by

$$\mathcal{R}_\delta(\bar{b}) = \mathcal{R}_\delta^{\text{coll.}}(\bar{b}) + \mathcal{R}_\delta^{\text{wide}}(\bar{b}), \tag{A.29}$$

where the contribution corresponding to collinear (soft or hard) emissions from the incoming legs (a and b) is expressed as

$$\mathcal{R}_\delta^{\text{coll.}}(\bar{b}) = (\mathcal{C}_a + \mathcal{C}_b) [L g_1(\alpha_s L) + g_2(\alpha_s L) - \ln 2 g'(\alpha_s L)] + (\mathcal{C}_a B_a + \mathcal{C}_b B_b) t(\alpha_s L), \tag{A.30}$$

with

$$g_1 = -\frac{1}{2\pi\beta_0\Lambda} [2\Lambda + \ln(1-2\Lambda)], \tag{A.31}$$

$$g_2 = \frac{K}{4\pi^2\beta_0^2} \left[\ln(1-2\Lambda) + \frac{2\Lambda}{1-2\Lambda} \right] - \frac{\beta_1}{2\pi\beta_0^3} \left[\frac{1}{2} \ln^2(1-2\Lambda) + \frac{\ln(1-2\Lambda) + 2\Lambda}{1-2\Lambda} \right], \tag{A.32}$$

$$g' = \frac{\partial g}{\partial L} = \frac{2}{\pi\beta_0} \frac{\Lambda}{1-2\Lambda}, \tag{A.33}$$

$$t = -\frac{1}{\pi\beta_0} \ln(1-2\Lambda), \tag{A.34}$$

and $g = L g_1 + g_2$. The functions g_1 and g_2 can easily be obtained from the principles of general final-state resummation of ref. [27].² Additionally the function resumming soft wide-angle emissions from all the three hard legs is

$$\mathcal{R}_\delta^{\text{wide}}(\bar{b}) = \frac{1}{2} t(\alpha_s L) \sum_{(\alpha\beta)} \mathcal{C}_{\alpha\beta} \left(\ln \frac{Q_{\alpha\beta}^2}{p_i^2} - h_{\alpha\beta}(R) \right), \quad (\text{A.35})$$

where the sum extends over the three dipoles and the jet-radius-dependent functions are given by

$$h_{ab}(R) = \frac{R^2}{2}, \quad (\text{A.36})$$

$$h_{aj}(R) = h_{bj}(R) = \ln R + \frac{1}{8} R^2 + \frac{1}{576} R^4 + \mathcal{O}(R^8). \quad (\text{A.37})$$

In the above we define $\mathcal{C}_a = (\mathcal{C}_{ab} + \mathcal{C}_{aj})/2$ and $\mathcal{C}_b = (\mathcal{C}_{ab} + \mathcal{C}_{bj})/2$. It turns out that $\mathcal{C}_i = C_F$ for quark leg i and $\mathcal{C}_i = C_A$ for gluon leg i .

Finally, the derivative of the radiator with respect to $\ln \bar{b}$ (up to NLL accuracy) is given by

$$\mathcal{R}'_\delta(\bar{b}) = \frac{\partial \mathcal{R}_\delta}{\partial \ln \bar{b}} = (\mathcal{C}_a + \mathcal{C}_b) g'(\alpha_s L), \quad (\text{A.38})$$

where g' is defined in eq. (A.33).

²See eq. (3.6), and the expressions (A.4) and (A.6), with $a = 1$ corresponding to the power of k_t in the definition of our observable.

Appendix B

Fixed-order expansion.

In order to expand the resummed distribution (given *formally* by eq. (4.18)) at fixed order, we first need to relate the PDFs of flavour i evaluated at the scale $\mu_f^2 \Delta^2$ to the PDFs at the factorisation scale μ_f^2 . The relevant expression can be obtained by solving the DGLAP evolution equation [92] at leading order to obtain ¹

$$f_i(x, \Delta^2 \mu_f^2) = f_i(x, \mu_f^2) \left(1 - \frac{1}{f_i(x, \mu_f^2)} \frac{\alpha_s}{\pi} \ln \frac{1}{\Delta} \sum_j \int_x^1 P_{ij}(\xi) f_j(x/\xi, \mu_f^2) \frac{d\xi}{\xi} \right), \quad (\text{B.1})$$

where $P_{ij}(\xi)$ are the corresponding leading-order Altarelli-Parisi splitting functions. For a fixed factorisation scale the expansion of the resummed formula (4.18) at fixed order is

$$\sigma_1(\Delta) = \sum_{\delta} \int d\mathcal{B}_{\delta} \frac{d\sigma_{0\delta}}{d\mathcal{B}_{\delta}} \Xi_{\mathcal{B}} \left(1 + G_{11} \frac{\alpha_s}{\pi} \ln \frac{1}{\Delta} + G_{12} \frac{\alpha_s}{\pi} \ln^2 \frac{1}{\Delta} \right), \quad (\text{B.2})$$

where

$$G_{11} = (\mathcal{C}_a + \mathcal{C}_b) 2 \ln 2 - 2(\mathcal{C}_a B_a + \mathcal{C}_b B_b) + \mathcal{C}_{ab} \frac{R^2}{2} + (\mathcal{C}_{aj} + \mathcal{C}_{bj}) \left(\ln R + \frac{R^2}{8} + \frac{R^4}{576} \right) - 2 \left(\mathcal{C}_{ab} \ln \frac{Q_{ab}}{p_t} + \mathcal{C}_{aj} \ln \frac{Q_{aj}}{p_t} + \mathcal{C}_{bj} \ln \frac{Q_{bj}}{p_t} \right) - P(\mathcal{B}), \quad (\text{B.3})$$

$$G_{12} = -(\mathcal{C}_a + \mathcal{C}_b), \quad (\text{B.4})$$

¹See ref. [27], page 59 and 56 for further details, including expressions of leading-order splitting functions.

with the process-dependent (on x_a and x_b) term (sum over j implied)

$$P(\mathcal{B}) = \frac{1}{f_a(x_a, \mu_{\mathcal{F}}^2)} \int_{x_a}^1 P_{aj}(\xi) f_j(x_a/\xi, \mu_{\mathcal{F}}^2) \frac{d\xi}{\xi} + \frac{1}{f_b(x_b, \mu_{\mathcal{F}}^2)} \int_{x_b}^1 P_{bj}(\xi) f_j(x_b/\xi, \mu_{\mathcal{F}}^2) \frac{d\xi}{\xi}. \quad (\text{B.5})$$

Bibliography

- [1] Azimuthal correlations in Z+jets events in proton-proton collisions at $\sqrt{s} = 13$ TeV. 10 2022.
- [2] M. Aaboud et al. Measurement of dijet azimuthal decorrelations in pp collisions at $\sqrt{s} = 8$ TeV with the ATLAS detector and determination of the strong coupling. *Phys. Rev. D*, 98(9):092004, 2018.
- [3] Morad Aaboud et al. Dijet azimuthal correlations and conditional yields in pp and $p+\text{Pb}$ collisions at $\sqrt{s_{NN}}=5.02\text{TeV}$ with the ATLAS detector. *Phys. Rev. C*, 100(3):034903, 2019.
- [4] Georges Aad et al. Measurement of Dijet Azimuthal Decorrelations in pp Collisions at $\sqrt{s} = 7$ TeV. *Phys. Rev. Lett.*, 106:172002, 2011.
- [5] Georges Aad et al. Measurement of the production cross section for Z/γ^* in association with jets in pp collisions at $\sqrt{s} = 7$ TeV with the ATLAS detector. *Phys. Rev. D*, 85:032009, 2012.
- [6] Georges Aad et al. Observation of a new particle in the search for the Standard Model Higgs boson with the ATLAS detector at the LHC. *Phys. Lett. B*, 716:1–29, 2012.
- [7] V. M. Abazov et al. Measurement of dijet azimuthal decorrelations at central rapidities in $p\bar{p}$ collisions at $\sqrt{s} = 1.96$ TeV. *Phys. Rev. Lett.*, 94:221801, 2005.
- [8] S. Agostinelli et al. GEANT4—a simulation toolkit. *Nucl. Instrum. Meth. A*, 506:250–303, 2003.
- [9] A. Aktas et al. Inclusive dijet production at low Bjorken x in deep inelastic scattering. *Eur. Phys. J. C*, 33:477–493, 2004.

- [10] Fawad Ali, Edward Moyses, Mohammad Humayun Khan, Emilio Cortina Labra, Andreas Pappas, Gaurav Sharma, Arthur Hennequin, bcouturi, PhD Riccardo M. BIANCHI, Amarjeet, Arya Bhosale, Sebastien Ponce, and Stefano Roberto Soleti. Hsf/phoenix: v2.11.4, October 2022.
- [11] G. Altarelli and G. Parisi. Asymptotic freedom in parton language. *Nuclear Physics B*, 126(2):298–318, 1977.
- [12] J. Alwall, R. Frederix, S. Frixione, V. Hirschi, F. Maltoni, O. Mattelaer, H. S. Shao, T. Stelzer, P. Torrielli, and M. Zaro. The automated computation of tree-level and next-to-leading order differential cross sections, and their matching to parton shower simulations. *JHEP*, 07:079, 2014.
- [13] Johan Alwall, Simon de Visscher, and Fabio Maltoni. QCD radiation in the production of heavy colored particles at the LHC. *JHEP*, 02:017, 2009.
- [14] Johan Alwall et al. A Standard format for Les Houches event files. *Comput. Phys. Commun.*, 176:300–304, 2007.
- [15] Johan Alwall et al. Comparative study of various algorithms for the merging of parton showers and matrix elements in hadronic collisions. *Eur. Phys. J. C*, 53:473–500, 2008.
- [16] Thomas Appelquist and J. Carazzone. Infrared singularities and massive fields. *Phys. Rev. D*, 11:2856–2861, May 1975.
- [17] R. B. Appleby and M. H. Seymour. Nonglobal logarithms in interjet energy flow with kt clustering requirement. *JHEP*, 12:063, 2002.
- [18] M. Bahr et al. Herwig++ Physics and Manual. *Eur. Phys. J. C*, 58:639–707, 2008.
- [19] A. Banfi, G. Marchesini, Yuri L. Dokshitzer, and G. Zanderighi. QCD analysis of near-to-planar three jet events. *JHEP*, 07:002, 2000.
- [20] A. Banfi, G. Marchesini, and G. Smye. Away from jet energy flow. *JHEP*, 08:006, 2002.
- [21] A. Banfi, G. Marchesini, and G. Smye. Azimuthal correlation in DIS. *JHEP*, 04:024, 2002.

- [22] A. Banfi, G. Marchesini, G. Smye, and G. Zanderighi. Out-of-plane QCD radiation in DIS with high $p(t)$ jets. *JHEP*, 11:066, 2001.
- [23] Andrea Banfi, Mrinal Dasgupta, and Yazid Delenda. Azimuthal decorrelations between QCD jets at all orders. *Phys. Lett. B*, 665:86–91, 2008.
- [24] Andrea Banfi, Frédéric A. Dreyer, and Pier Francesco Monni. Next-to-leading non-global logarithms in QCD. *JHEP*, 10:006, 2021.
- [25] Andrea Banfi, Frédéric A. Dreyer, and Pier Francesco Monni. Higher-order non-global logarithms from jet calculus. *JHEP*, 03:135, 2022.
- [26] Andrea Banfi, Giuseppe Marchesini, and Graham Smye. Away-from-jet energy flow. *Journal of High Energy Physics*, 2002(08):006–006, aug 2002.
- [27] Andrea Banfi, Gavin P. Salam, and Giulia Zanderighi. Principles of general final-state resummation and automated implementation. *JHEP*, 03:073, 2005.
- [28] Andrea Banfi, Gavin P. Salam, and Giulia Zanderighi. Phenomenology of event shapes at hadron colliders. *JHEP*, 06:038, 2010.
- [29] Johannes Bellm et al. Herwig 7.0/Herwig++ 3.0 release note. *Eur. Phys. J. C*, 76(4):196, 2016.
- [30] Alexander Belyaev, Neil D. Christensen, and Alexander Pukhov. CalcHEP 3.4 for collider physics within and beyond the Standard Model. *Comput. Phys. Commun.*, 184:1729–1769, 2013.
- [31] F.A. Berends and W.T. Giele. Recursive calculations for processes with n gluons. *Nuclear Physics B*, 306(4):759–808, 1988.
- [32] F.A. Berends, H. Kuijf, B. Tausk, and W.T. Giele. On the production of a w and jets at hadron colliders. *Nuclear Physics B*, 357(1):32–64, 1991.
- [33] Daniele Bertolini, Tucker Chan, and Jesse Thaler. Jet Observables Without Jet Algorithms. *JHEP*, 04:013, 2014.

- [34] Christian Bierlich et al. Robust Independent Validation of Experiment and Theory: Rivet version 3. *SciPost Phys.*, 8:026, 2020.
- [35] Christian Bierlich et al. A comprehensive guide to the physics and usage of PYTHIA 8.3. 3 2022.
- [36] Thomas Binoth, C. Buttar, P. J. Clark, and E. W. Nigel Glover, editors. *Proceedings, 65th Scottish Universities Summer School in Physics: LHC Physics (SUSSP65): St. Andrews, UK, August 16-29, 2009*, Boca Raton, Florida, 2012. CRC Pr.
- [37] J. D. Bjorken and E. A. Paschos. Inelastic electron-proton and γ -proton scattering and the structure of the nucleon. *Phys. Rev.*, 185:1975–1982, Sep 1969.
- [38] F. Bloch and A. Nordsieck. Note on the radiation field of the electron. *Phys. Rev.*, 52:54–59, Jul 1937.
- [39] Enrico Bothmann et al. Event Generation with Sherpa 2.2. *SciPost Phys.*, 7(3):034, 2019.
- [40] Andy Buckley et al. General-purpose event generators for LHC physics. *Phys. Rept.*, 504:145–233, 2011.
- [41] Andy Buckley, James Ferrando, Stephen Lloyd, Karl Nordström, Ben Page, Martin Rüfenacht, Marek Schönherr, and Graeme Watt. LHAPDF6: parton density access in the LHC precision era. *Eur. Phys. J. C*, 75:132, 2015.
- [42] Matteo Cacciari, Gavin P. Salam, and Gregory Soyez. The anti- k_t jet clustering algorithm. *JHEP*, 04:063, 2008.
- [43] Matteo Cacciari, Gavin P. Salam, and Gregory Soyez. FastJet User Manual. *Eur. Phys. J. C*, 72:1896, 2012.
- [44] John Campbell, Joey Huston, and Frank Krauss. *The Black Book of Quantum Chromodynamics: A Primer for the LHC Era*. Oxford University Press, 12 2017.
- [45] John Campbell and Tobias Neumann. Precision Phenomenology with MCFM. *JHEP*, 12:034, 2019.

- [46] Stefano Carrazza, Alfio Ferrara, Daniele Palazzo, and Juan Rojo. APFEL web: a web-based application for the graphical visualization of parton distribution functions. *Journal of Physics G: Nuclear and Particle Physics*, 42(5):057001, mar 2015.
- [47] Peter A Carruthers. *Introduction to unitary symmetry*. Number 27 in Interscience tracts on physics and astronomy. Interscience Publishers, 1966.
- [48] S. Catani, Yu.L. Dokshitzer, M.H. Seymour, and B.R. Webber. Longitudinally-invariant kt -clustering algorithms for hadron-hadron collisions. *Nuclear Physics B*, 406(1):187–224, 1993.
- [49] S. Catani, Yuri L. Dokshitzer, M. H. Seymour, and B. R. Webber. Longitudinally-invariant k_{\perp} -clustering algorithms for hadron-hadron collisions. *Nucl. Phys. B*, 406:187–224, 1993.
- [50] S. Catani, F. Krauss, R. Kuhn, and B. R. Webber. QCD matrix elements + parton showers. *JHEP*, 11:063, 2001.
- [51] S. Catani and M. H. Seymour. A General algorithm for calculating jet cross-sections in NLO QCD. *Nucl. Phys. B*, 485:291–419, 1997. [Erratum: Nucl.Phys.B 510, 503–504 (1998)].
- [52] S. Catani and L. Trentadue. Resummation of the QCD Perturbative Series for Hard Processes. *Nucl. Phys. B*, 327:323–352, 1989.
- [53] S. Catani, L. Trentadue, G. Turnock, and B. R. Webber. Resummation of large logarithms in e^+e^- event shape distributions. *Nucl. Phys. B*, 407:3–42, 1993.
- [54] S. Catani, B. R. Webber, and G. Marchesini. QCD coherent branching and semiinclusive processes at large x . *Nucl. Phys. B*, 349:635–654, 1991.
- [55] Stefano Catani, Stefan Dittmaier, Michael H. Seymour, and Zoltan Trocsanyi. The Dipole formalism for next-to-leading order QCD calculations with massive partons. *Nucl. Phys. B*, 627:189–265, 2002.
- [56] Stefano Catani and Massimiliano Grazzini. Infrared factorization of tree level QCD amplitudes at the next-to-next-to-leading order and beyond. *Nucl. Phys. B*, 570:287–325, 2000.

- [57] Serguei Chatrchyan et al. Observation of a New Boson at a Mass of 125 GeV with the CMS Experiment at the LHC. *Phys. Lett. B*, 716:30–61, 2012.
- [58] Serguei Chatrchyan et al. Event Shapes and Azimuthal Correlations in $Z + \text{Jets}$ Events in pp Collisions at $\sqrt{s} = 7$ TeV. *Phys. Lett. B*, 722:238–261, 2013.
- [59] Yang-Ting Chien, Rudi Rahn, Solange Schrijnder van Velzen, Ding Yu Shao, Wouter J. Waalewijn, and Bin Wu. Recoil-free azimuthal angle for precision boson-jet correlation. *Phys. Lett. B*, 815:136124, 2021.
- [60] Yang-Ting Chien, Rudi Rahn, Ding Yu Shao, Wouter J. Waalewijn, and Bin Wu. Precision boson-jet azimuthal decorrelation at hadron colliders. 5 2022.
- [61] John C. Collins, Davison E. Soper, and George Sterman. Factorization for short distance hadron-hadron scattering. *Nuclear Physics B*, 261:104–142, 1985.
- [62] John C. Collins, Davison E. Soper, and George F. Sterman. Transverse Momentum Distribution in Drell-Yan Pair and W and Z Boson Production. *Nucl. Phys. B*, 250:199–224, 1985.
- [63] Eric Conte, Benjamin Fuks, and Guillaume Serret. MadAnalysis 5, A User-Friendly Framework for Collider Phenomenology. *Comput. Phys. Commun.*, 184:222–256, 2013.
- [64] A. Daleo, T. Gehrmann, and D. Maitre. Antenna subtraction with hadronic initial states. *JHEP*, 04:016, 2007.
- [65] M. Dasgupta and G. P. Salam. Resummation of non-global QCD observables. *Phys. Lett. B*, 512:323–330, 2001.
- [66] Mrinal Dasgupta, Kamel Khelifa-Kerfa, Simone Marzani, and Michael Spannowsky. On jet mass distributions in $Z + \text{jet}$ and dijet processes at the LHC. *JHEP*, 10:126, 2012.
- [67] Mrinal Dasgupta and Gavin P. Salam. Accounting for coherence in interjet E_t flow: A case study. *JHEP*, 03:017, 2002.

- [68] J. de Favereau, C. Delaere, P. Demin, A. Giammanco, V. Lemaître, A. Mertens, and M. Selvaggi. DELPHES 3, A modular framework for fast simulation of a generic collider experiment. *JHEP*, 02:057, 2014.
- [69] Celine Degrande, Claude Duhr, Benjamin Fuks, David Grellscheid, Olivier Mattelaer, and Thomas Reiter. UFO - The Universal FeynRules Output. *Comput. Phys. Commun.*, 183:1201–1214, 2012.
- [70] Yazid Delenda, Robert Appleby, Mrinal Dasgupta, and Andrea Banfi. On QCD resummation with k_t clustering. *JHEP*, 12:044, 2006.
- [71] Yazid Delenda and Kamel Khelifa-Kerfa. On the resummation of clustering logarithms for non-global observables. *JHEP*, 09:109, 2012.
- [72] Robin Devenish and Amanda Cooper-Sarkar. *Deep Inelastic Scattering*. Oxford University Press, 11 2003.
- [73] Günther Dissertori, Ian G. Knowles, and Michael Schmelling. *Quantum Chromodynamics: High Energy Experiments and Theory*. Oxford University Press, 05 2009.
- [74] Yuri L. Dokshitzer. Calculation of the Structure Functions for Deep Inelastic Scattering and $e^+ e^-$ Annihilation by Perturbation Theory in Quantum Chromodynamics. *Sov. Phys. JETP*, 46:641–653, 1977.
- [75] Yuri L. Dokshitzer, Valery A. Khoze, Alfred H. Mueller, and S. I. Troian. *Basics of perturbative QCD*. 1991.
- [76] Yuri L. Dokshitzer, G. D. Leder, S. Moretti, and B. R. Webber. Better jet clustering algorithms. *JHEP*, 08:001, 1997.
- [77] S. D. Drell and Tung-Mow Yan. Massive Lepton Pair Production in Hadron-Hadron Collisions at High-Energies. *Phys. Rev. Lett.*, 25:316–320, 1970. [Erratum: *Phys.Rev.Lett.* 25, 902 (1970)].

- [78] R. K. Ellis, W. J. Stirling, and B. R. Webber. *QCD and Collider Physics*. Cambridge Monographs on Particle Physics, Nuclear Physics and Cosmology. Cambridge University Press, 1996.
- [79] Stephen D. Ellis and Davison E. Soper. Successive combination jet algorithm for hadron collisions. *Phys. Rev. D*, 48:3160–3166, 1993.
- [80] Richard P. Feynman. Very high-energy collisions of hadrons. *Phys. Rev. Lett.*, 23:1415–1417, Dec 1969.
- [81] Jeffrey R. Forshaw, Michael H. Seymour, and Andrzej Siodmok. On the Breaking of Collinear Factorization in QCD. *JHEP*, 11:066, 2012.
- [82] Rikkert Frederix and Stefano Frixione. Merging meets matching in MC@NLO. *JHEP*, 12:061, 2012.
- [83] Rikkert Frederix, Stefano Frixione, Valentin Hirschi, Fabio Maltoni, Roberto Pittau, and Paolo Torrielli. Four-lepton production at hadron colliders: aMC@NLO predictions with theoretical uncertainties. *JHEP*, 02:099, 2012.
- [84] S. Frixione. A General approach to jet cross-sections in QCD. *Nucl. Phys. B*, 507:295–314, 1997.
- [85] S. Frixione, Z. Kunszt, and A. Signer. Three jet cross-sections to next-to-leading order. *Nucl. Phys. B*, 467:399–442, 1996.
- [86] Stefano Frixione and Bryan R. Webber. Matching NLO QCD computations and parton shower simulations. *JHEP*, 06:029, 2002.
- [87] W. T. Giele and E. W. N. Glover. Higher-order corrections to jet cross sections in e^+e^- annihilation. *Phys. Rev. D*, 46:1980–2010, Sep 1992.
- [88] W. T. Giele, E. W. Nigel Glover, and David A. Kosower. Higher order corrections to jet cross-sections in hadron colliders. *Nucl. Phys. B*, 403:633–670, 1993.

- [89] T. Gleisberg, Stefan. Hoeche, F. Krauss, M. Schonherr, S. Schumann, F. Siegert, and J. Winter. Event generation with SHERPA 1.1. *JHEP*, 02:007, 2009.
- [90] Tanju Gleisberg and Stefan Hoeche. Comix, a new matrix element generator. *JHEP*, 12:039, 2008.
- [91] W. Greiner, S. Schramm, and E. Stein. *Quantum chromodynamics*. 2002.
- [92] V. N. Gribov and L. N. Lipatov. Deep inelastic e p scattering in perturbation theory. *Sov. J. Nucl. Phys.*, 15:438–450, 1972.
- [93] David J. Gross and Frank Wilczek. Ultraviolet behavior of non-abelian gauge theories. *Phys. Rev. Lett.*, 30:1343–1346, Jun 1973.
- [94] G.'t Hooft. A planar diagram theory for strong interactions. *Nuclear Physics B*, 72(3):461–473, 1974.
- [95] John E. Huth et al. Toward a standardization of jet definitions. In *1990 DPF Summer Study on High-energy Physics: Research Directions for the Decade (Snowmass 90)*, pages 0134–136, 12 1990.
- [96] F James. Monte carlo theory and practice. *Reports on Progress in Physics*, 43(9):1145, sep 1980.
- [97] Frederick James and Lorenzo Moneta. Review of High-Quality Random Number Generators. *Comput. Softw. Big Sci.*, 4(1):2, 2020.
- [98] S. Kanda et al. Study of two particle azimuthal correlations in e^+e^- annihilation at $\sqrt{s} = 58$ GeV. *Phys. Rev. D*, 52:4872–4876, 1995.
- [99] Vardan Khachatryan et al. Azimuthal decorrelation of jets widely separated in rapidity in pp collisions at $\sqrt{s} = 7$ TeV. *JHEP*, 08:139, 2016.
- [100] Vardan Khachatryan et al. Measurement of dijet azimuthal decorrelation in pp collisions at $\sqrt{s} = 8$ TeV. *Eur. Phys. J. C*, 76(10):536, 2016.

- [101] K. Khelifa-Kerfa and Y. Delenda. Eikonal amplitudes for three-hard legs processes at finite- N_c . *Phys. Lett. B*, 809:135768, 2020.
- [102] Kamel Khelifa-Kerfa and Yazid Delenda. Non-global logarithms at finite n_c beyond leading order. *Journal of High Energy Physics*, 2015(3), mar 2015.
- [103] K. J. Kim and K. Schilcher. Scaling violation in the infinite-momentum frame. *Phys. Rev. D*, 17:2800–2808, May 1978.
- [104] Toichiro Kinoshita. Mass singularities of feynman amplitudes. *Journal of Mathematical Physics*, 3(4):650–677, 1962.
- [105] Hagen Kleinert and Verena Schulte-Frohlinde. *Critical Properties of Φ^4 -Theories*. WORLD SCIENTIFIC, 2001.
- [106] R. Kleiss and W. James Stirling. Spinor Techniques for Calculating p anti- $p \rightarrow W^{+-} / Z^0 + \text{Jets}$. *Nucl. Phys. B*, 262:235–262, 1985.
- [107] Ronald Kleiss and Roberto Pittau. Weight optimization in multichannel monte carlo. *Computer Physics Communications*, 83(2):141–146, 1994.
- [108] S. Kluth. Jet physics in e^+e^- annihilation from 14 to 209 gev. *Nuclear Physics B - Proceedings Supplements*, 133:36–46, 2004. Proceedings of the 10th High-Energy International Conference on Quantum ChromoDynamics.
- [109] Stefan Kluth. Tests of quantum chromo dynamics at e^+e^- colliders. *Reports on Progress in Physics*, 69(6):1771–1846, may 2006.
- [110] David A. Kosower. Antenna factorization of gauge theory amplitudes. *Phys. Rev. D*, 57:5410–5416, 1998.
- [111] F. Krauss. Matrix elements and parton showers in hadronic interactions. *JHEP*, 08:015, 2002.
- [112] Pierre L’Ecuyer. Good parameters and implementations for combined multiple recursive random number generators. *Operations Research*, 47(1):159–164, 1999.

- [113] T. D. Lee and M. Nauenberg. Degenerate systems and mass singularities. *Phys. Rev.*, 133:B1549–B1562, Mar 1964.
- [114] Maurice Lévy and Joseph Sucher. Eikonal approximation in quantum field theory. *Phys. Rev.*, 186:1656–1670, Oct 1969.
- [115] Leif Lonnblad. Correcting the color dipole cascade model with fixed order matrix elements. *JHEP*, 05:046, 2002.
- [116] L.Tomlinson. *Azimuthal decorrelation between leptons in the Drell-Yan process as a probe of infrared QCD: Phenomenology, predictions and measurement of a novel collider observable using perturbative resummation techniques*. PhD thesis, University of Manchester, 2014.
- [117] Fabio Maltoni and Tim Stelzer. MadEvent: Automatic event generation with MadGraph. *JHEP*, 02:027, 2003.
- [118] Michelangelo L. Mangano, Mauro Moretti, Fulvio Piccinini, Roberto Pittau, and Antonio D. Polosa. ALPGEN, a generator for hard multiparton processes in hadronic collisions. *JHEP*, 07:001, 2003.
- [119] A. D. Martin, W. J. Stirling, R. S. Thorne, and G. Watt. Parton distributions for the LHC. *Eur. Phys. J. C*, 63:189–285, 2009.
- [120] Makoto Matsumoto and Takuji Nishimura. Mersenne twister: A 623-dimensionally equidistributed uniform pseudo-random number generator. *ACM Trans. Model. Comput. Simul.*, 8(1):3–30, jan 1998.
- [121] O. Mattelaer and K. Ostrolenk. Speeding up MadGraph5_aMC@NLO. *Eur. Phys. J. C*, 81(5):435, 2021.
- [122] Nicholas Metropolis, Arianna W. Rosenbluth, Marshall N. Rosenbluth, Augusta H. Teller, and Edward Teller. Equation of state calculations by fast computing machines. *The Journal of Chemical Physics*, 21(6):1087–1092, 1953.
- [123] A H Mueller. *Perturbative QCD*. WORLD SCIENTIFIC, 1989.

- [124] T Muta. *Foundations of Quantum Chromodynamics*. WORLD SCIENTIFIC, 1987.
- [125] Paolo Nason. A New method for combining NLO QCD with shower Monte Carlo algorithms. *JHEP*, 11:040, 2004.
- [126] G. Parisi and R. Petronzio. Small Transverse Momentum Distributions in Hard Processes. *Nucl. Phys. B*, 154:427–440, 1979.
- [127] Michael E. Peskin and Daniel V. Schroeder. *An Introduction to quantum field theory*. Addison-Wesley, Reading, USA, 1995.
- [128] Tilman Plehn. *Lectures on LHC Physics*. Springer, 2015.
- [129] H. David Politzer. Reliable perturbative results for strong interactions? *Phys. Rev. Lett.*, 30:1346–1349, Jun 1973.
- [130] J. Pumplin, D. R. Stump, J. Huston, H. L. Lai, Pavel M. Nadolsky, and W. K. Tung. New generation of parton distributions with uncertainties from global QCD analysis. *JHEP*, 07:012, 2002.
- [131] E. Reya. Perturbative quantum chromodynamics. *Physics Reports*, 69(3):195–333, 1981.
- [132] Gavin P. Salam. Towards jetography. *The European Physical Journal C*, 67(3-4):637–686, may 2010.
- [133] Gavin P. Salam and Gregory Soyez. A Practical Seedless Infrared-Safe Cone jet algorithm. *JHEP*, 05:086, 2007.
- [134] Albert M Sirunyan et al. Azimuthal separation in nearly back-to-back jet topologies in inclusive 2- and 3-jet events in pp collisions at $\sqrt{s} = 13$ TeV. *Eur. Phys. J. C*, 79(9):773, 2019.
- [135] Torbjörn Sjöstrand, Stefan Ask, Jesper R. Christiansen, Richard Corke, Nishita Desai, Philip Ilten, Stephen Mrenna, Stefan Prestel, Christine O. Rasmussen, and Peter Z. Skands. An introduction to PYTHIA 8.2. *Comput. Phys. Commun.*, 191:159–177, 2015.

- [136] George F. Sterman and Steven Weinberg. Jets from Quantum Chromodynamics. *Phys. Rev. Lett.*, 39:1436, 1977.
- [137] Peng Sun, Bin Yan, C. P. Yuan, and Feng Yuan. Resummation of High Order Corrections in Z Boson Plus Jet Production at the LHC. *Phys. Rev. D*, 100(5):054032, 2019.
- [138] G. 't Hooft. Dimensional regularization and the renormalization group. *Nuclear Physics B*, 61:455–468, 1973.
- [139] G. 't Hooft and M. Veltman. Regularization and renormalization of gauge fields. *Nuclear Physics B*, 44(1):189–213, 1972.
- [140] Roberto Vega and Jose Wudka. Covariant method for calculating helicity amplitudes. *Phys. Rev. D*, 53:5286–5292, May 1996.
- [141] Stefan Weinzierl. Introduction to Monte Carlo methods. 6 2000.
- [142] M. Wobisch and T. Wengler. Hadronization corrections to jet cross-sections in deep inelastic scattering. In *Workshop on Monte Carlo Generators for HERA Physics (Plenary Starting Meeting)*, pages 270–279, 4 1998.
- [143] R. L. Workman et al. Review of Particle Physics. *PTEP*, 2022:083C01, 2022.
- [144] H. Yang et al. Back-to-back azimuthal correlations in Z +jet events at high transverse momentum in the TMD parton branching method at next-to-leading order. 4 2022.
- [145] Naima Ziani, Kamel Khelifa-Kerfa, and Yazid Delenda. Jet mass distribution in Higgs/vector boson + jet events at hadron colliders with k_t clustering. *Eur. Phys. J. C*, 81:570, 2021.